Influence of Constituents' Properties on the

Fracture Properties of High Strength Concrete

by

Jeffrey Ramzi Karam

B.S.C.E., Washington University in St. Louis

(1995)

SUBMITTED TO THE DEPARTMENT OF CIVIL AND

ENVIRONMENTAL ENGINEERING

IN PARTIAL FULFILLMENT

OF THE REQUIREMENTS FOR THE

MASTER OF SCIENCE

IN CIVIL AND ENVIRONMENTAL ENGINEERING

at the

MASSACHUSETTS INSTITUTE OF TECHNOLOGY

January, 1997

Signature of Author ____ _____

Department of Civil and Environmental Engineering

ember, 1996

Certified by _____ _____

Büyüköztürk

pervisor

Certified by ____ _____

Joseph M. Sussman

Chairman, Departmental Committee on Graduate Students

Influence of Constituents' Properties on the Fracture Properties of High Strength Concrete

by
Jeffrey Ramzi Karam

Submitted to the Department of Civil and Environmental Engineering
January, 1997 in partial fulfillment of the
requirements for the degree of
Master of Science in Civil and Environmental Engineering

Abstract

The mechanical properties of concrete are known to be highly dependent on the characteristics of the interfacial region. Through the use of admixtures the properties of the interfacial region have been altered such that concretes of exceptional strength are now achievable. As with most engineering materials, the improved strength comes at the expense of ductility. The objective of this research was to ascertain how the properties of the basic constituents of concrete affect the ductility. An interface fracture energy methodology was used to study the influence of various internal parameters. The parameters investigated for normal and high strength mortars were: aggregate size, aggregate volume fraction, and aggregate type. Additionally, a novel code-like equation was developed in order to predict the fracture energy of a cementitious composite based on the material properties of the constituents.

Conclusions from the ductility analysis can be summarized as follows: 1.) smaller maximum size of aggregate leads to greater ductility, 2.) with normal strength mixtures ductility is inversely related to volume fraction, and 3.) with high strength mixtures the ductility is directly related to volume fraction.

The novel equation was shown to be a good preliminary step in the development of a concrete fracture energy equation.

Keywords: High strength concrete, interface fracture mechanics, fracture energy, ductility.

Thesis Supervisor: Oral Büyüköztürk

Title: Professor of Civil and Environmental Engineering

Dedication

To my parents: Ramzi and Susan Karam

who always encourage and support me.

Acknowledgments

I would like to thank all the people who have helped me throughout my stay at MIT, in particular:

Professor Oral Büyüköztürk, my thesis advisor. He gave me this topic to work on and assisted me in all phases of the research required. His expertise in this field made my thesis work significantly less difficult.

Brian Hearing, a fellow graduate student who assisted me in many ways. I appreciate his help in the laboratory and in the development of some conclusions: particularly in the development of the fracture energy equation. Without his assistance my thesis would have been much more difficult and less complete.

My undergraduate advisor, Professor Thomas Harmon of Washington University in St. Louis who encouraged me to attend graduate school and in particular suggested that I apply to MIT. Without his advice I would never have applied and you would not be reading this.

W. R. Grace Co. of Cambridge, MA. and Bates Brothers who donated silica fume and superplasticizers, and granite respectively.

Table of Contents

List of Figures

List of Tables

Nomenclature

a_c	initial crack length
E_c	modulus of elasticity of concrete
$\overline{E}$	$\frac{E}{(1-\nu^2)}$, plain strain modulus
f_c	compressive strength of concrete
f_r	modulus of rupture
f_t	splitting tensile strength
G	fracture energy
K	stress intensity factor
k_a k_v	aggregate size factor, and volume fraction factor for novel equation
l_{ch}	characteristic length
Q	measure of ductility proposed by Jeng and Shah
S, b, t	loading geometry
α, β	Dundurs' elastic mismatch parameters
v	coarse aggregate volume fraction
Γ	interface fracture strength
σ_{22}, σ_{12}	normal stress and shear stress
μ	shear modulus
ν	Poisson's ratio

γ angle of incidence for impinging crack

Ψ phase angle

$\hat{L}$ reference length

T applied traction loading

Chapter 1

Introduction

1.1 Background

For nearly a century the constituents and behavior of concrete remained relatively unchanged. However, during the last three decades significant research has been undertaken in order to improve the mechanical properties of concrete [*Aitcin and Laplante, 1992*]. Through the use of mineral and chemical admixtures, primarily developed in the 1970's, researchers have been able to improve strength, stiffness, durability and other properties of concrete. The most noteworthy admixtures developed are air-entraining mixtures, superplasticizers, also known as high range water reducers (HRWR) and silica fume. Air entrainment improves the freeze-thaw resistance by creating voids for frozen water to occupy. Superplasticizers decrease the water necessary for hydration by reducing trapped water in the cement grain flakes and silica fume enhances the durability and strength of concrete by improving the bond strength and decreasing porosity. Use of these admixtures, with careful material selection, can regularly produce concrete with compressive strengths above 100 MPa (69,000psi).

1.2 Introduction to Relation between Interface Properties and Ductility

The ability of high strength concrete (HSC) to support high compressive loads has made its use in columns and other compression members obvious. Other applications of HSC have come more slowly mainly due to the reluctance of design engineers. The reluctance is founded in the lack of ductility and relatively low tensile strengths exhibited by HSC. The lack of ductility may be attributed to the

same attributes which improve the other mechanical properties of concrete, that is the altered properties of the interface. Increased bond strength between concrete phases through the use of admixtures enhances the mechanical properties of the composite however the ductility is sacrificed. By altering the constituents of concrete, it is known that the behavior of the interfacial region, and therefore composite, is altered. If the characteristics of this region can be optimized by altering only the basic constituents perhaps a HSC with superior ductility can be obtained and its use can become more widespread.

1.3 Research Objective

Recently, the mortar-aggregate interface has been the subject of several investigations at MIT [*Büyüköztürk and Lee, 1993; Oumera, 1991; Lee, 1993; Trende, 1995; Büyüköztürk and Hearing, 1996*]. The purpose of the works has been characterization of the interfacial region of various material combinations and its influence on crack propagation. These works utilized two phase model to asses the fracture properties of the mortar-aggregate interface. This simplification is commonly employed, however verification of the conclusions' applicability to real concrete is then necessary.

The purpose of this research is to investigate the affect of various material combinations on the fracture properties of real concrete through interface fracture and basic fracture concepts. Material selection is chosen as the primary variable because it represents an affordable alternative to other means of ductility enhancement. Research limited by this constraint seems to have been eclipsed recently by investigations of fiber reinforcement, however due to the high costs the widescale use of fibers outside laboratories seems doubtful. This research will expand the base of the previous investigations from two phase models to real concrete. Whenever possible the same material combinations and mix proportions

were used as those previously investigated in order to ensure compatibility. The applicability of the knowledge obtained in past works to real concrete will be addressed. Additionally, the applicability of analytical models developed at MIT, to real concrete will also be covered briefly.

1.4 Research Approach and Scope

1.4.1 Interface Properties in Concrete

Concrete is often studied as a two phase model consisting of only mortar and an aggregate. These models have proven to be useful in the past, however they fail to account for the properties of the interface while it has been shown by several researchers that the behavior of concrete is highly dependent on this region [*He and Hutchinson, 1989; Büyüköztürk and Lee, 1993; Goldman and Bentur, 1989*]. It is known that microcracks tend to propagate around the aggregate first, which allows one to conclude that the fracture resistance of this area is less than that of the mortar [*Mitsui et al., 1992*]. An understanding of the physical properties of the interface will make it possible to then alter them in order to improve the crack resistance of the composite as a whole.

A great deal can be learned by studying crack propagation in the interfacial region. Depending on the bond strength and the properties of the aggregate two possible crack scenarios are evident in the failure of cementatious materials. If an aggregate that is weaker than the bond strength is chosen, the crack will penetrate the aggregate and the interface properties will have little contribution to crack resistance. Meanwhile a strong aggregate will deflect the crack through the interface and a crack path with many bends and bifurcations can be observed. The total energy consumed may be greater in either case. In the first case the fracture path is planar but the energy release rate per unit extension of crack could be

larger. In the second case the crack path is longer and therefore may consume more energy.

Analytical models representing these two crack scenarios have been developed at MIT. Kitsutaka et al. [*1993*] analyzed transgranular cracking on mortar specimens containing an aggregate inclusion. Büyüköztürk and Hearing [*1996*] followed this work with a finite element code to simulate interfacial cracking. Both works by themselves provide relevant information however, because they analyzed simple composite models it is not known how appropriate their conclusions are for true concrete.

1.4.2 Research Approach

It is clear that the properties of the aggregate have a significant effect on the behavior of the interface and therefore the composite. Specifically, the maximum aggregate size (MSA), volume fraction and aggregate type all can have an appreciable effect. An investigation of how these parameters, for both normal strength concrete (NSC) and HSC, influence ductility is undertaken. Both strengths were tested in order to isolate the effect of silica fume on the properties of the interface. Silica fume enhances the properties of the interface by reducing the porosity and inhomogeneity in the region immediately surrounding the aggregates, also known as the transition zone. By improving the strength of the interface the strength of HSC has been increased significantly. However the increase in strength has come at the expense of a corresponding decrease in ductility [*Oumera, 1991*]. Hence more research is needed to characterize the interfacial region in order to optimize both ductility and strength.

1.4.3 Scope of Research

Considering the dearth of knowledge regarding material selection's effect on the ductility of concrete an experimental investigation was undertaken. The

characteristic length, a measure of ductility developed by Hillerborg, is used to characterize several different mixtures of concrete. The measure has been used to quantify the ductility of concrete, glass, rock and other materials [*Zhou et al., 1995*]. The variables studied in this work are: mortar strength, aggregate type, MSA and volume fraction. Precracked three point bending beams meeting RILEM specifications and standard laboratory cylinders for compression and split cylinder tests were used for each material combination obtained by the permutation of the investigation parameters. In all over 110 beams and 110 cylinders were tested over 13 weeks to adequately asses the properties.

1.5 Thesis Organization

Chapter 1 gives a brief introduction to the history of concrete and the developments which led to HSC. The scope and objective of the research and the thesis organization are also presented.

Chapter 2 contains a discussion of the properties of HSC. Included are the advantages and disadvantages of HSC compared to NSC, its use in construction around the world and its engineering properties.

Chapter 3 provides relevant information on Interface Fracture Mechanics. Specifically addressed is the competition between crack deflection and penetration.

Chapter 4 is a summary of the works previously completed at MIT which have led to this work. The works have led to several Master's thesis, journal articles and a Ph.D. thesis.

Chapter 5 outlines the testing program and material selection for HSC. The material selection as it pertains to this work as well as a background of parameters not investigated here is given.

Chapter 6 contains the discussion of the experimental results obtained from this work. Most notably a discussion about various material combinations and their ductilities is presented.

Chapter 7 consists of comparisons of the results of this work to previously completed analytical results and the development of a novel code-like equation to predict the fracture energy of a composite based solely on the properties of the constituents.

Chapter 8 is a summary and conclusion of this work. In addition recommendations for future work will also be made.

Chapter 2

High Strength Concrete

The purpose of this chapter is to give a basic introduction to the behavior of HSC. It is important that some familiarity with the material be acquired before research to improve the properties can be accomplished. Also included are past uses of HSC in construction. By examining how the material has been used future applications can be realized.

2.1 Definition of HSC

It is important to note that the definition is not a rigid or consistent one. Many researchers seem to define HSC as simply concrete with compressive strengths above what is considered standard. In 1984 American Concrete Institute (ACI) Committee 363 defined high strength as having a compressive strength above 41 MPa. The looser definition above is often accepted due to strength variations from region to region and over time.

2.2 Advantages and Disadvantages of HSC

Due to the improved compressive strength the natural application of HSC is to compression members. In the past HSC has been used most frequently for the columns of high rise buildings. Besides the improved final strength other properties which make HSC efficient for this use include the increased early strength and increased resistance to creep and shrinkage. The higher strength allows smaller cross-sectional areas to be utilized to carry loads which decreases the dead load on the structure and increases the area of rentable floor space on the lower floors. The improved creep and shrinkage resistance lead to appreciable savings because construction time can be shortened because formwork removal can start earlier and therefore be used more often [*Aitcin and Laplante, 1992, Oumera, 1991*].

For example, the Water Point Tower in Chicago was designed to have the same size columns throughout the building which allowed the use of the same formwork for every column. This design required that the compressive strength be varied from floor to floor [*Aitcin and Laplante, 1992*]. The variation of compressive strengths by floor can be seen in Figure 2.1. Finally, the decreased creep and shrinkage also makes HSC more suitable for prestressing because prestressing can start earlier and the losses are diminished [*Malier, 1992*].

To this point the only advantages mentioned have been strength, creep and shrinkage however there are many other beneficial characteristics of HSC. Most notably are the improved modulus of elasticity, durability, shear strength and resistance to freeze thaw cycles [*Malier, 1992*] Because not only the strength is increased, concrete of these types are often referred to as high-performance concrete (HPC). Although the aforementioned attributes are found in the concrete tested for this research, the term HSC will be used herein and regarded as synonymous.

HSC is not without its negative qualities. The two major weaknesses are its lack of ductility and low tensile strength relative to HSC. In Figure 2.2 the stress strain curves for three different concretes are given. By observing the post-peak behavior it is apparent that HSC rapidly loses its ability to carry load. The lack of ductility is a major concern because it leads to the reluctance of structural engineers to call for its use. Presently this is one of the factors most limiting its everyday use [*Malier, 1992*]. The relatively low tensile strength creates significant problems. Typically in NSC the tensile strength is 10-15% of the compressive strength, while HSC's tensile strength is between 5-7% of the compressive strength. For HSC used solely in compression this does not pose a problem, however in beams tension cracking can seriously jeopardize the long term performance of the member.

Another significant negative is that there is less knowledge about the behavior of HSC. Many of the empirical equations in ACI codes were developed for NSC and they

are not applicable to HSC. With future research, ACI should be able to alleviate this situation.

2.3 Use of HSC in Construction

Despite the fact that reliable HSC is easily achievable, most structural concrete elements are still made with 20 to 40 MPa concrete. It is argued that in most cases this strength is adequate due to member sizing governed by deflections or space requirements of reinforcing steels, cables, vibrating pokers, etc. In the past new technologies requiring new design considerations have been met with similar skepticism. Comparable remarks were made regarding the introduction of prestressed concrete and even about the first use of reinforcing steel by Hennebique and Coignet. However today, both practices are now widely used and accepted as means of construction [*Malier, 1992*].

There are many situations in which HSC would be advantageous. Specifically HSC has been used in the past for a variety of structures including buildings, bridges, offshore structures, highways and nuclear containment [*Mehta and Aitcin, 1990; Paulson et al., 1991; Haug and Jakobsen., 1990; Helland, 1990; Larrard et al., 1990*]. Some additional and specific examples of the use of HSC are given in Table 2.1. It is suited for these applications not only due to the improved compressive strengths, but also due to improved modulus of elasticity, durability, shear strength, and high early strength [*Malier, 1992*].

HSC was first used in the U.S. in 1965 for the columns of the Lake Point Tower in Chicago. The compressive strength was at the time an impressive 50 MPa. In the 1970's compressive strengths continued increasing. In Chicago 60 MPa was used for the first 28 of 79 stories for the Water Tower building shown in Figure 2.1, and 75 MPa concrete was used in the River Plaza. Then in 1982, 100 MPa concrete elements were used for the Chicago Mercantile Building. Later in the same decade 120 MPa concrete elements were used in the Two Union Square building in Seattle [*Mehta and Aitcin, 1990*]. For centuries concrete's compressive strength remained in the range of 20 to 40 MPa; then in

only 17 years the strength doubled from 50 to 100 MPa. Mix Proportions for some examples of HSC used in high rises are shown in Table 2.2.

The use of HSC in bridge engineering has also increased recently. HSC is appropriate for bridges due to the improved short term strength, workability, durability and improved modulus of elasticity [*Malier, 1992*] The French Ministry of Public Works and the National Project on New Concretes teamed up to build an experimental HPC bridge in the town of Joigny, France. The bridge, shown in Figure 2.3, is a balanced continuous three-span bridge, with span lengths of 34, 46 and 34 meters. Preliminary designs for ordinary concrete (35 MPa) and HSC (60 MPa) showed that the quantity of concrete could be reduced from 1,395 m^3 to 985 m^3. This 30 percent reduction led to a 24 percent load reduction on the piers, abutments and foundations. The decreased dead load also decreased the number of prestressing strands required [*Malier et al., 1992*] HSC has also successfully been used for the deck of the Roize Bridge and in the arch of the Rance arch bridge shown in Figure 2.4 [*Causse and Montens, 1992; De Champs and Monachon, 1992*].

HSC has also been used for several offshore structures in the North Sea which have been tested in-situ and have given very encouraging results. Haug and Jakobsen [*1990*] undertook the testing of approximately one thousand concrete cores from gravity based platforms from the locations seen in Figure 2.5 The goal of their research was to show that the in-situ strength of the concrete was higher than assumed as basis for the Norwegian code NS 3473. They found that with stringent quality control and good curing conditions the design compressive strength with slipformed cell walls could have been safely increased by 10%, with slipformed shafts 5% and with all non-slipformed parts 0%. The actually strengths were increased by more than these percentages, however they felt that larger increases in design strength should be taken in steps [*Haug and Jakobsen, 1990*].

HSC can also be used successfully for highway pavements to improve abrasion resistance. During the winter months in Norway cars are permitted to use studded tires

which damage the road in heavily populated areas to the point where it needs repair nearly every year or two. A major national program to investigate concrete as an alternative to asphalt was undertaken with success. By carefully selecting aggregates Helland [*1990*] was able to achieve the same resistance from 100-120 MPa concrete as that of granite. Today 100-130 MPa concrete is used for both new and the repair and maintenance of old highway pavements [*Helland*, 1990].

In 1990 Larrard et al. undertook the mix design of HSC for use in the nuclear power plant Civaux II. The requirements for the material were a compressive strength of 65-70 MPa and an improved air tightness. Obviously in the case of an accident containment of the radioactive particles is critical. Upon completion of their investigation Larrard et al. claimed the use of "the new generation of concretes will therefore be a major leap forward in French nuclear power plant" technology [*1990*].

2.4 Behavior of HSC

The use of HSC will increase only with an increased awareness of the basic behavior of the material. Presently one main factor limiting the use of HSC is reluctance of designers [*Aitcin and Laplante, 1992*] Without knowing the properties characteristic of HSC designers will fail to use the material in situations where it could be structurally and/or economically more efficient. In order to rectify this problem, this section will discuss the basic engineering properties typical of HSC.

2.4.1 Stress-Strain Behavior

There is a common understanding that engineering materials become more brittle as the strength is increased. In the quest to make and safely use HSC this has proven to be the main limitation. Aside from compressive strength, the major difference between HSC and NSC is the post peak load behavior. As seen in the stress-strain diagram of Figure 2.2, the nearly linear descending portion of the curve for HSC is representative of the rapid loss of the materials ability to carry load. In order to ensure the redistribution of forces and to give ample warning before collapse of a member the post peak behavior of HSC must become more like that of NSC [*Bjerkeli et al., 1990*].

The inherent brittleness of HSC can be understood by examining the behavior on a microscopic level. Failure of a cementatious material has two stages; first there is failure of the bond between the aggregate and the mortar, known as interface cracks, then mortar cracks form and propagate to bridge the interface cracks. Examples of these cracks are shown graphically in Figure 2.6. NSC under loading experiences these cracking scenarios with a gap in time between them due to the difference in strength of the mortar and bond. However, with HSC the ductility is observed to be smaller because the differential in stress levels at which the bond and mortar cracking takes place becomes small [*Oumera, 1991*].

Crack formation and propagation has been studied rather extensively for NSC. The progression of cracking can be seen in Figure 2.7. Shrinkage cracks and cracks caused by bleeding exist before the member experiences load. Progression of these and other cracks begins at loads lower than 65% of the ultimate, with bond cracks around the largest aggregates occurring first. Then, at nearly 85% of the ultimate load mortar cracks begin to form and bridge the bond cracks. Finally, failure occurs when the cracks form parallel to the applied load, at which point splitting occurs [*Liu et al., 1972*].

The development of microcracks in HSC has not been studied as extensively. It is accepted that the addition of silica fume densifies the paste in the vicinity of the aggregate which leads to improved bond strength. The improvement in bond strength is responsible for the larger linear portion of the stress strain curve for HSC as compared to NSC. The linearity allows one to conclude that failure of the bonds occurs at a higher stress ratio. However as mentioned earlier, the stronger bonds also result in a more brittle behavior of the composite because the onset of cracking begins relatively near the ultimate load [*Oumera, 1991*].

2.4.2 Ductility of HSC

Qualitatively it is not difficult to characterize the ductility of a material. Usually the post peak behavior of the stress strain curves are studied and a material which has a longer and flatter tail is said to be more ductile. However, quantitatively there is no uniformly accepted measure. Improvement of the ductility of concrete has been the subject of much

research lately. Some of these works have also suggested equations to quantify ductility. Two of the more well known measures are the characteristic length, l_{ch}, by Hillerborg and the parameter Q by Jeng and Shah. In research similar to this work, Zhou et al. found that the measure proposed by Hillerborg was a more appropriate indication of ductility than that developed by Jeng and Shah [*1985*].

The theory showing that the characteristic length is an appropriate measure is presented in Section 3.5. This measure has been used to quantify the brittleness of concrete, rock, glass and other materials. Specifically, it has been used for concrete by Hilsdorf and Brameshuber [*1991*], Zhou et al. [*1995*] and Tasdemir et al. [*1996*]. The value of l_{ch} for ordinary concrete is in the range of 0.1 to 1.0m with an average value of 0.2 to 0.4m. With the smaller the number representing a more brittle material [*Hillerborg, 1989*]. Zhou et al. report values of l_{ch} ranging from 0.08 to 0.33m for concretes with compressive strengths ranging from 81 to 115 MPa, irrespectively [*1995*].

2.4.3 Modulus of Elasticity

The modulus of elasticity is a very meaningful material parameter in structural analysis and design. It is used to calculate stress, strains and deflection of members and structures. The modulus of concrete depends on several properties including the ambient moisture, loading conditions and rate, modulus of cement-paste matrix, porosity and composition of the transition zone, and the modulus of the aggregate [*Mehta, 1986*].

The empirical equation that the ACI proposes can not be satisfactorily applied to concretes considered high-strength. ACI-318 predicts the modulus of elasticity of concrete as,

$$E_c = 33 w_c^{1.5} \sqrt{f_c'} \qquad (2.1)$$

where E_c is in pounds per square inch (psi), w_c is the air dry weight of concrete in pounds per cubic foot, and f_c' is the compressive strength of concrete in psi: all at the time of

testing [*Shih et al., 1989*]. Shih et al. proposed the following empirical equations which give a better relation between compressive strength and the modulus of elasticity for HSC:

$$E_c = 55{,}000\sqrt{f_c'} - 120{,}000 \text{ psi} \qquad (2.2)$$

$$\text{for } 3{,}000 \text{ psi} < f_c' < 12{,}000 \text{ psi}$$

$$E_c = 4{,}660\sqrt{f_c'} - 1{,}370 \text{ MPa} \qquad (2.3)$$

$$\text{for } 21 \text{ MPa} < f_c' < 83 \text{ MPa}$$

ACI-318 has proposed an equation for HSC which is similar to 2.2, which is:

$$E_c = 57{,}000\sqrt{f_c'} \text{ psi} \qquad (2.4)$$

Carrasquillo et al. and ACI Committee 363 feel that the equation 2.4 overestimates the modulus of elasticity for compressive strengths above 6,000 psi. Therefore, upon further investigation, they proposed the following equation for compressive strengths in the range of 3,000 to 12,000 psi:

$$E_c = 40{,}000\sqrt{f_c'} + 1.0x10^6 \text{ psi} \qquad (2.5)$$

However, they have conceded that the modulus of elasticity predicted by this equation is below that that many researchers have reported.

The three empirical equations suggested previously are depicted graphically in Figure 2.8. By noting the wide scatter of results it seems apparent that not one equation can adequately predict the modulus of elasticity for concretes with compressive strengths in the range of HSC. Therefore further research is necessary in this area.

2.4.4 Tensile Strength

Application of HSC to flexural members has come slowly due to the relatively lower tensile strength compared to NSC. Although tensile strength is not often

considered important it does effect the extent and size of cracking in flexural members. The tensile strengths of NSC is usually assumed to be 10% of the compressive strength [*Wang and Salmon, 1985*]. For HSC the tensile strength does not increase proportionally with the compressive strength and is usually assumed to be only 5-7 % of the compressive strength.

Tensile strength in flexure, known as the modulus of rupture, is an important measure when cracking and deflection of beams is considered. It is generally accepted that an average value of f_r for NSC is

$$f_r = 0.62\sqrt{f_c}\ \text{MPa} \tag{2.6}$$

For concretes as high in strength as 83 MPa Carrasquillo et al. [*1981*] the previous equation has been modified to

$$f_r = 0.94\sqrt{f_c}\ \text{MPa} \tag{2.7}$$

Both equations are empirical and their results have significant scatter, therefore they should used carefully for design purposes.

2.4.5 Creep and Shrinkage

Comparatively little research has been done on creep and shrinkage of HSC compared to NSC [*Penttala et al., 1990*]. Based on experimental research by Paulson, Nilson and Hover [*1991*] on HSC beams it seems that the ACI Building Code drastically over predicts the time dependent deformations. Less than accurate predictions seriously curtail the efficient use of HSC in applications it would otherwise be suitable for [*Paulson et al., 1991*] For buildings in the range of 100-150 stories creep deformation of the columns may be as important as strength for floor levelness and exterior skin movement [*Collins, 1989*].

Qualitatively one would surmise that the effects of creep in HSC will be diminished compared to NSC due to the decrease in water used [*Penttala et al., 1990, Paulson et al., 1991*]. Yet, anything that reduces the free water content will promote shrinkage by either hydration or drying. With low w/c ratios concrete loses free water by hydration because the cement is not able to find enough water to complete its transformation. This situation will yield higher autogenous shrinkage and lower drying shrinkage [*Larrard, 1990*]. Penttala et al. found that the shrinkage of HSC is of the same magnitude as that of NSC [*1990*]. However, Paulson et al. [*1991*] found that for 83 MPa concrete under uniform compression had a creep coefficient approximately half of NSC's

As with the modulus of elasticity, this is an area in which more research is necessary. With a change in the creep coefficient of the ACI Building Code HSC could be used more extensively in situations where it seems it is already more efficient.

2.4.6 Freeze-Thaw Resistance of HSC

Freeze-thaw resistance of concrete depends primarily on material, production and environmental properties. The later two parameters are nearly standard to HSC and NSC, therefore only the first will be discussed. The most important material parameter is the w/(c+s) ratio, silica fume content and the air void distribution, which can only be obtained through the use of air entraining agents. However, air entrainment causes instability of the air voids and a decrease in strength due to increased porosity [*Hammer and Sellevold, 1990*].

When low w/(c+s) ratios are used, as with HSC, the capillary pore size and volume are decreased. With less porosity there is also less permeability and a smaller amount of water freezeable. Therefore HSC exhibits more resistance to freeze/thaw cycles than NSC [*Hammer and Sellevold, 1990*]. This makes the use of HSC for highways and parking decks attractive because replacements, which are usually very expensive, can be reduced.

2.5 Summary

The aim of this chapter was to provide a fundamental understanding of HSC and its properties. At the onset, the apparent lack of a rigid definition for HSC was addressed. This was followed by a discussion of the attributes that make HSC more and less attractive than NSC. Based on these attributes, past uses of the material were given in order to demonstrate how HSC may be used in the future.

Next, the engineering properties of HSC were presented. It was explained that HSC is characterized by a more linear ascending portion of the stress strain curve than NSC due to the lag time in the formation of cracks of the interface and mortar. This may also be responsible for the more rapidly decreasing stress strain curve following the post peak load. Also presented was the measure that will be used to quantify the ductility of the concretes tested. Next, some empirical equations suggested to ACI to evaluate the modulus of elasticity based on compressive strength were discussed. Finally, the tensile strength, creep and shrinkage, and freeze-thaw resistance of HSC were addressed. The tensile strength of HSC does not increase at the same rate as the compressive strength, thereby limiting its applications to flexural members due to cracking. The effect of creep and shrinkage is also diminished due to the decrease of water in the system. It was also shown that HSC exhibits more resistance to freeze-thaw cycles than does NSC making its use for highways and parking decks more efficient.

Table 2.1 Examples of HSC in use.
[*Malier, 1992*]

Types of Structure	Properties Improved	Practical Examples
Bridges	Short term strength, workability, durability, deferred deformation, strength	Joigny, Rance, Perthuiset, Louhans, Champs du Comte, Sylans, Ré, Auzon (All in France)
Offshore Structures	Durability, compression and shear, workability, abrasion and impact	Gullfaks B, C (Norway), Tere Neuve (Canada), Terre Adéle (France)
High-Rise Buildings	Compression and shear, workability, short term strength, constraint	Water Tower Place (USA), Nova Scotia (Canada), 2 Union Square Seattle (USA), 1 Wacker Drive Chicago (USA), 181 Wacker Chicago (USA), 225 Wacker Chicago (USA), NW Hospital, Chicago (USA), Arche Paris, and Chibune R. S. (Japan)
Highways	Abrasion, impact, freeze-thaw, shear, durability, workability	Valerenga (Norway), Ranasfoss BR. (Norway), Shestad TU. (Norway), Highway 86 (Paris), Paris Airport
Nuclear Structures	Durability, strength, water tightness	Civeaux (France)

Tale 2.2 Mix proportions for HSC used in high-rises.
[*Lee, 1993*]

Building	Avg. 28 day compressive strength	Component Materials in 1 -m^3 concrete batch, kg/ m^3							
		Cementitious materials			Total Water	Fine Aggregate	Coarse Aggregate	Superplasticizer L/m^3	Water/Cement ratio by weight
		PC	FA	SF					
Water Tower Place, Chicago	65	500	60	-	178	608	1068	-	0.32
Commerce Tower, Houston	65	390	100	-	161	575	1141	-	0.33
International First Plaza, Dallas	80	360	150	-	148	603	1157	3	0.29
Experimental Column, Montreal	90	500	-	30	135	700	1100	15	0.25

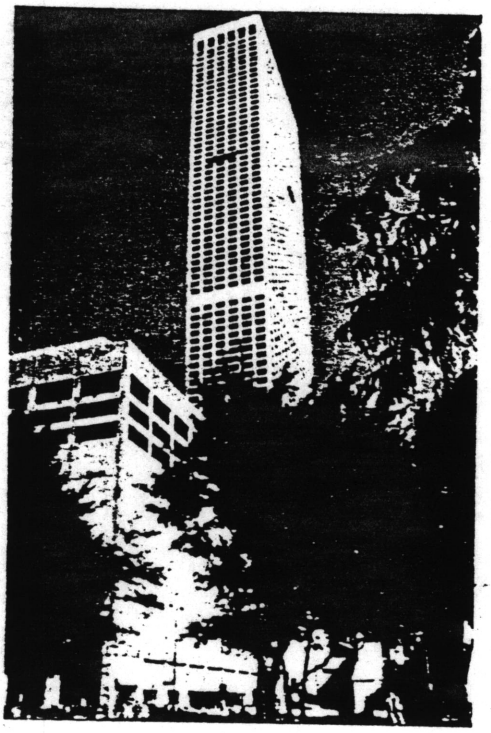

Water Tower Place, Chicago

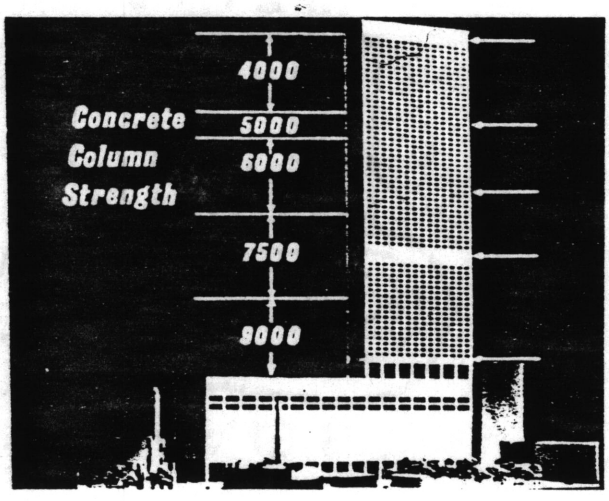

Figure 2.1 Variation of Compressive Strength by Floor
[*Malier, 1992*]

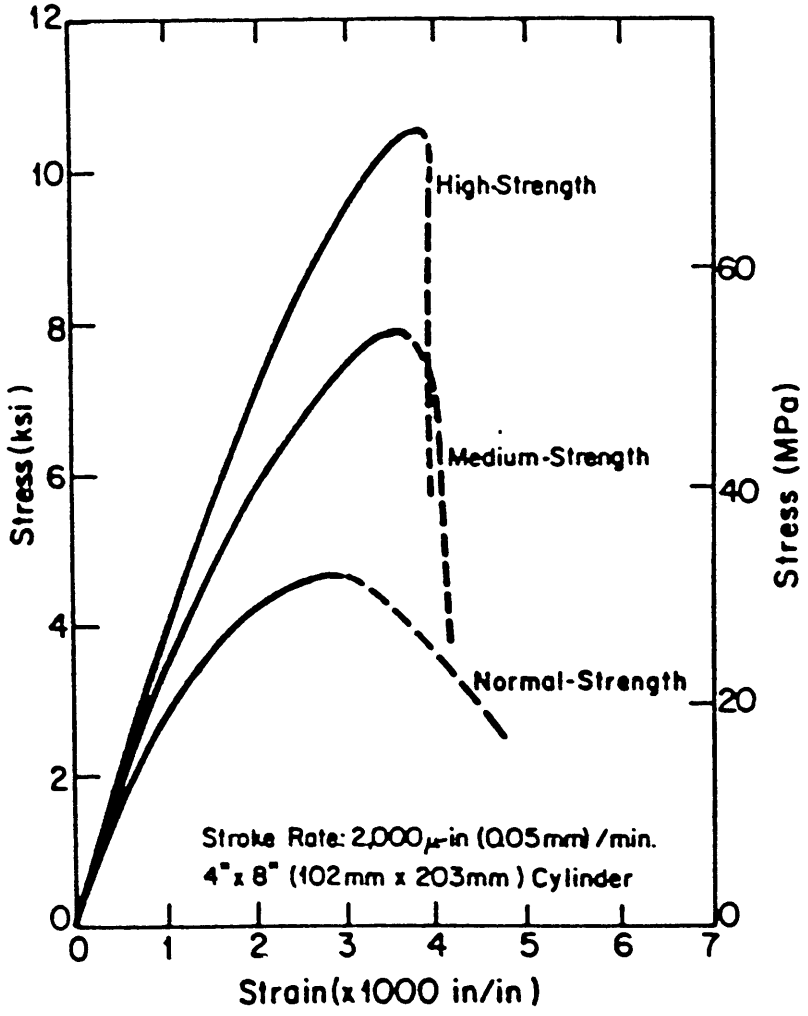

Figure 2.2 Stress-Strain Curves for Normal, Medium and High Strength Concretes.
[*Carrasquillo et al., 1981*]

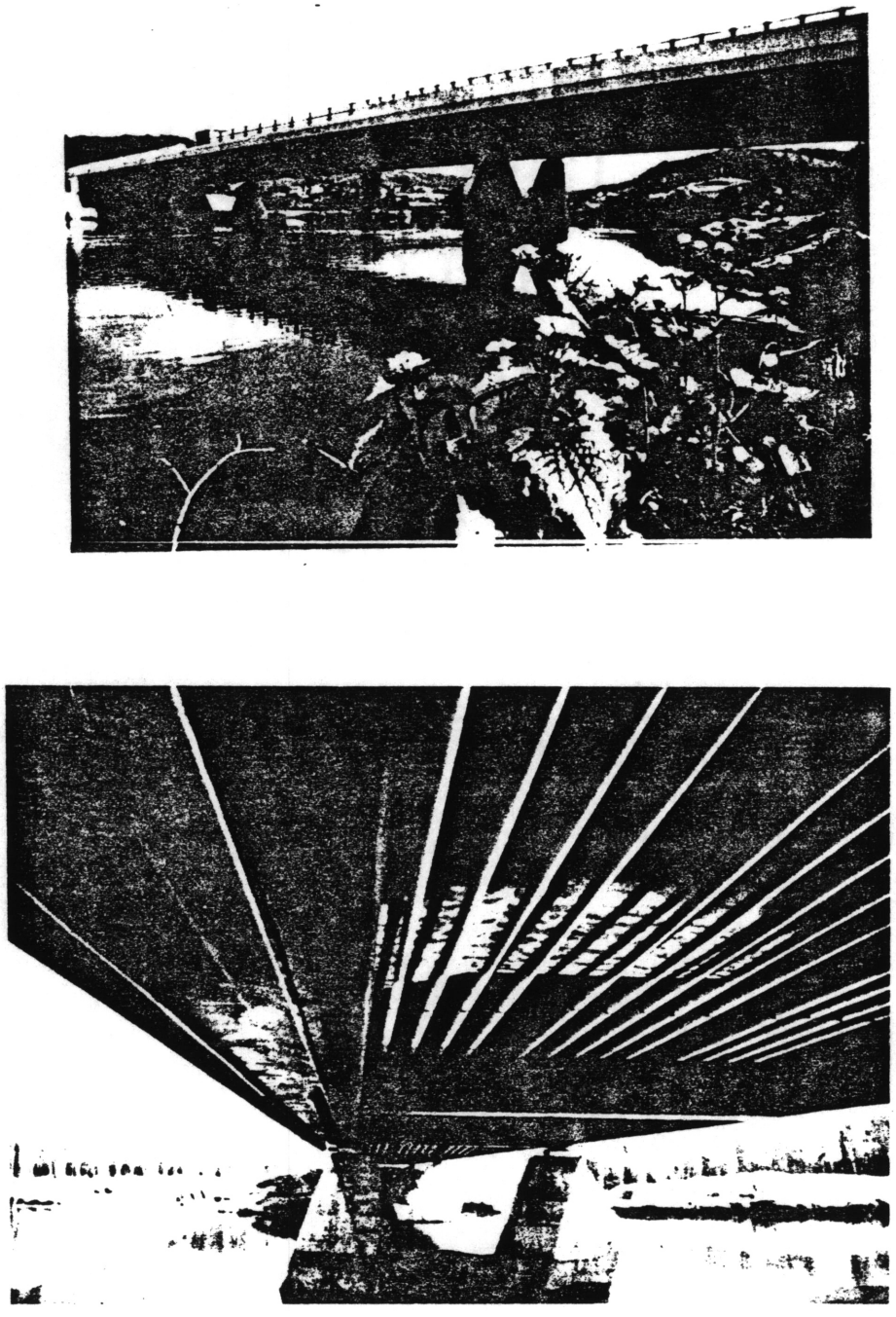

Figure 2.3 The Bridge of Joigny
[*Malier et al., 1992*]

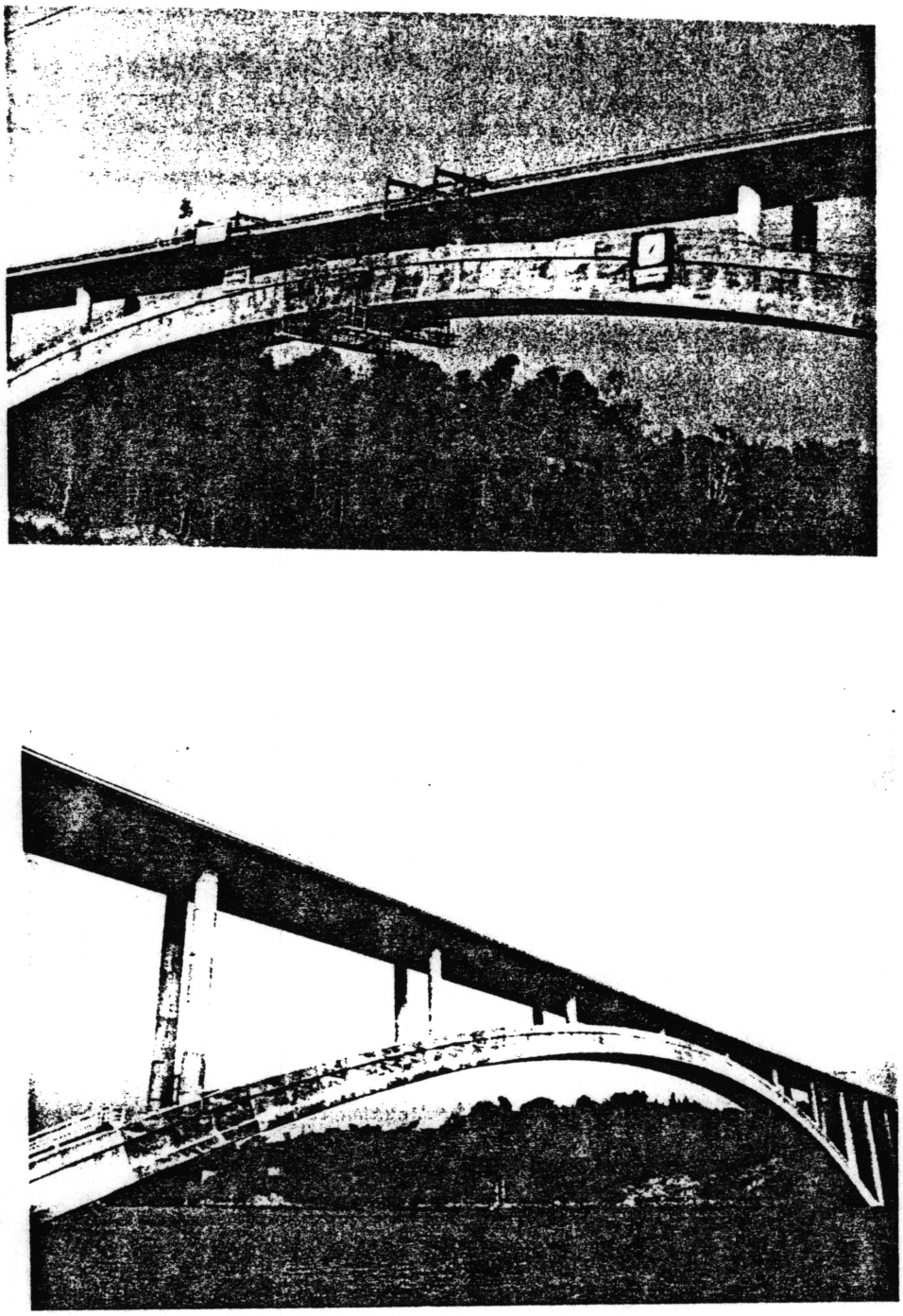

Figure 2.4 Rance Arch Bridge
[*DeChamps and Monachon, 1992*]

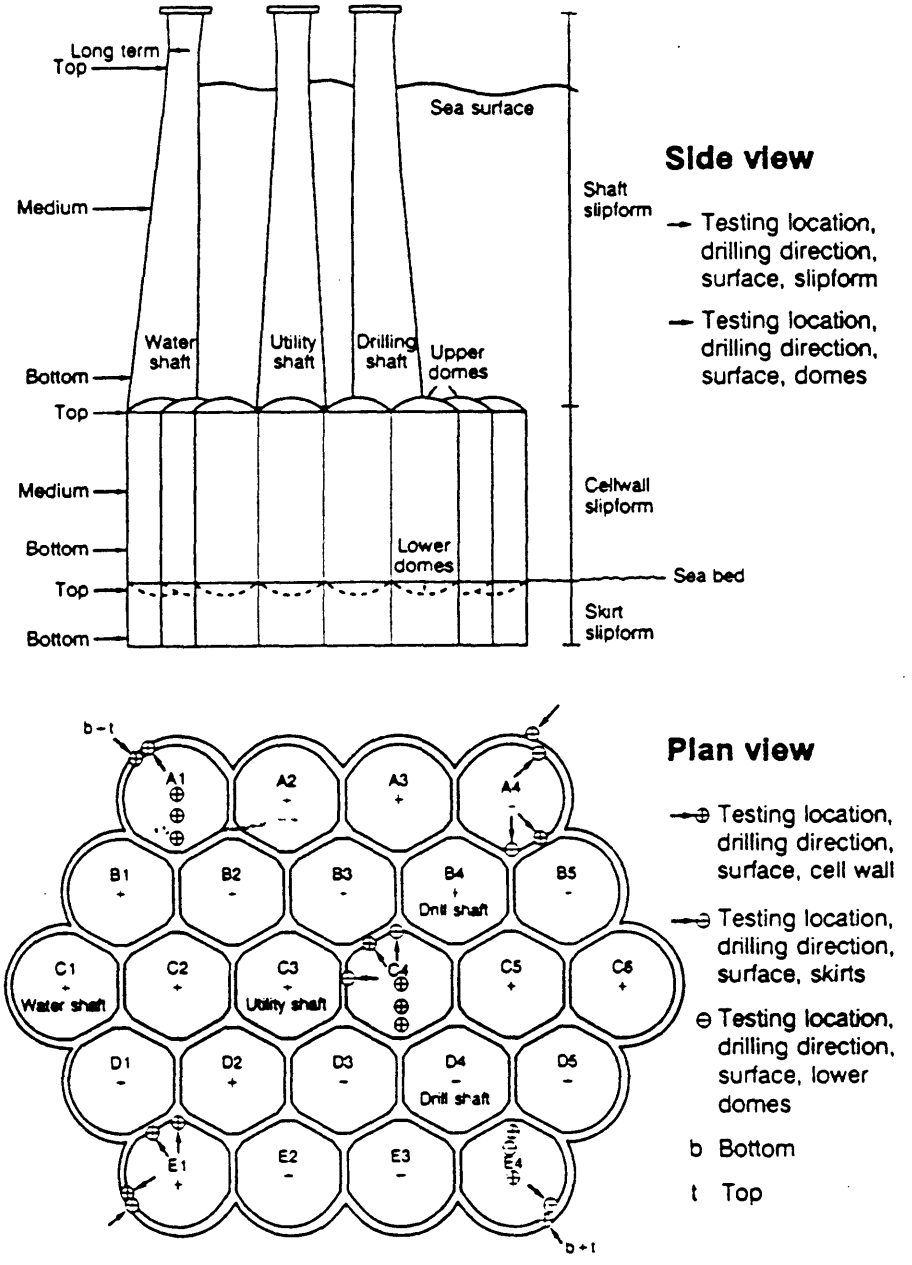

Figure 2.5 Locations of Testing Cores for Offshore Platforms
[*Haug and Jakobsen, 1992*]

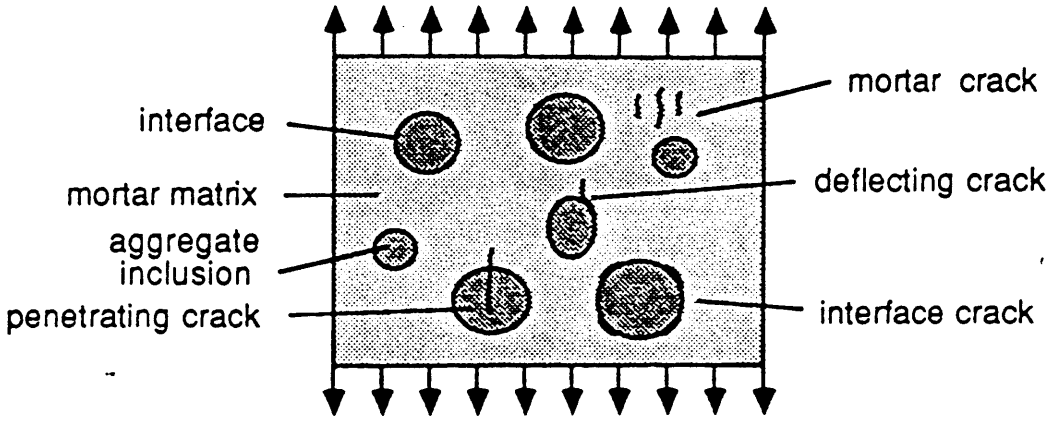

Figure 2.6 Types of Cracks Observed in Concrete
[*Lee, 1993*]

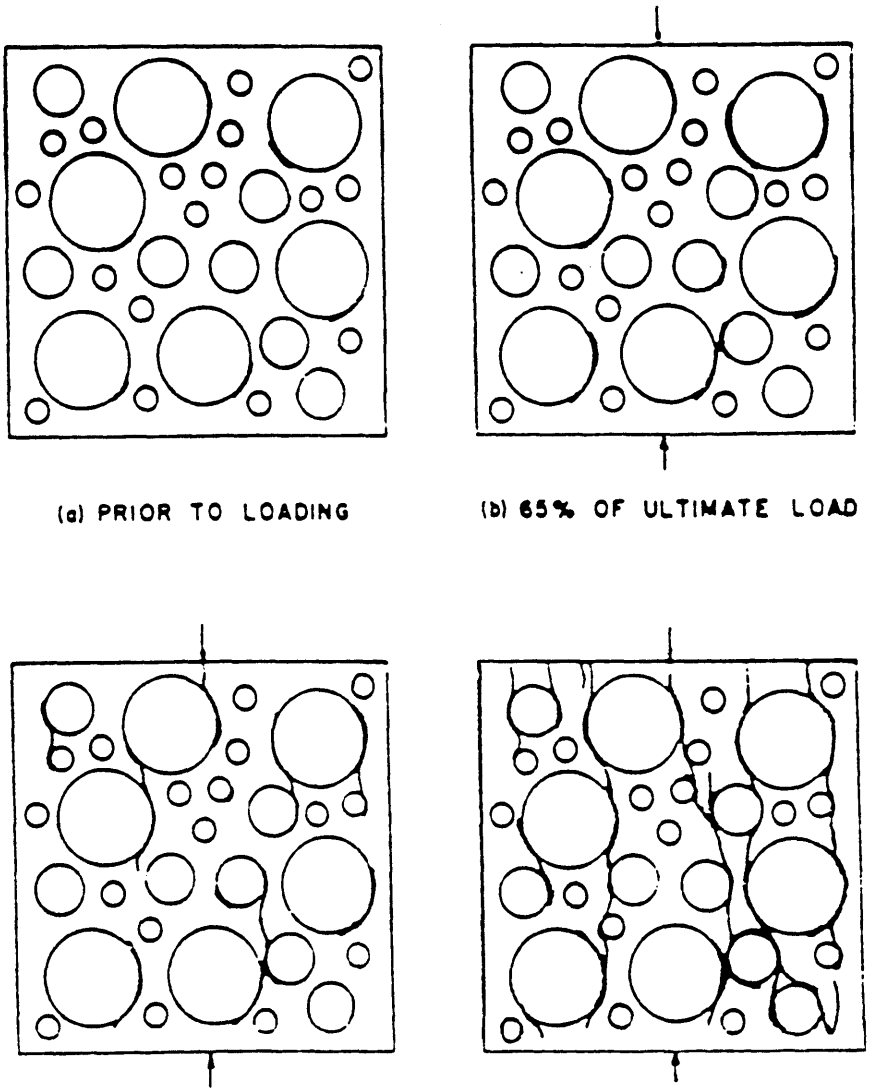

Figure 2.7 Progression of Microcracking in HSC
[*Liu et al., 1972*]

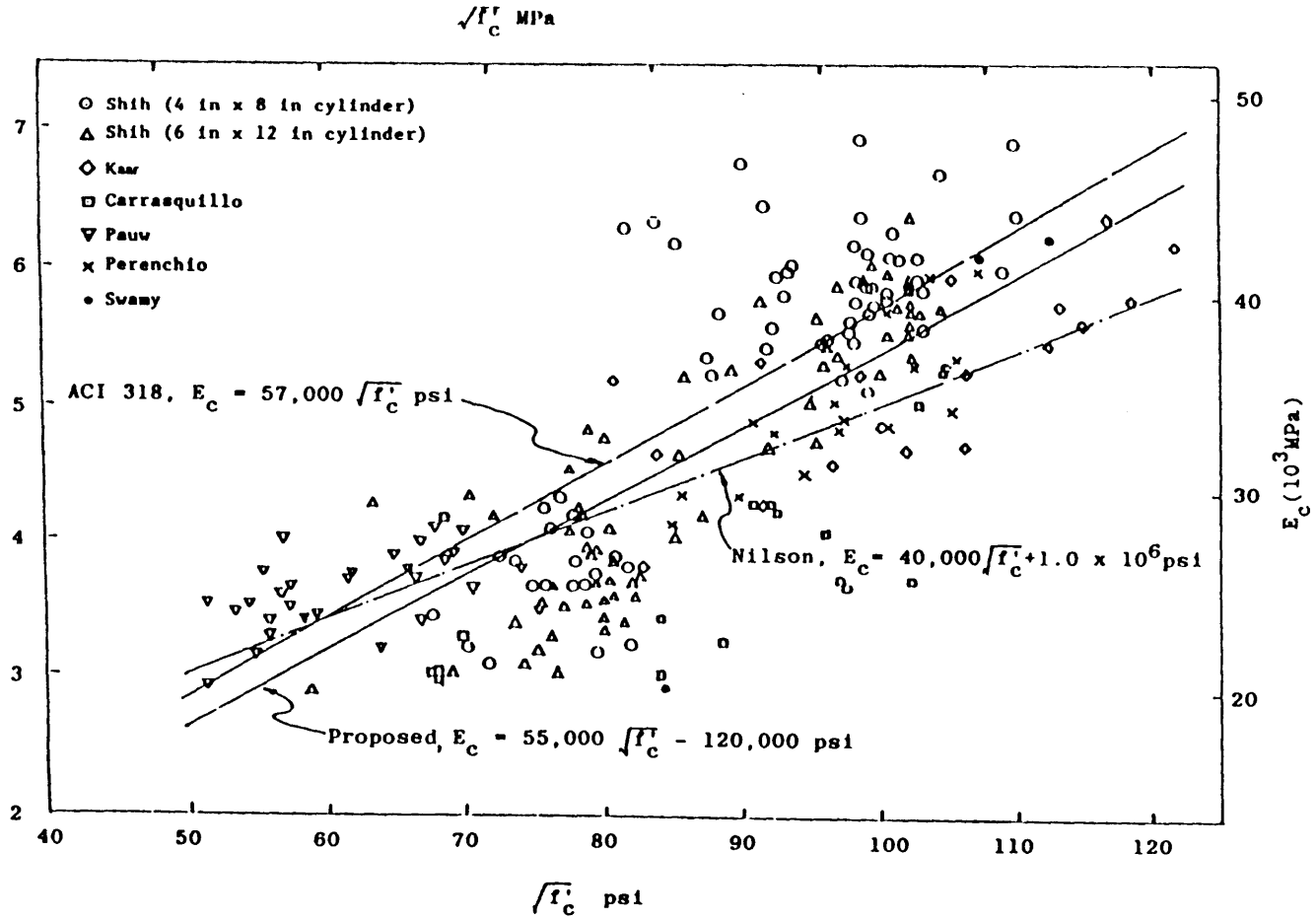

Figure 2.8 Modulus of Elasticity versus Concrete Strength
[*Shih et al., 1989*]

Chapter 3

Interface Fracture Mechanics

It has been shown by several researchers that the mechanical behavior of concrete is highly dependent on the properties of the interfacial region [*He and Hutchinson, 1989; Büyüköztürk and Lee, 1993; Goldman and Bentur, 1989*]. Interfaces, which represent discontinuities, are intrinsic to concrete and their structural performance is generally influenced by them [*Büyüköztürk and Lee, 1993*]. Load transfer between the phases of concrete depends on the degree of contact between the phases of concrete and the cohesive forces of the interface [*Lee and Büyüköztürk, 1995*]. The microstructure of these zones is higher in porosity and has larger pore sizes than the microstructure of the bulk paste. The porosity is highest near the aggregate and decreases with distance until it reaches the level of the paste. If a sufficient number of aggregates are present the interface zones may overlap and failure may occur at premature stress levels [*Snyder, 1992*]. In HSC incorporating silica fume this region is more compact and smaller which allows a more efficient transfer of stress from the paste to the aggregate [*Nilsen et al., 1992*]. The improved interface then leads to enhanced strength, stiffness and durability. However, as with most engineering materials, the improved strength comes at the expense of decreased ductility [*Lee and Büyüköztürk, 1995*]. By employing the two phase model of concrete suggested earlier in connection with fracture mechanics it is possible to characterize these interfacial regions and examine ways in which to improve them.

Some of this chapter is a summary of a similar chapter in the Ph.D. thesis of Lee [*1993*].

3.1 Bimaterial Elasticity

By investigating the behavior of a semi-infinite free crack lying along an interface between two homogeneous isotropic planes Dundurs developed the moduli mismatch parameters which govern interface crack fields in plane strain. The system studied is often referred to as a bimaterial. A bimaterial is defined as a composite of two homogeneous materials with continuity of traction and displacement across interfaces maintained. The parameters, known as Dundurs' parameters for the bimaterial shown in Figure 3.1, are given by:

$$\alpha = \frac{\overline{E}_1 - \overline{E}_2}{\overline{E}_1 + \overline{E}_2} \tag{3.1}$$

and

$$\beta = \frac{1}{2}\frac{\mu_1(1-2\nu_2) - \mu_2(1-2\nu_1)}{\mu_1(1-\nu_2) - \mu_2(1-\nu_1)} \tag{3.2}$$

where $\overline{E} = \frac{E}{(1-\nu^2)} = \frac{2\mu}{(1-\nu)}$ is the plain strain modulus and E, μ and ν are Young's modulus, shear modulus and Poisson's ratio with the subscripts referring to the two materials [*Dundurs, 1969*]. The parameter α describes the relative stiffness of the two materials. If material one is extremely stiff when compared to material two α becomes nearly equal to 1; if the values of stiffnesses are reversed α converges to -1. In most mortar-aggregate combinations β can be neglected, and only α need be considered [*Lee and Büyüköztürk, 1995*].

3.2 Crack Tip Fields

Consider the bimaterial of Figure 3.1 which contains a semi-infinite traction-free crack lying along the interface of the two materials. For plane

problems the normal and shear stresses of the singular filed acting on the interface a distance r ahead of the crack tip are given by:

$$\sigma_{22} + i\sigma_{12} = \frac{K_1 + iK_2}{\sqrt{2\pi r}} r^{i\varepsilon} \tag{3.3}$$

where $i \equiv \sqrt{-1}$, and the oscillation index is

$$\varepsilon = \frac{1}{2\pi} \ln\left(\frac{1-\beta}{1+\beta}\right) \tag{3.4}$$

The amplitude factors K_1 and K_2 depend linearly on the applied loads and the geometry of the specimen.

The interface fracture of a bimaterial can now be expressed in terms of two parameters: G, the energy release rate and ψ the phase angle. The energy release rate per unit length of crack extension along an interface is given by:

$$G = \frac{\left(\frac{1}{\bar{E}_1} + \frac{1}{\bar{E}_2}\right)}{2\cosh^2(\pi\varepsilon)}\left(K_1^2 + K_2^2\right) \tag{3.5}$$

where $\cosh^2(\pi\varepsilon)=1/(1-\beta^2)$ [*Büyüköztürk and Lee, 1993*]. The phase angle, which represents the contribution of shear to the opening of the interface crack, equals:

$$\Psi = \tan^{-1}\left(\frac{\mathrm{Im}\left(K\hat{L}^{i\varepsilon}\right)}{\mathrm{Re}\left(K\hat{L}^{i\varepsilon}\right)}\right) \tag{3.6}$$

with $\hat{L}$ defined as the reference length. The choice of $\hat{L}$ is somewhat arbitrary. In order to measure the proportion of Mode I to Mode II in the vicinity of the crack it is necessary to specify a length because the ratio of the shear traction to

normal traction varies slowly with the distance to the tip when β is assumed not equal to zero [*Lee, 1993*]. Modes of stressing , defined I, II, and III are depicted in Figure 3.2. Note that if Ψ is equal to zero, the bimaterial is stressed in pure Mode I and when $\Psi = 90°$ pure Mode II cracking occurs [*Lee and Büyüköztürk, 1995*].

3.3 Interfacial Fracture Toughness

In elastically homogeneous brittle solids, cracks propagate such that Mode I conditions are maintained at the crack tip. In concrete this does not occur because in the region of the interface the relative fracture toughnesses of the interface and aggregate play a role [*Büyüköztürk and Lee, 1993*]. Therefore the fracture mode of an interface of dissimilar materials is usually mixed. Symmetry is lost even when the geometry and loading conditions are symmetric with respect to the crack plane. Additionally, the interface is usually more brittle than either of the materials being connected and an interface crack tends to stay in the interface once propagation has begun.

For an interfacial crack, K can be defined by

$$KL^{i\varepsilon} = YT\sqrt{L}e^{i\psi} \tag{3.7}$$

where T is the applied traction loading, L is a length used to describe the crack length or the uncracked ligament length, and Y is a dimensionless real positive number. ψ is the phase angle of $KL^{i\varepsilon}$ and is often referred to as the phase angle of the stress intensity factor, or just the phase angle. Y and $\hat{\Psi}$ depend on the ratios of various applied loads and lengths and for a traction prescribed problem on α and β.

Knowing the peak value of T at the onset of cracking it is possible to calculate the interface fracture toughness. The value obtained, however, is also a

function of ψ so it becomes necessary to characterize the interface through a toughness curve of K versus ψ. Generally K is known to increase with an increase in phase angle. By employing equation 3.5, the current practice is to use a graph of G_c versus $\hat{\Psi}$. With the toughness curve it is important to state $\hat{L}$ because it effects the value of $\hat{\Psi}$ as shown by equation 3.6. The freedom of choice in $\hat{L}$ arises due to a simple transformation rule from $\hat{L}$ to $\hat{\Psi}$. Letting ψ_1 be associated with L_1 and ψ_2 with L_2, it is possible to show

$$\Psi_2 = \Psi_1 + \varepsilon \ln\left(\frac{L_2}{L_1}\right) \tag{3.8}$$

Therefore the transformation from one to the other can easily be made [*Rice, 1988*].

As will be shown below it is possible to transform toughness data. Let $\hat{L}$ be a length that characterizes the size of the fracture process zone, or the size of the fracture process zone at fracture and let $\hat{\Psi}$ be defined by equation 3.6. It is assumed that small scale yielding or a small scale fracture process zone exists therefore $\hat{L}$ lies within the dominance of the K field. The criteria for interface cracking can then be given by

$$G = \Gamma_i\left(\hat{\Psi}, \hat{L}\right) \tag{3.9}$$

$\Gamma_i\left(\hat{\Psi}, \hat{L}\right)$ is the critical value of energy release rate required for a crack to advance in the interface in the presence of a combination of traction with the relative proportion measured by $\hat{\Psi}$.

3.4 Crack Propagation in Bimaterials

A crack impinging an interface can take two courses upon reaching the aggregate: penetration or deflection. Examples of each of these scenarios developed by He and Hutchinson [*1989*], will be examined in this section. The first example, denoted A type, has a crack approaching an interface at a right angle which either penetrates material 1 or is deflected 90° into the interface. The second situation, B type, is more general; the crack can hit the interface at a variable angle and the competition between penetration and deflection is examined [*He and Hutchinson, 1989*]. It is possible to use an energy based criteria based on energy release rate to study the competition between crack paths in the interfacial region [*Büyüköztürk and Lee, 1993*].

3.4.1 Crack Perpendicular to Interface

By using the examples developed by He and Hutchinson it is possible to depict the possible cracking scenarios when a crack approaches an aggregate at a right angle to the interface. Consider a semi-infinite reference crack with a = 0. A symmetric loading with respect to the reference crack is applied and the traction ahead of the crack is

$$\sigma_{xx}(0,y) = k_1(2\pi y)^{-\lambda} \tag{3.10}$$

where λ is real and depends on α and β according to

$$\cos\lambda\,\pi = \frac{2(\beta-\alpha)}{1+\alpha}\left(1-\lambda^{2}\right)+\frac{\alpha+\beta^{2}}{1-\beta^{2}} \tag{3.11}$$

λ as a function of α for β=0 is shown in Figure 3.3 and k_1 is proportional to the applied load. The crack is then assumed to advance in one of three possible ways seen in Figure 3.4 a. The first possibility is penetration and the other two

λ as a function of α for β=0 is shown in Figure 3.3 and k_1 is proportional to the applied load. The crack is then assumed to advance in one of three possible ways seen in Figure 3.4 a. The first possibility is penetration and the other two possibilities are deflection. If deflection occurs the crack could either propagate as one crack or it could be deflected in both directions [*He and Hutchinson, 1989*].

When the crack is advancing the stress state at the tip of the crack is in pure Mode I and the ratio of penetration to deflection is given by

$$\frac{G_d}{G_p} = \left[\frac{1-\beta^2}{1-\alpha}\right]\frac{\left[|d|^2 + |e|^2 + 2\,\mathrm{Re}(de)\right]}{c^2} \tag{3.12}$$

where c is dimensionless and d and e are dimensionless complex valued functions of α and β.

It is now possible to asses the tendency of the crack to be deflected by the interface or pass through it [*He and Hutchinson, 1989*]. In a bimaterial a crack will likely be deflected if

$$\frac{\Gamma_i}{\Gamma_2} < \frac{G_d}{G_p^{\max}} \tag{3.13}$$

with Γ_i is the toughness of the interface as a function of the loading phase angle, Γ_2 is the Mode I toughness of material 2, G_d is the energy release rate of a deflected crack and $G_p^{\max}$ is the maximum energy release rate of the penetrated crack [*Büyüköztürk and Lee, 1993*]. Conversely the crack will penetrate the aggregate if the inequality is reversed. Typically with deflection the crack propagates to only

one side because the ratio of $\frac{G_d}{G_p^{\max}}$ is larger [*He and Hutchinson, 1989*]. $\frac{G_d}{G_p^{\max}}$ is plotted as a function of α in Figure 3.5. It is interesting to note on this figure that as the absolute value of the elastic mismatch parameter, α increases the crack becomes more likely to deflect at the interface.

For α not too different from zero the critical ratio is approximately ¼ and when $\alpha = ½$ the ratio becomes nearly ½ [*He and Hutchinson, 1989*]. These values are found by the following procedure. First, the angle of crack propagation is defined as γ, and is shown in Figure 3.6. Considering only Mode I cracking for an equation derived by Hussain et al. [*1974*] the energy release rate for penetration, $\gamma = 0°$, is found to dissipate approximately four times more energy than deflection, $\gamma = 90°$. For $\gamma = 0°$ $G(0) = G_p = \frac{K_I^2}{E}$, while for $\gamma = \pi/2$, $G\left(\frac{\pi}{2}\right) = G_d = 0.256\frac{K_I^2}{E}$. The equations were developed for an elastic homogeneous material under Mode I cracking, however they can be used to characterize the interface between two dissimilar materials having similar elastic properties [*Oumera, 1991*].

3.4.2 Propagation of an Oblique Crack

The competition between penetration and deflection for an oblique crack is not unlike the previous condition. The possible cracking scenarios are depicted in Figure 3.4 b. However, now the angle of penetration, ω_1, into material 1 must be determined. The crack's path will be that which maximizes the energy release rate [*He and Hutchinson, 1989*].

The energy release rate of the penetrating crack is given by

$$G_p = \frac{1-\nu_1}{2\mu_1}|c|^2 k_1^2 a^{1-2\lambda_1} \tag{3.14}$$

The maximum energy release rate with respect to ω_1, for a fixed a is $G_p^{\max}$, therefore the ratio $\frac{G_d}{G_p^{\max}}$ can be found. Results of this ratio as a function of α are given in Figure 3.7 for $\omega_2 = 45°$. In considering this figure a few interesting conclusions can be drawn. When material 1 is stiff compared to material 2, $\alpha > 0$, the maximum energy release rate of a penetrating crack is only slightly larger than the deflected crack. When $\alpha > 0.5$ the maximum energy release rate of a penetrating crack is the same as for $\omega_2 = 0°$. That is, the critical penetrating crack coincides with the deflecting crack. When material 1 is more compliant the energy release rate of penetration exceeds that of deflection [*He and Hutchinson, 1989*].

3.5 Applications of Fracture to this Work

The purpose of this work is to expand the knowledge acquired by other interfacial fracture mechanics studies done at MIT to apply the concepts to true concrete. Through characterization of the interface the overall behavior of concrete can be enhanced. In this work fracture mechanics is employed to investigate the ductility of concrete, because at present it is the main negative limiting the use of HSC.

Interface fracture mechanics is useful in the characterization of small samples with a few aggregate inclusions, however in addition to describing the interfacial properties it is necessary to quantify the ductility of the concrete as a whole. The material behavior can be described by the stress-crack tip opening displacement along the crack face, also known as the tension softening curve. The shape of this curve is representative of concrete's ductility and contains information about the tensile strength and the fracture energy, which is calculated as the area under the curve. From this curve one can define the characteristic length as

$$l_{ch} = \frac{EG_F}{f_t^2} \tag{3.15}$$

where E is the modulus of elasticity, G_F is the fracture energy and f_t is the tensile strength of concrete. This measure has been shown to be particularly suitable to describe the ductility of concrete [*Hilsdorf and Brameshuber, 1991; Tasdemir et al., 1996; Zhou et al., 1995*].

However, because the fracture toughness, K_{Ic}, is easier to determine through testing than G_F it is necessary to manipulate equation 3.19 by using

$$K_{Ic}^2 = EG_F \tag{3.16}$$

to obtain

$$l_{ch} = \frac{K_{Ic}^2}{f_t^2} \tag{3.17}$$

With this equation to quantify the ductility of the global materials, and the knowledge obtained on interface fracture from the smaller models it should be possible to characterize, and therefore optimize, the interfacial properties of HSC.

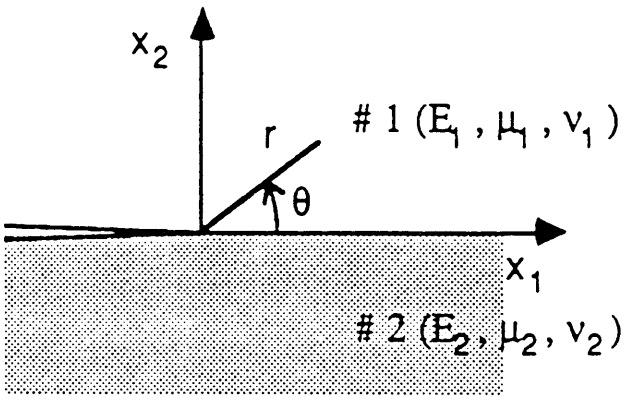

Figure 3.1 Example of a Bimaterial
[*Hutchinson and Suo, 1992*]

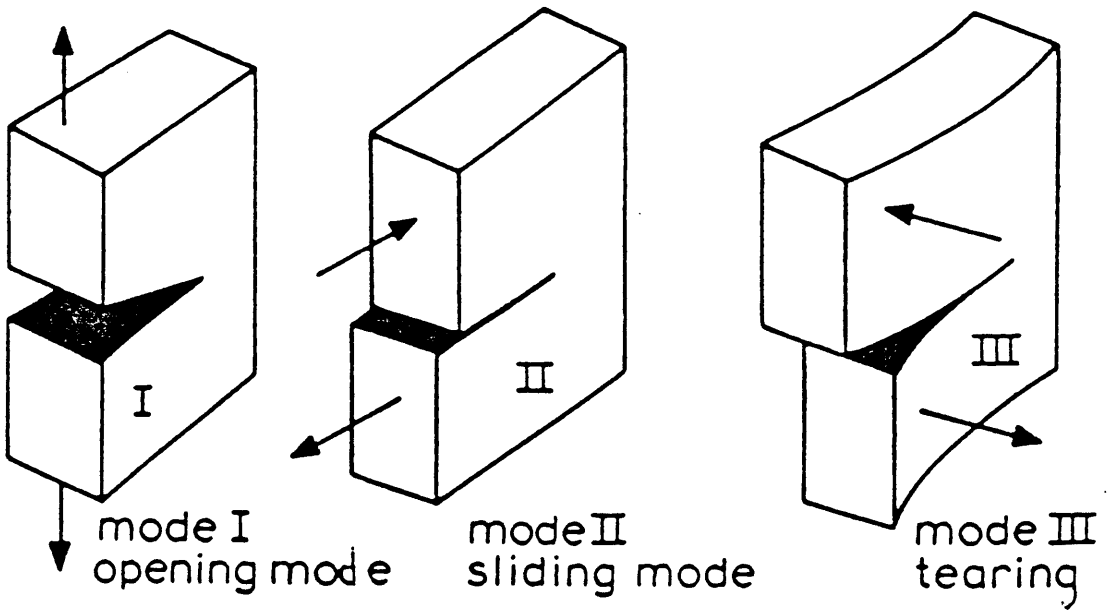

Figure 3.2 Cracking Modes
[*Broek, 1978*]

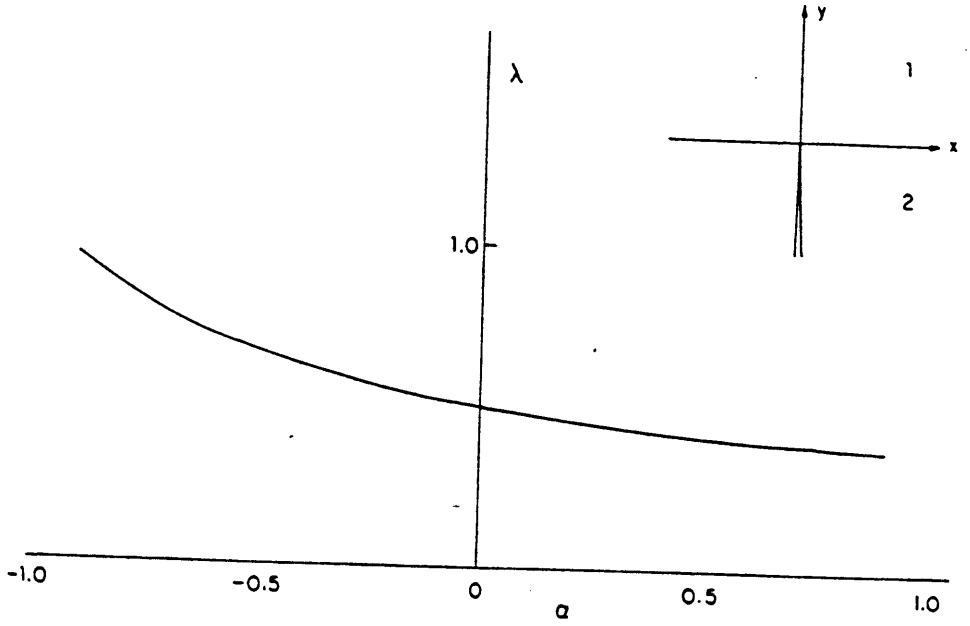

Figure 3.3 λ as a function of α for β=0
[*He and Hutchinson, 1989*]

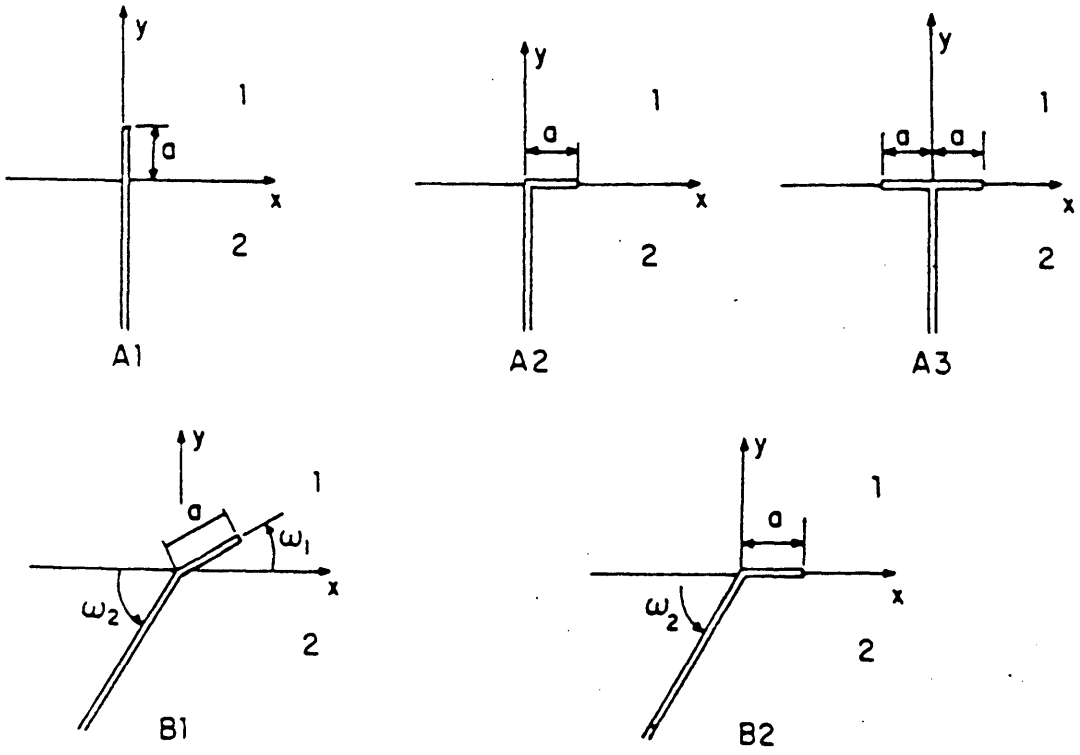

Figure 3.4 Possible Crack Paths at Interface of Bimaterial
[*He and Hutchinson, 1989*]

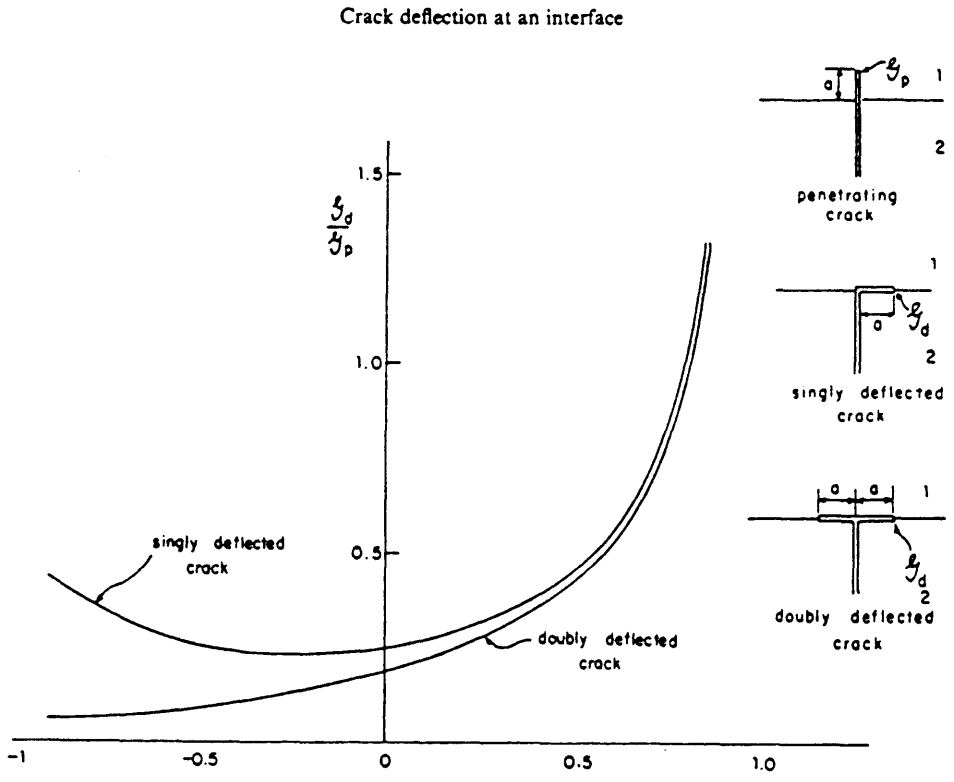

Figure 3.5 $\frac{G_d}{G_p^{\max}}$ is plotted as a function of α

[*He and Hutchinson, 1989*]

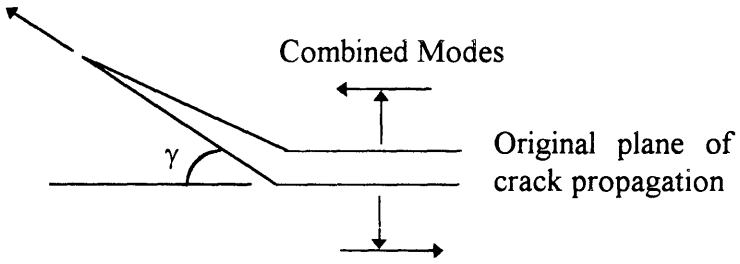

Figure 3.6 Crack Propagation under Combined Mode I and II
[*Oumera, 1991*]

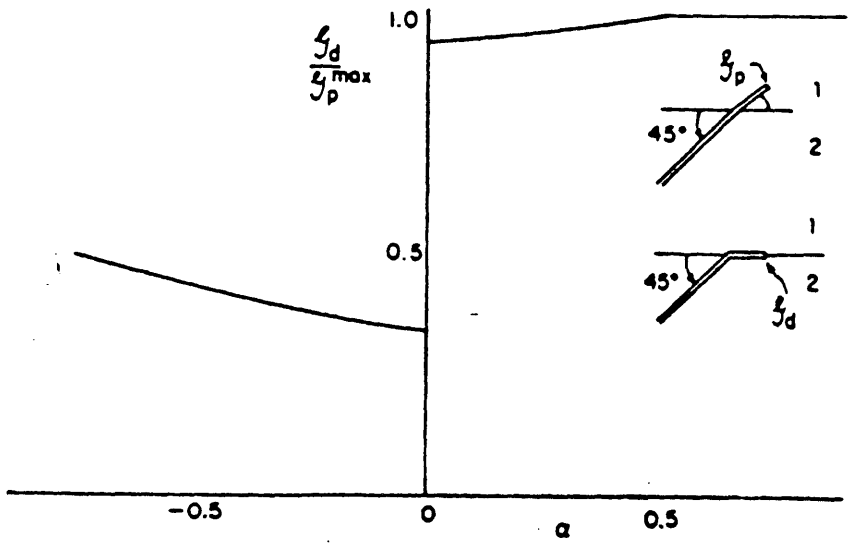

Figure 3.7 Ratio of ratio of energy release rate of deflected crack to maximum energy release rate of penetrating crack at same a for asymptotic when $a = 0$ (β=0) [*He and Hutchinson, 1989*]

Chapter 4

Previous MIT Research

As mentioned in the introduction, this work is a continuation of previous works completed at MIT on related topics. This work will follow those in that the characteristic length of real concrete will be examined in attempt to correlate the crack initiation and progression of cracks from the two phase models to real concrete. The conclusions drawn from previous works will be discussed within this chapter as well as their anticipated practicality for this work. In chronological order the works are:

"Crack propagation in the Aggregate-Mortar Interface Regions of Concrete" by Oumera [1991],

"Interface Fracture in High Strength Concrete" by Lee [*1993*],

"Fracture Behavior of High Strength Concrete Composite" by Kitsutaka et al. [*1993*],

"Interface Fracture of High Strength Concrete: Size Effect and Aggregate Roughness" by Trende [*1995*] and

"Improving the Ductility of High Performance Concrete Through Mortar-Aggregate Interfaces" by Büyüköztürk and Hearing [*1996*].

4.1 Oumera [*1991*]

The objective of Oumera's work was to approximate the interfacial fracture toughness of the aggregate-mortar interface of NSC and HSC using a model consisting of a round aggregate embedded in a mortar plate. Oumera made two basic assumptions: first that concrete can be modeled as a two phase material of mortar and aggregate, and second that concrete can be modeled as a circular aggregate embedded in mortar. The samples

tested, shown in Figure 4.1, were 4" in height x 3" in length x 1" in width with a 1.5" diameter aggregate inclusion centrally located. The two types of aggregates were chosen to represent the two possible cracking scenarios. Granite which is a strong aggregate was chosen to deflect the impinging crack and marble was chosen so that the crack would penetrate the aggregate. Three mortar strengths were used for each aggregate type in order to asses the effect of silica fume on the interface.

To understand the most important conclusions from the work it is first necessary to consider Figure 4.2. The angle of hit, γ, is defined as the angle between the crack path and the tangent to the inclusion at the point of contact. When the aggregate inclusion is granite, Oumera found that the crack was deflected in every case regardless of the value of γ. In the specimens containing marble both penetration and deflection were observed. For various mortar strengths the critical angles differ. For medium strength mortar containing marble γ_{cr} is bounded by 32° and 60°. Below 32° the crack was found to deflect in every case, while it penetrated in every case above 60°. Similarly, the bounds for high strength mortar with marble are 54° and 74°.

By examining specific cases in which similar fracture paths were evident some conclusions were drawn about the effect of mortar strength and aggregate type. Figure 4.3 depicts cracking scenarios for the three different mortar strengths. Despite the increase in mortar strength of 132% the failure load only increases around 20%. Therefore, one can conclude that the contribution of the mortar, when penetration occurs, is small. On the other hand, when the angle of hit is such that deflection occurs with the weak aggregate, as shown in Figure 4.4, the mortar significantly affects the behavior of the composite. With the same percentage increase in mortar strength (132%) a corresponding increase of 47% in failure load is achieved. Oumera attributes 13% of this increase to the contribution of the mortar an the other 34% directly to the improved interface. Leading one to safely conclude that the interface of HSC is much stronger than NSC.

By examining the data which resulted in Figure 4.5, a discussion about the granite inclusions can be undertaken. In this case a 46% increase in the compressive strength of the mortar results in a 14% increase in the failure load. 10% of this improvement is attributed to the improved strength of the mortar and 4% is from the improved interface. In contrasting Figures 4.4 and 4.5 it is found that the increase in composite strength from medium to high strength mortar is smaller than was found for the marble inclusions. Oumera attributes this behavior to marble, which is close in composition to limestone, because it is believed to react chemically with mortar thereby strengthening the interface.

In conclusion and very briefly, granite deflects the crack in every case and the weak aggregate, marble, is deflected only when there is a small angle of incidence. The aggregates used in this study are granite and limestone. It is suspected that granite will in fact deflect the crack in real concrete and limestone, being similar to marble will be penetrated in most, if not all cases.

4.2 Lee [1993]

The objective of the work completed by Lee for his Ph. D. thesis was threefold. One objective was to study and characterize the fracture behavior of the mortar-aggregate interface in HSC with silica fume through novel interface fracture models. Secondly, an experimental and numerical investigation of cracking scenarios in interfacial regions of two-phase composite models was undertaken.

A composite model was developed to study the competition between crack propagation and deflection in interfacial regions. The model, shown in Figure 4.6, is a beam of mortar and an inclusion of one of two aggregate types. The two aggregates chosen were limestone and granite, which are the same types used in this research. The loading configuration was altered so that cracking ranged from Mode I to Mode II. The angle of inclination of the aggregate, γ was also varied to investigate the tendency of crack propagation to deflect or penetrate. The angles used were 90°, 60°, and 30° with respect to the impinging crack.

Phase I of Lee's work examined crack propagation scenarios in interfacial regions. Under three point bending, the granite inclusions were found to deflect the crack in nearly every case, that is interfacial propagation was found. Under four point bending both crack paths were found for granite. Penetration was found only in the highest strength limestone mixture with $\gamma = 90°$. Generally, cracking loads of a mortar/limestone system were lower than the granite systems.

Phase II consisted of numerical analysis of the model by a finite element method based on interface fracture mechanics concepts. The only test specimen examined in this phase was the case with γ equal to 90°. As an example the weakest mortar/granite system under four point bending was discussed in his thesis. In this system the phase angle of the deflected crack was found to be 37°. The Mode I fracture energy of granite, Γ_g, is 17.5 J/m^2 and the interface fracture energy, $\Gamma_i(37°)$, is approximately 5.0 J/m^2. The ratio of $G_d/G_p^{\max}$, from He and Hutchinson is 0.37. Therefore, the ratio $\Gamma_i(37°)/\Gamma_g = 5.0/17.5 = 0.28$. Since this is less than 0.37 deflection of the impinging crack is predicted by equation 3.13. Similar calculations were carried out for 14 other mixtures and the failure paths were compared to those observed in the experiments. For Phase III it was observed that 10 of the 14 specimens failed as predicted by numerical analysis, and in general good correlation between the two models was found [*Lee, 1993*].

4.3 Kitsutaka et al. [*1993*]

Kitsutaka et al. modeled concrete as a two phase composite and studied transgranular cracking from an analytical and experimental standpoint. The objective was to investigate the influence of aggregate on the fracture behavior of two-phase HSC. For the experimental portion concrete beams with circular inclusions were used and the load-displacement curves were studied to asses fracture behavior. The numerical analysis method using cohesive force models was suggested to predict the load-displacement behavior of HSC with transgranular cracking.

Parameters studied in this investigation were the strengths of the aggregate and the

mortar matrix, the volume fraction, and the arrangement of aggregate. Load line displacement curves were used to evaluate the fracture behavior of the mixtures. Limestone and granite were chosen as the weak and strong aggregates respectively. It was observed that the crack path of all the low strength mortar specimens was deflection. Penetration and deflection was observed in the high strength mortar. It is interesting to note that in the left side of Figure 4.7 that the load line displacement curves for the low strength mortar systems are not particularly sensitive to aggregate type while on the right side the curves are affected.

With Type 3 specimens and the high strength mortar the peak load is about 40 percent greater than mortar alone. However, the post-peak load is steep, which represents brittle behavior. Kitsutaka et al. [*1993*] attribute this to the larger volume fraction inhibiting the development of a fracture process zone in the mortar matrix which reduces the total energy absorption during cracking. To understand this and the other factors a numerical modeling method using cohesive force approach for transgranular cracking was proposed. Results from the model developed will be compared to laboratory data obtained in Chapter 7.

4.4 Trende [*1995*]

The main objective relevant to this work was the evaluation of the influence of aggregate roughness on the interface fracture parameters. Two aggregates were used with a consistent 28-day 83 MPa mortar. Both aggregates were chosen to deflect the crack so that the influence of the roughness would be more evident. For Chelmsford and Mason granite four and three surface roughnesses, respectively, were used. The data demonstrates an increasing fracture toughness for increased roughness, with the exception of the smooth surface. The roughest and smoothest surfaces for the Chelmsford granite have critical stress intensity factors that are on the same order. Typically one would expect an increase in interface fracture toughness with an increase in surface roughness, however in this case, according to Trende, the increased porosity decreases the total bonding area.

To quantify his results from a ductility standpoint, it is necessary to employ equation 3.17. Knowing that the tensile strength is increased only marginally with time due to roughness [*Mehta, 1986*] and that K_{Ic} increases appreciably [*Trende, 1995*], one can qualitatively conclude that the characteristic length will increase with an increase in surface roughness.

Also of note, among Trende's recommendations for future work is the objective of this work, he suggests: "Investigate the real concrete behavior with altered interface characteristics, correlate the results with those from composite model studies, and make recommendations for the design of high performance concrete" [*1995*].

4.5 Büyüköztürk and Hearing [1996]

The work of Büyüköztürk and Hearing [*1996*] is similar to that of Kitsutaka et al. in that an analytical model to study crack propagation was developed. However, Büyüköztürk and Hearing's work examined crack propagation through the interface rather than transgranular cracking. Granite was used in the laboratory specimens because it has shown the tendency to deflect an impinging crack. In fact, in all of the specimens interface fracture was observed. Interface properties were altered by varying the surface roughness of the aggregates and the strength of the mortar. Failure loads were found to increase with increased roughness and mortar strength. The stress-strain curves shown in Figure 4.8, demonstrate that the NSC is more ductile than both HSC mixtures and that the rougher aggregate leads to a more ductile HSC.

Results of the analytical model were shown to compare favorably to the laboratory tests. The relative post peak ductility was decreased with high strength mortar and increased with surface roughness. It was concluded that the fracture model can be used to study the influence of fracture parameters on the behavior of the composite. Possible future work mentioned include the extension of his fracture modeling techniques to the global material behavior of real concrete. This model's predictions will be compared to data obtained in the laboratory in Chapter 7.

4.6 Relation to This Work

Because all of the previous work entailed the modeling of concrete as a two phase composite, there is a need for research on true concrete specimens. The applicability of the conclusions drawn from the simple models are not yet known to extend to real concrete. The most obvious conclusion predicted from the simple models which should be found to apply to the failure of true concrete is that the weak aggregate, limestone, usually fails to deflect the crack while granite concretes fail interfacially. These crack paths will result in a planar failure path for limestone and a tortuous path for granite. It is suspected that the longer crack path will result in a larger characteristic length since greater energy consumption is expected.

In order to predict the failure path based on material properties it is necessary to solve the range of phase angles from

$$\Gamma_i(\hat{\psi}) < \left(\frac{G_d}{G_p^{msc}}\right)\Gamma_1 \tag{4.1}$$

The results of solutions for $G_d/G_p^{\max}$ for semi-infinite crack planes with respect to elastic mismatch parameters [*He and Hutchinson, 1989*] are applied with results from previous work in the interfacial fracture energy [*Büyüköztürk and Lee, 1993*] to compute the range of phase angles for the different material combinations tested in this work. The granite specimens were calculated to have a high tendency to deflect the crack. For penetration a phase angles greater than 78° for NSC and 75° for HSC is required. This supports the trend found in the laboratory where it was observed that penetration rarely occurred in granite mixes. Conversely, the limestone mixes were found to have a smaller phase angle range which represents a higher tendency for transgranular failure. As with granite, this trend was observed in the laboratory for both NSC and HSC. Therefore, the model developed by Kitsutaka et al. [*1993*] is most applicable to limestone concretes while the model of Büyüköztürk and Hearing [*1996*] is useful for granite concretes. Their predictions are compared to the data obtained in this testing series and are shown later in

Table 6.1. Also by studying equation 4.1, one can theoretically maximize ductility by using a strong aggregate with a low interface to aggregate fracture toughness ratio.

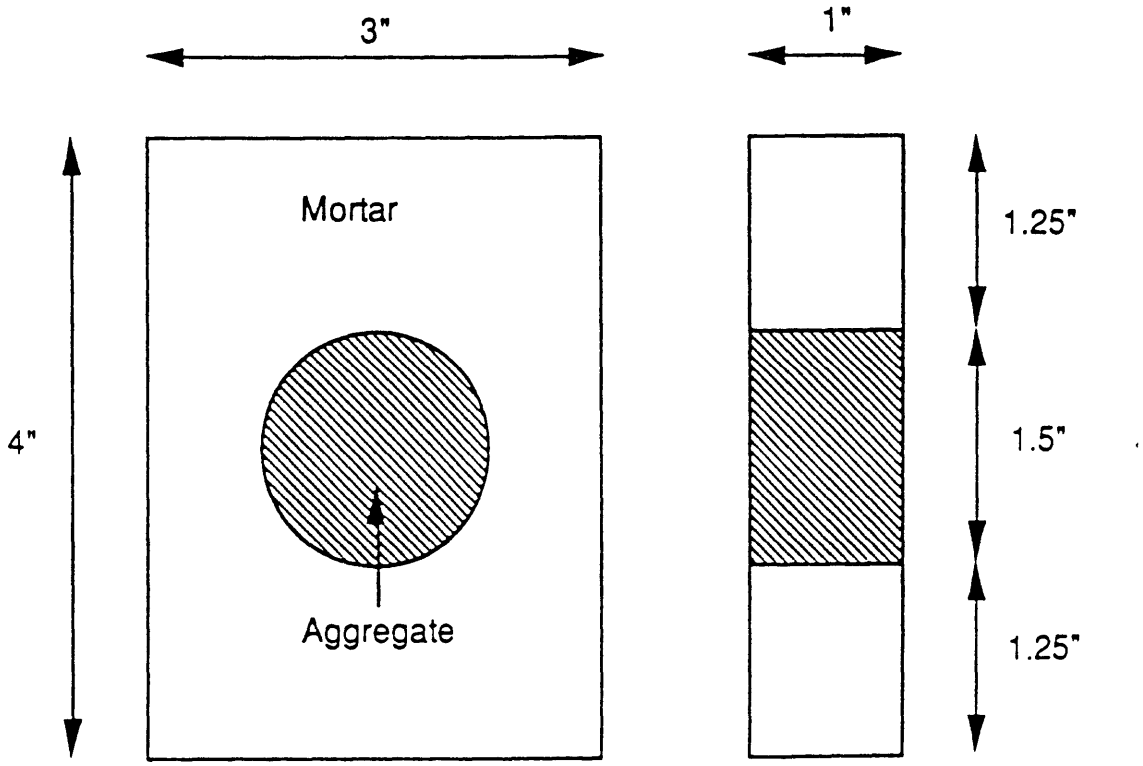

Figure 4.1 Testing Specimens used by Oumera

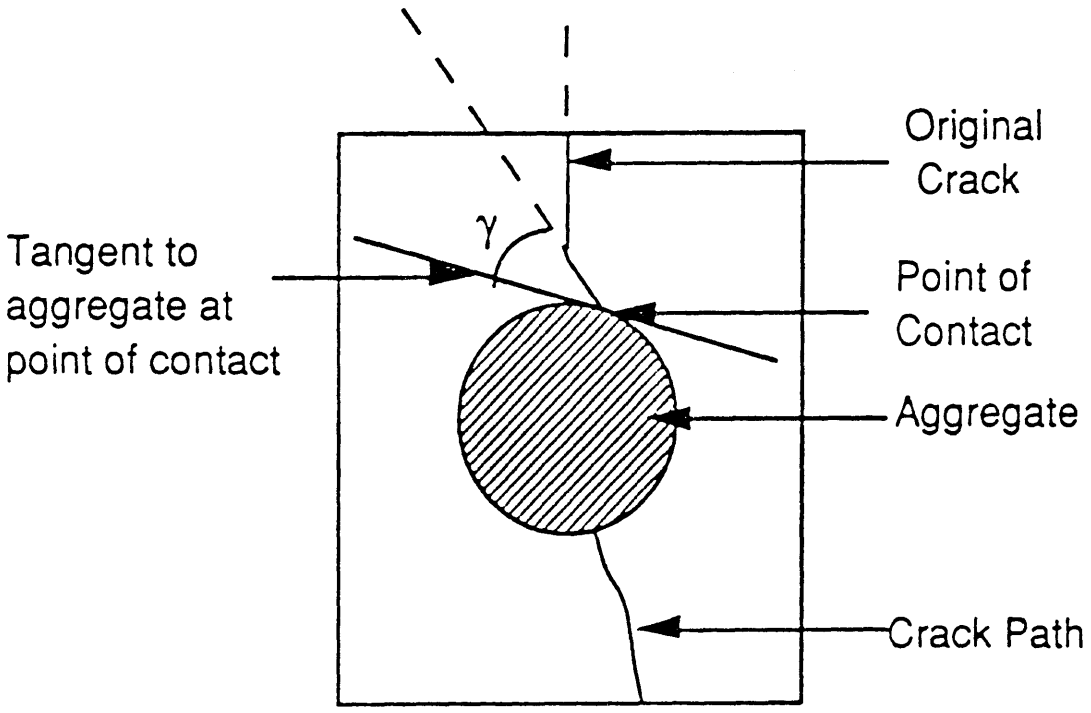

Figure 4.2 Angle of Incidence of Crack Propagation at the Interface
[*Oumera, 1991*]

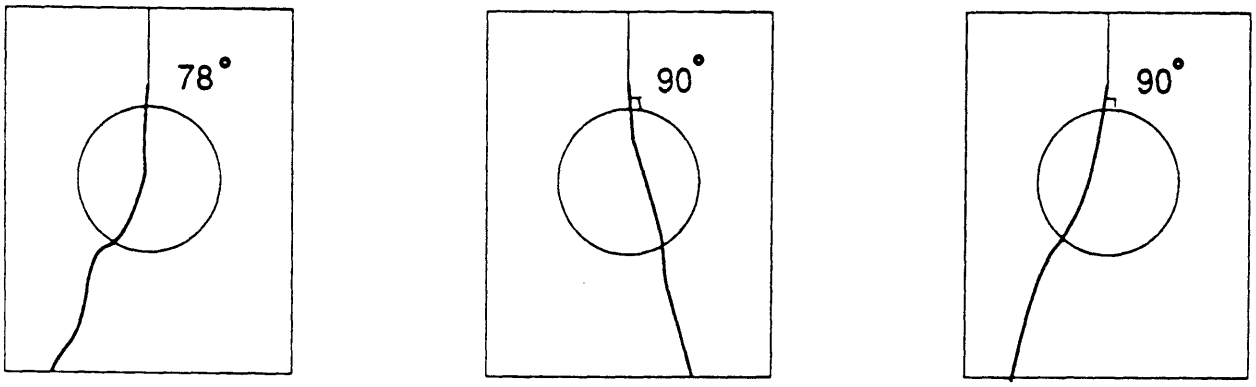

Figure 4.3 Failure Loads for Different Mortar Strengths and Marble Inclusions for Penetration
[*Oumera, 1991*]

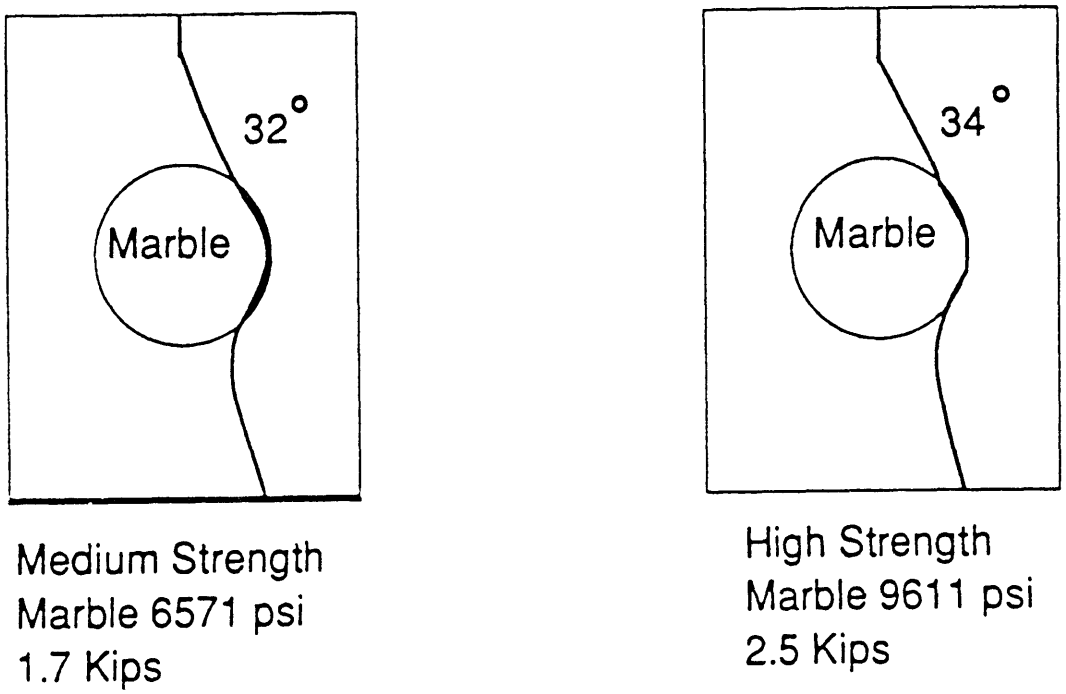

Figure 4.4 Failure Loads for Different Mortar Strengths and Marble Inclusions for Deflection
[*Oumera, 1991*]

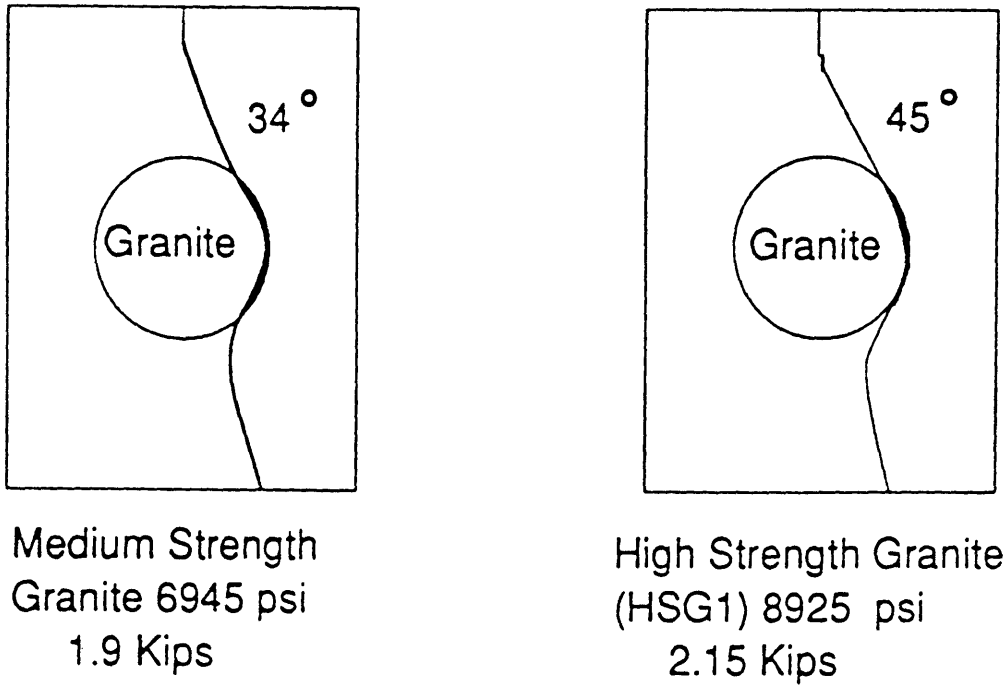

Figure 4.5 Failure Loads for Different Mortar Strengths and Granite Inclusions [*Oumera, 1991*]

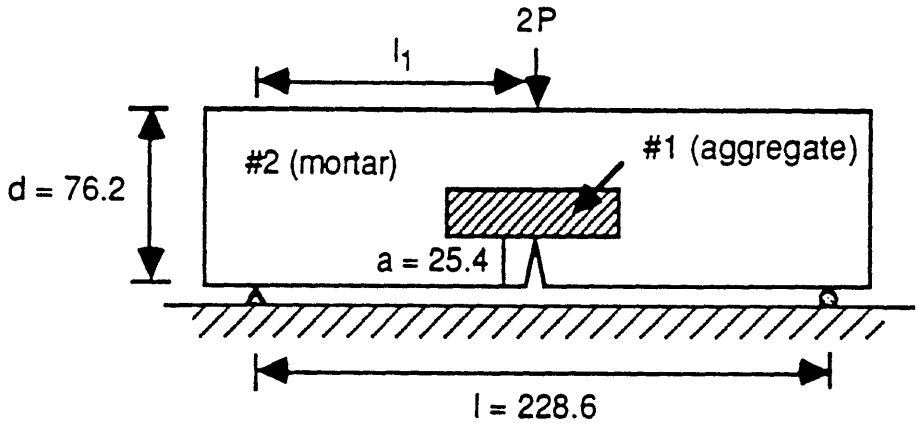

Figure 4.6 Testing Specimens used by Lee
[*Lee, 1991*]

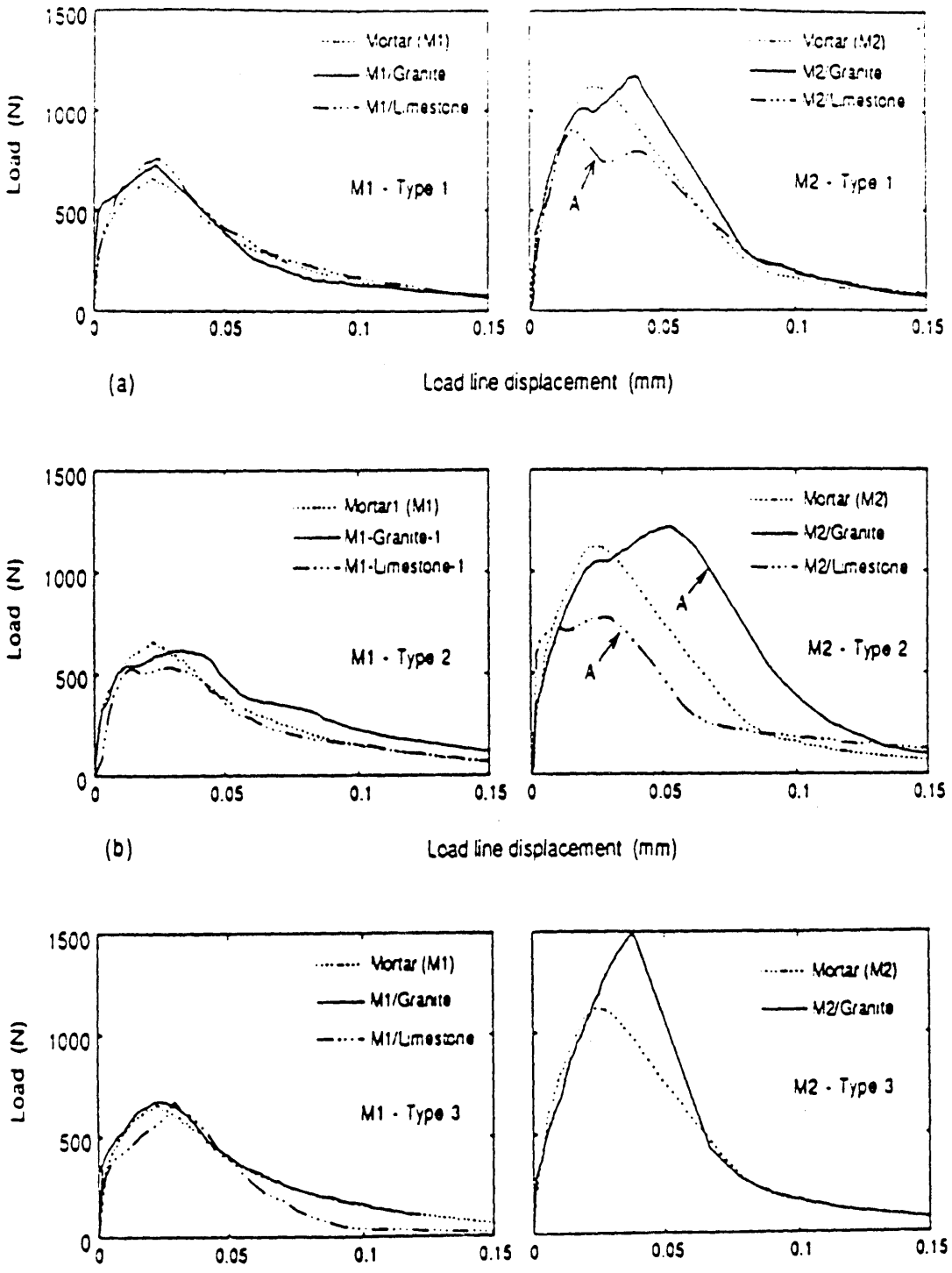

Figure 4.7 Load Line Displacement Curves
[*Kitsutaka et al, 1993*]

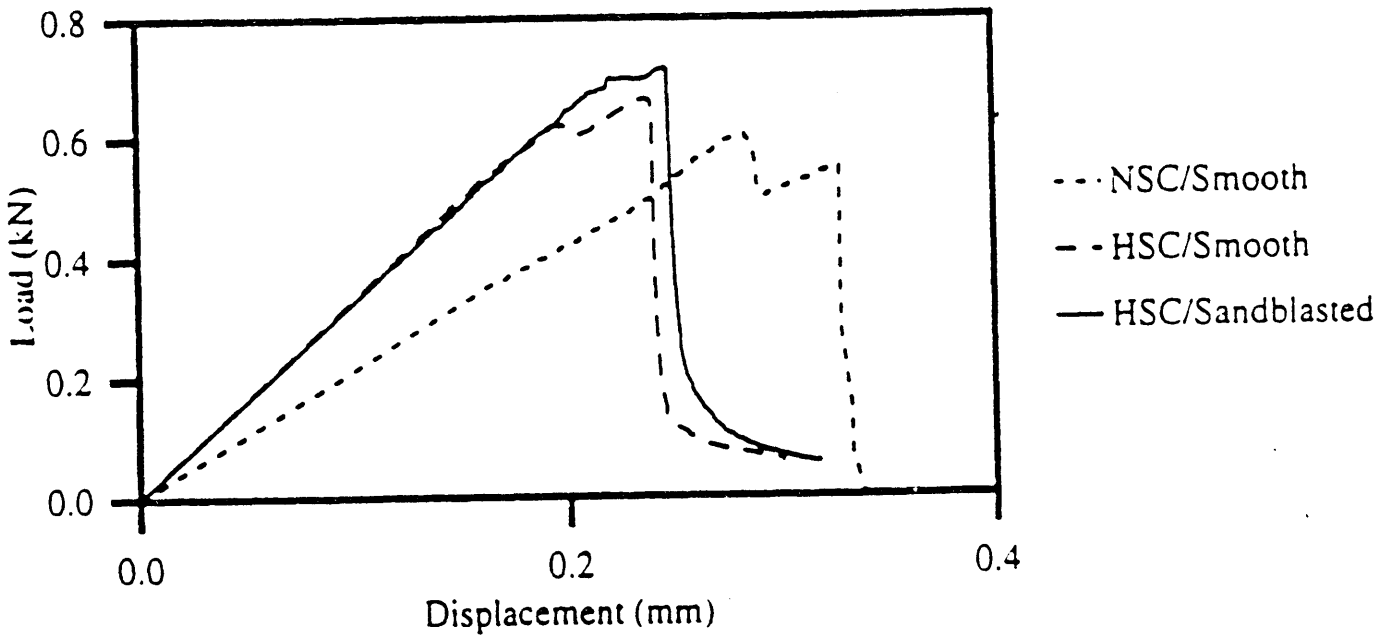

Figure 4.8 Stress Stain Curves for Concretes of Different Mortar Strengths and Aggregate Roughnesses
[*Büyüköztürk and Hearing, 1996*]

Chapter 5

Experimental Program

By studying concrete as a composite material, and studying the properties of the components and the interactions between them, a more thorough understanding of its behavior can be obtained [*Giaccio et al., 1992*]. This chapter will detail the testing program and material selection for this work. Following the description of the variables investigated in this work a general discussion about how these and other parameters are known to affect the behavior of the composite. Discussion regarding parameters not investigated in this work are also included for completeness. The variables studied and discussed are constrained to material properties of the basic constituents which can easily be specified by the mix designer. This constraint is important because in order for the use of HSC to become commonplace it must be made with low cost materials and current techniques [*Mehta and Aitcin, 1990*].

The chapter is divided into two parts: Testing Program and Material Selection.

TESTING PROGRAM

5.1 Mix Design

Due to the limited use of HSC and unfamiliarity of the material, mix designers often proportion the constituents empirically. Extensive lab testing then becomes necessary to ensure that the concrete's properties meet the design specifications. This uncertainty arises because for HSC there are no stringent guidelines similar to ACI 211 "Recommended Practice for Selecting Proportions

for Concrete Mixtures" for NSC. Therefore, it seems that the best approach to mix design of HSC is to rely on past successes. The mix design for this research followed the work already completed by Trende [*1995*], Lee [*1993*], Oumera [*1991*] and Büyüköztürk and Hearing [*1996*]. Their mix designs were used because they had been used successfully, and because results could then be more easily correlated between their works and this study.

For this research, NSC as well as HSC was made. The NSC, with a w/c ratio of 0.5, was made with standard techniques using only water, aggregates and Type III cement. In addition to these constituents, HSC required the use silica fume and superplasticizers to achieve the w/c of 0.22. For each of the two mortar strengths several material parameters were also studied. In order to contrast the different possible cracking scenarios granite and limestone aggregates were used to show deflection and penetration, respectively. Another parameter which has been shown to influence the behavior of the composite is the maximum size of the aggregate (MSA). It is generally accepted that the mechanical properties of cementatious composites are improved with a small MSA. Therefore three varying aggregate sizes were chosen. The coarse aggregates were separated into three categories: small, medium and large. Small coarse aggregates, for this study, are defined as all those smaller than ½". Medium coarse aggregates are those that fall in the range of ½" to ¾" and large are those greater than ¾" but less than 1". Before use the aggregates were separated by the corresponding sieves, washed and air-dried for 24 hours. Another parameter which has been the subject of less research, but is felt to have an appreciable affect is volume fraction of the coarse aggregate. Typically 35% volume fraction is used. Therefore 25%, 35% and 45% were examined for this work. Each of the variables mentioned led to 36 total mixtures examined. To record data it was necessary to devise a nomenclature which is shown in Figure 5.1. The exact mix proportions for each combination are reported in the appendix.

Production of concrete for testing requires that a stringent guide be followed in order to ensure consistency. Before any materials were place in the mixing machine its walls were wet down. The constituents were then placed in the mixing machine in the order specified on the machine: water, aggregate, cement, then sand. For HSC, the admixtures were added last. The mixes were typically left in the mixer for ten minutes or until the mix was satisfactory by visual inspection. After this time, the concrete was placed in the beam molds and cylinders at which point tamping began. The cylinders were cast in thirds and tamped 25 times. The beams were tamped for approximately one minute each. Then, in order to decrease the voids and inhomogeneity of the mix, all of the forms and cylinders were placed on a vibrator for approximately one minute. After which the initial cracks of 50mm, which is equal one-third of the beam depth, were placed in the beams. Then all forms were covered with damp towels and sealed. The following day, the specimens were then demolded and placed in warm baths of tap water for one week before testing.

5.2 Test Specimens

5.2.1 Three Point Bending Beams

The RILEM Technical Committee 89-FMT on Fracture Mechanics of Concrete-Test Methods proposed in 1990 a recommendation to measure the material fracture toughness, K_{Ic}. For the MSA used in this research the dimensions shown in Figure 5.2 were suggested by RILEM. For each of the 36 concrete mixes three to four beams were cast, yielding a total of over 110 beams tested. All beams were tested under three point bending at a constant rate of 0.1mm/min on the 1 kip INSTRON shown in Figure 5.3.

diameter. For each of the 36 mixtures three to four cylinders were cast yielding over 110 cylinders in total. All cylinders were tested on the 60 kip Baldwin universal testing machine shown in Figure 5.4, with the exception of a very few which were tested on the 100 kip INSTRON, shown in Figure 5.5. One of the cylinders was tested in compression and the remaining two/three cylinders were tested in accordance with ASTM C496. This procedure, called the split-cylinder test, is completed by placing the cylinder on its side so that the compressive load is applied along the length. The cylinder will then split in half at the critical tensile stress, which is computed by the following equation which is based on the theory of elasticity for a homogeneous material in a biaxial state of stress:

$$f_t = \frac{2P_c}{\pi dl} \tag{5.1}$$

The value is defined as the splitting tensile strength. There are some inaccuracies which can result from use of this equation. First of all concrete is not a homogenous material. Secondly, this is not a measure of direct tensile strength. However, in spite of these weaknesses, direct tension tests give no better correlation to tensile related failures therefore this test, which is easier to do, is commonly used [*Wang and Salmon 1985*].

5.3 Measurement of Ductility

With the beam dimensions and critical loads, the stress intensity factor can easily be computed through the use of some empirical equations. For three point bending beams with a_c, initial crack length, b the beam depth, t the beam thickness, P_c as the critical load and S as the span, the fracture toughness equation form RILEM is given by:

P_c as the critical load and S as the span, the fracture toughness equation form RILEM is given by:

$$K_{Ic} = 3P_c \frac{S\sqrt{\pi a_c} g_1(a_c/b)}{2b^2 t} \tag{5.2}$$

where

$$g_1\left(\frac{a_c}{b}\right) = \frac{1.99 - \left(\frac{a_c}{b}\right)\left(1 - \frac{a_c}{b}\right)\left[2.15 - 3.93\frac{a_c}{b} + 2.70\left(\frac{a_c}{b}\right)^2\right]}{\sqrt{\pi}\left(1 + 2\frac{a_c}{b}\right)\left(1 - \frac{a_c}{b}\right)^{3/2}} \tag{5.3}$$

For the dimensions used in this testing series the value of g_1 is 1.08. With the stress intensity factor and the split cylinder tensile strength the characteristic length can be computed from equation 3.17, presented in Section 3.5.

MATERIAL SELECTION

This section will detail the materials chosen for this research as well as giving a brief outline of some of the parameters not studied in this work. When possible, past research both from MIT and elsewhere will be cited to asses what is already known to affect the performance of concrete composites.

5.4 Cement and Water Cement Ratio

Cement is defined as a material with adhesive and cohesive properties which make it able to bond mineral fragments into a compact whole. The type of cements of interest to Civil Engineers are known as hydraulic cements which set and harden with the addition of water. Hydraulic cements are composed of mainly lime and silica which, with the addition of water react to form a hardened material

[*Troxell et al., 1968*]. HSC can easily be made with any of the five types of cement identified by the American Society for Testing and Materials (ASTM). Ordinarily Type I is used which has no special properties and reaches design strength in 28 days. For this research Type III cement was used to give high early strength.

It is well known that one of the most general parameters to characterize concrete is the w/c ratio. Two ratios were used in this investigation, 0.5 and 0.22. Water cement ratios on the order of 0.5 are used to obtain normal strength mortars, while ratios below around 0.25 are used to obtain high strength. Normal strength mortar was made with standard techniques using only water, aggregates and Type III cement. In addition to these constituents, high strength mortars required the use of HRWR and silica fume. The admixtures and their affects on concrete are discussed in following sections.

5.5 Aggregates

Although aggregates are usually inert, granular materials which serve as a filler, proper selection is essential. Aggregates should be strong, durable and economical [*Troxell et al., 1968*]. The coarse aggregate should be well graded and comprised of equidimensional particles. Suggested aggregates include dense limestone or an igneous rock of the following types: granite, syenite, diorite, gabbro or diabase [*Giaccio, 1992*].

Classification based solely on aggregate type is not sufficient. Aggregates are usually classified further by the following properties: whether they are natural or manufactured; according to their petrography; by their specific gravity; whether they are crushed or natural; whether they are inert or reactive; and most frequently by the maximum size. Based on the last criteria aggregates are divided into two major classes, fine aggregates and coarse aggregates. Fine aggregates are defined

as aggregate which pass a No. 4 sieve, which has an opening of 3/16 in (4.75mm) [*Popovics, 1979*]. It is common to refer to coarse aggregate as simply aggregate; therefore, for the remaining part of this work the word aggregate alone will mean coarse aggregate.

5.5.1 Fine Aggregate

In order to keep the water demand low, well graded fine aggregates should be used. For fine aggregates a clean natural sand or crushed rock that is without clay or silt is adequate. With NSC a fineness modulus of about 2.4 is recommended, however with HSC a fineness modulus of up to 3.0 can be used. The higher modulus will help keep the water content low and in turn improve the strength [*Troxell et al., 1968*].

The fine aggregate used for this study was donated by Boston Sand & Gravel and had the characteristics shown in Table 5.1. The fineness modulus for the fine aggregate was 2.65, which is nearly the average of the fineness modului recommended for NSC and HSC. Before each batching the fine aggregate to be used was air-dried for 24 hours to ensure that little excess water was present. Immediately before placing the fine aggregate in the mix it was sifted with a No. 10 sieve to reduce clumping.

5.5.2 Coarse Aggregate

Compared to NSC, a higher quality control of aggregates is necessary for HSC. In NSC the bond is almost always the weaker leak making the aggregate selection less important [*Mehta and Aitcin, 1990*]. Parameters which must be more strictly controlled are grading, mineralogy, and maximum aggregate size (MSA). For concretes of a given consistency and cement content a well graded mixture yields higher strength since less water is required for acceptable workability [*Troxell et al., 1968*]. Mineralogy can positively or adversely affect

the bond strength of the mortar-aggregate interface depending on the chemical or physical reactions which may take place [*Popovics, 1979*]. The interaction between the mortar and aggregate is discussed in relation to bond strength later in this section. Research regarding the effect of MSA has yielded conflicting evidence therefore an assessment of its effect is one of the aims of this research.

5.5.2.1 Selection of Aggregate Type

The coarse aggregates used in this research were specifically chosen to show the two different cracking scenarios that are possible when a cementatious material fails. Due to the differences in strength and fracture energy of the aggregates, different crack paths will occur and thus a different fracture energy and characteristic length of the concrete composite can be observed. The failure crack can either penetrate the aggregate, if it is weaker than the bond, or travel around it if it is not. Limestone being a relatively weak aggregate was chosen to exhibit the first scenario, and granite, a strong aggregate, was chosen for the second. One or both of these aggregates were also used in the research by Oumera [*1991*], Kitsutaka et al. [*1993*], Lee [*1993*], Trende [*1995*] and Büyüköztürk and Hearing [*1996*]. Other benefits to choosing these aggregates are, namely: they are commonly used for other similar research, they are used in the field and they are available locally. The limestone was purchased from Plymouth Quarries. The granite was donated by Bates Brothers located in Weymouth, Massachusetts.

5.5.2.2 Mineralogy

As discussed earlier, the bond strength in HSC is greater than that of NSC and may be responsible for the increase in brittleness associated with HSC. Part of this work aims at characterizing the bond between the aggregate and matrix such that the bond can be made strong enough to maintain higher strength, yet weak enough so that cracks will propagate through the interface rather than the aggregate. In order to alter the bond, one must have an understanding of the

physical, chemical and mechanical interactions at the interfaces [*Zhang and Gjørv, 1990*]. Each of these interactions is depicted in Figure 5.6.

Physical Interaction

Concretes comprising aggregates which are well polished and have no chemical interaction with the matrix have only the physical bond to rely on for stress transfer. In these situations the interface strength is extremely small or negligible even with a strong matrix. Therefore, selection of smooth and inert aggregates should be avoided if possible in order to ensure a more ductile fracture [*Zhang and Gjørv, 1990*]. The granite and limestone used for this research were not exceptionally smooth. They were both used as found; that is, the natural roughness was adequate and it was not necessary to intentionally roughen them.

Chemical Bond

It is common for aggregates in Portland cement concrete to contain particles that are chemically active [*Popovics, 1979*]. If there is a chemical interaction between the aggregate and cement, as with some carbonate rocks, the bond strength may be very strong [*Zhang and Gjørv, 1990*]. However, there are also chemical reactions which can have adverse effects. The most common is an alkali-silica reaction. A gel, which swells and induces cracking, is produced by the reaction between the alkalis and active siliceous minerals and rock types. This reaction is not typical of aggregates used in this research but is presented in order for future works to avoid the problem.

A reaction which can effect limestone, an aggregate used in this work, can also be observed. The reaction, which causes cracking, is an alkali-carbonate reaction. The active materials are excessive cement alkali in moist environments and argillaceous dolomitic limestones. The cracking comes about due to large

expansion; this is most commonly seen in sidewalks and floor slabs, which often have cracks which penetrate to two-thirds of the depth. In order to avoid these effects several precautions can be made. Most simply, nonreactive rocks should be used, or at least blended with reactive rocks. Also, the use of a low cement content, with the cement containing less than 0.4% alkalis calculated as sodium oxide, is known to diminish the effects. In addition, allowing the concrete to dry before sealing will lead to better results [*Popovics, 1979*].

Despite the previous highlights on the possible negatives, a limited chemical reaction can in some cases be favorable for the bond between the aggregate and cement paste. For example, the lime-silica reaction that occurs at high temperatures can be used for high-pressure steam curing. This reaction is considered beneficial because it is not accompanied by significant expansion. In general, there is no consistent way in which to determine whether or not an aggregate will cause expansion or have other negative effects. It seems that the best manner to determine an aggregate's properties is to rely on past performances [*Popovics, 1979*].

Mechanical Bond

Mechanical bonding is simply an interlocking of the aggregate surface and the cement. When aggregates which are porous or rough are used the cement paste or cement hydration products may penetrate into the pores on the aggregate surface. The penetrations will form a connection between the aggregate and matrix [*Zhang and Gjørv, 1990*]. It is obvious that this interlock will vary directly with the surface roughness and will effect the bond strength and ductility [*Troxell et al., 1968*]. Despite the fact that the water requirement of smooth aggregates is less than that of rough, concrete mixtures containing a rough textured or crushed

aggregate have a somewhat higher compressive strength and relatively higher tensile strength than concrete with smooth aggregates [*Popovics, 1979*].

5.5.2.3 Maximum Size of Aggregate

There is general controversy surrounding the effects of MSA. Most feel that, as in NSC, an appreciable role is played by the MSA in effecting the properties of concrete. It is widely accepted that an increase of MSA leads to an increase in the size and heterogeneity of the transition zone. Also, larger aggregates are more likely to have internal defects. Defects are more likely because during the size reduction process internal defects are often eliminated from previously large aggregates in the formation of smaller ones. Any remaining large aggregates are still likely to have flaws which will reduce the crack resistance of the concrete [*Mehta and Aitcin, 1990*]. Nonetheless, research by Wittman [*1989*] and Mihashi et al. [*1989*] has found that the fracture energy increases with an increase in MSA.

Due to the apparent lack of a rigorous understanding of the influence MSA has on concrete this variable was chosen to be studied for this research. Experience shows that it is difficult to produce HSC with an MSA above 25 mm and with most aggregates 10-12 mm is optimum [*Mehta and Aitcin, 1990*]. Therefore the aggregates investigate here will be limited by the upper range and will be smaller than what is considered optimum.

5.5.2.4 Percent Aggregate by Volume

Percent aggregate by volume to the author's knowledge is a parameter which has not been studied extensively. Nonetheless, it appears that an appreciable effect can be played by the volume fraction. For example, if the aggregate deflects the crack a more tortuous crack path will be evident with increasing aggregate percentage. Even if the aggregate does not deflect the crack

the volume fraction will effect the mechanical properties of the composite. For example, if the aggregate itself is more ductile than the interface the system will behave in a more ductile manner than if the crack had been deflected rather than penetrating the aggregate. Further, with an increase in the number of aggregates the transition zones may become so plentiful that they will overlap and become a critical weak-link [*Snyder, 1992*].

Typically 35% coarse aggregate by volume is used. Therefore 25%, 35% and 45% were examined for this research. These percentages were used for each aggregate type and size, giving 18 mixture combinations for each strength of mortar.

5.5.2.5 Shape of Aggregate

Since the shape of aggregates are typically irregular from a geometric point of view it is difficult to measure and therefore quantify the effect aggregate shape has on the properties of concrete. For this research aggregate shape was not specifically chosen as a parameter but the two aggregate types studied do typically have different shapes. The limestone aggregates were typically well rounded, while the granite aggregates were more oblong and flatter. It would have been desirable to have consistency with respect to shape, however the aggregates used were typical of those found in this area.

Aggregate shape has not been shown to be a critical factor in mix design. However, when it is necessary to make concrete with exceptional tensile strength, well rounded aggregates are recommended. Nonetheless there are some guidelines which should be followed. Equidimensional particles are preferred to flat or elongated aggregates because they can be packed tighter. Improved packing leads to a decrease in required water, cement paste, or mortar for a given workability. Flat particles when orientated in a plane tend to form water and air voids

underneath which jeopardizes the strength and durability of concrete [*Mehta and Aitcin, 1990*].

5.5.2.6 Roughness of Aggregates

Surface roughness of the aggregates was not specifically studied as part of this research but was another property that varied between the aggregates. The limestone typically had rounder edges, while the granite had sharper edges. Some influence would arise from this difference, however since these properties are typical of the aggregates it is not something that can easily be altered on a large scale so they aggregates were used as found.

Concrete mixtures containing a rough textured or crushed aggregate has a somewhat higher compressive strength and relatively higher tensile strength at early ages than concrete with smooth aggregates of otherwise identical mixtures. However, at later times the influence of roughness is diminished [*Mehta and Aitcin, 1986*]. Lee [*1993*] found that the interface toughness, K_{Ic}, is lower for polished surfaces as compared to regular surfaces. Theoretically this should be true, however Trende [*1995*] found that an increase from smooth to the roughest surface led to smaller or equal fracture toughnesses. Trende attributes this atypical behavior to increased porosity in the vicinity of the aggregates with increasing roughness. Nonetheless, Trende's data demonstrates the expected increase in fracture toughness for increased roughness with the exception of the smooth surface. Knowing that the tensile strength is increased only marginally over time and that the fracture toughness increases dramatically, one can conclude from the characteristic length equation that the ductility increases with roughness.

5.6 Admixtures

To make HSC it is necessary to obtain the most compact microstructure possible when solidification begins. One way to do this is to lower the volume of

water not used to hydrate the cement grains during the first step of hydration. In order to do this it is necessary to use chemical admixtures to limit the free water and maintain workability. By eliminating the excess water the cement particles can be packed more closely together [*Aitcin and Laplante, 1992*]. The most common way of eliminating excess water is through the use of admixtures. It is estimated that 80 % of the concrete made today in North America contains one or more chemical admixture [*Ghosh and Nasser, 1995*].

Ideally, it would be possible to provide additional water later on to completely hydrate all the cement particles. This would make it possible to take advantage of the binding properties of the hydrated calcium silicates that could be developed from the anhydrous cement grains. By carrying this to the extreme, concrete with a w/c ratio of 0.16 has been made which had a compressive strength of 280 MPa. In fact, when trying to decrease the w/c ratio it becomes evident that at some point the factor limiting the compressive strength is not the intrinsic strength of the hydrated cement past and the aggregate, but the compressive strength of the aggregate itself [*Aitcin and Laplante, 1992*].

5.6.1 Superplasticizers

Since water molecules have high surface tension, the cement-water system tends to form flocs which trap large amounts of water. Upon evaporation, the entrapped water creates voids. It is widely accepted that these voids have a detrimental effect on the strength. It is also known that if the excess entrapped water can be eliminated greater improvements in strength can be achieved than through the addition of more cement. The reduction in water leads to a stronger and more homogenous transition zone which improves load transfer between the phases of concrete [*Mehta and Aitcin, 1990*].

In the, 1970's the advent of high range water reducing admixtures, also known as superplasticizers, made it possible to make low w/c ratio concretes while providing adequate workability. Superplasticizers are derived from naphthalene or melamine sulfonate formaldehyde. They are a high molecular weight, anionic, surfactant with polar groups in the hydrocarbon chain [*Mehta and Aitcin, 1990*]. Normal water reducers tend to form spherical microgel flocs when used in high quantities, however superplasticizers do not and thus are able to disperse the cement grains [*Aitcin and Laplante, 1992*, *Mehta and Aitcin, 1990*].

The use of superplasticizers has become standard practice for HSC. They are typically used to make high slump concretes with w/c ratios of 0.3 or less [*Mehta and Aitcin, 1990*]. The HSC mix design for this work had a w/c ratio of 0.22. The superplasticizer used was the same as that for the previous MIT work mentioned. The brand name is WRDA-19, which is an aqueous solution of naphthalene sulfonate with a low viscosity. This, as well as the silica fume, was donated by W. R. Grace of Cambridge.

5.6.2 Silica Fume

Silica fume is another admixture developed in the 1970's that is often used to make HSC. Silica fume is a byproduct from the production of silicon and ferrosilicon alloys. The waste generated from this procedure is characterized by extremely fine ground spherical particles. The average diameter of these particles is nearly 100 times smaller than an average cement particle. Cement's specific surface is only 300-400 m^2/kg while silica fume's is in the area of 400-700 m^2/kg [*Lee, 1993*].

Addition of silica fume to concrete mixes can have positive effects including the reduction of bleeding and permeability and an increase in durability. However, silica fume is used primarily to improve the compressive strength.

Strength is improved due to the decrease in w/c ratio and an improved bond between the mortar and aggregate. An improved interface makes that region less of a weak link of the system and cracking occurs at higher stress levels [*Lee, 1993*].

The silica fume used for this research was the same as that used in the previous works already mentioned. Silica fume can come in two forms: slurry and powder. The slurry form of Force 10,000 is 48% silica fume, 2% foreign particles and 50% water. The powder form, with the same brand name, requires the addition of slightly more water. For this research silica fume in slurry form was used for the limestone mixtures and powder form was used for the granite. This change was not anticipated and was unavoidable due to the fact that the materials were donated.

5.7 Summary

This chapter contained a discussion regarding material selection for the production of HSC and the testing series for this research. A brief review of material selection was necessary because the mix proportioning of HSC is sometimes chosen empirically, which can sacrifice the ability to adequately predict the mechanical properties of the composite.

Any ASTM certified cement can easily be used to make HSC. It was shown that the variability in concretes is largely attributable to the properties of the coarse aggregate. The most important difference observable depends on the relative aggregate and interfacial strength. Depending on these properties the aggregate will either deflect or be penetrated by an impinging crack. Varying MSA was also shown to have an appreciable affect on the properties of the interface, and therefore the composite. A larger MSA was shown to have negative effects on this region for several reasons including: an increase in size and inhomogeneity of

the transition zone and poorer packing which leads to the accumulation of free water. The other variable studied as part of this work was coarse aggregate volume fraction. This variable, which has not been studied extensively, could dramatically influence the behavior of the composite. The effects will discussed further in the results and conclusions sections. Also included in this chapter but not directly variables in this research are shape and roughness of the aggregates. It has not been shown that either parameter has a significant affect on the behavior of the composite, however some influence can be observed. This chapter presented information regarding the admixtures used. HRWR are used to lower the w/c ratio while maintaining adequate workability. Silica fume is usually used to increase the density of the transition zone and thereby increase the amount of load transfer between the two phases.

The motivation for the mix design was discussed after the variables to be studied were presented. The mix design follows the work already completed at MIT in hopes of achieving similar success and compatibility between results. Details regarding the dimensions of the beams and testing procedures for all specimens were presented. In all over 110 beams and 100 cylinders were tested for this research.

Sieve No.	Opening	Opening [inch]	Weight ret.	Passing [%]	Total ret. [%]
8	2.36	0.0937	0	22.76	22.76
16	1.18	0.0469	921	39.22	61.98
30	0.60	0.0234	1587	23.01	84.99
50	0.30	0.0117	931	10.77	95.76
100	0.15	0.0059	436	4.22	---
Pan	---	---	171	---	---
Σ			4046	99.98	265

Fineness Modulus: (=Σ Total Ret./100=**2.65**)

Table 5.1 Fineness Modulus of Fine Aggregate Obtained from Boston Sand and Gravel

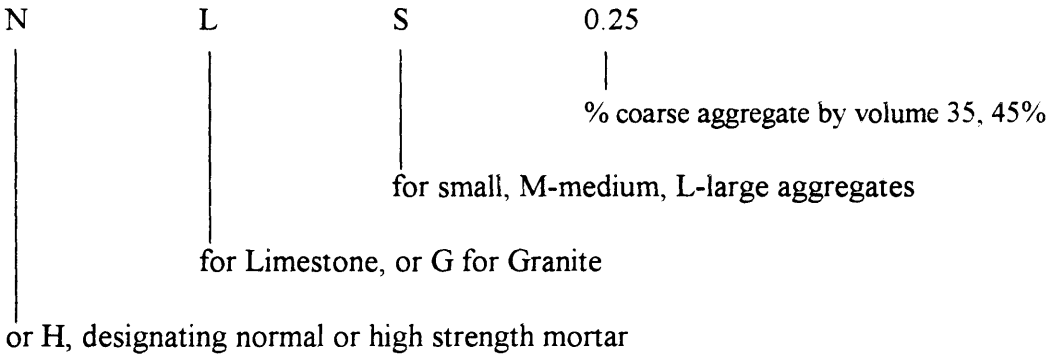

Figure 5.1 Nomenclature for Testing Series

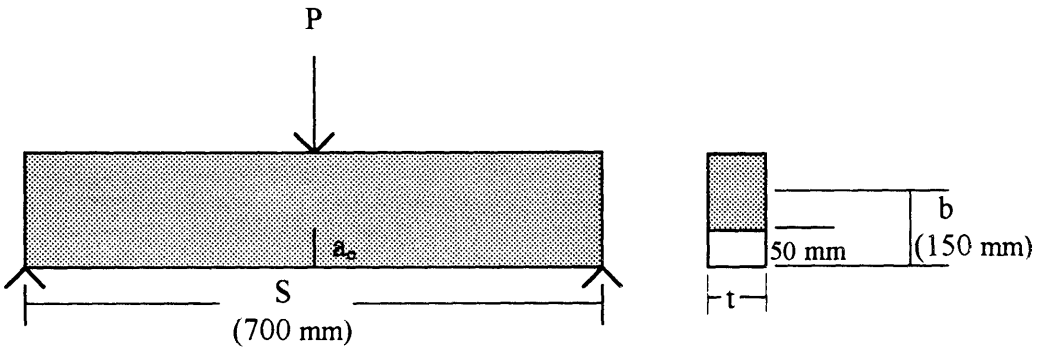

Figure 5.2 Dimensions of Three Point Bending Beams as Recommended by RILEM Technical Committee 89-FMT on Fracture Mechanics of Concrete-Test Methods

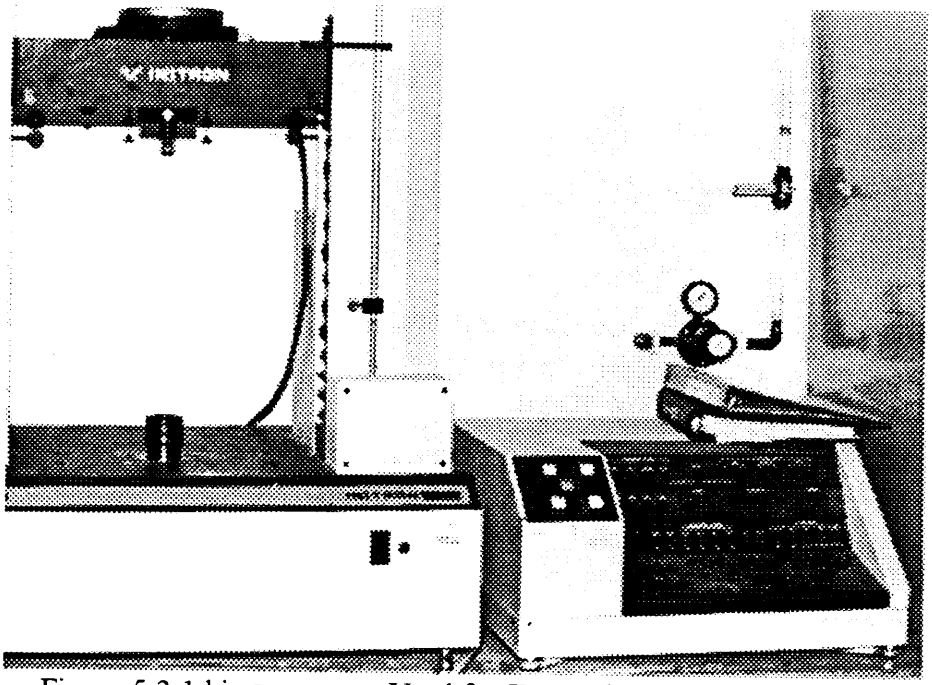

Figure 5.3 1 kip INSTRON. Used for Tests of Three Point Bending Beams

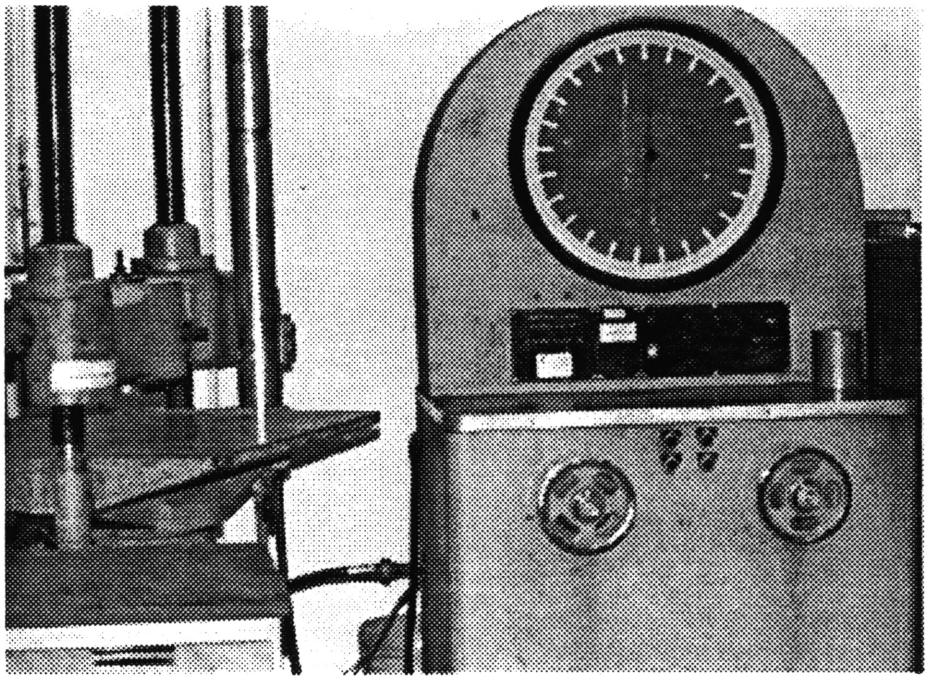

Figure 5.4 60 kip Baldwin. Used for Split Cylinder Tests and most Compression Tests.

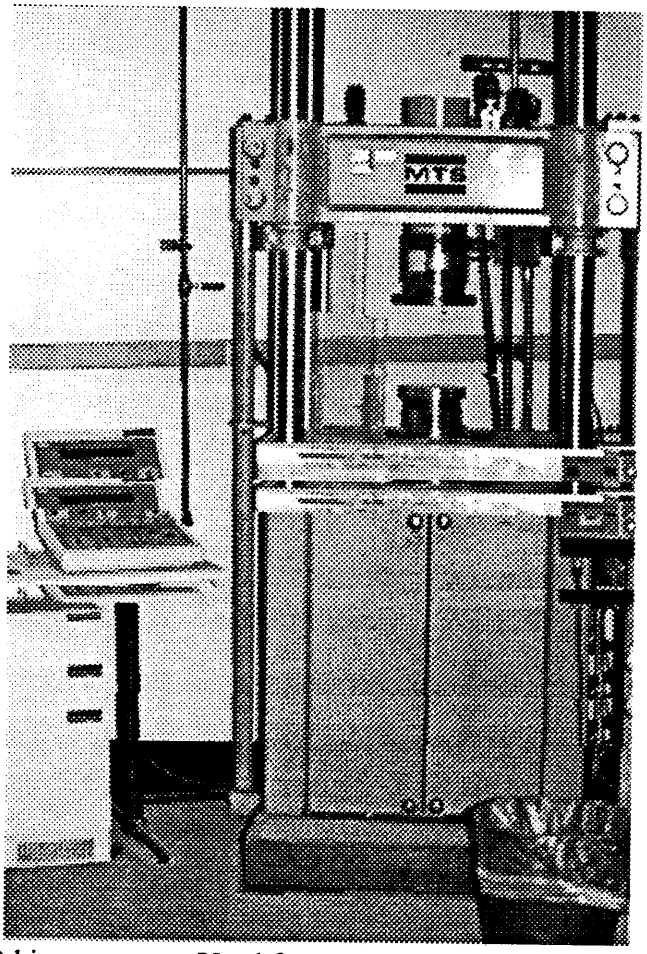

Figure 5.5 100 kip INSTRON. Used for Tests of some High Strength Cylinders.

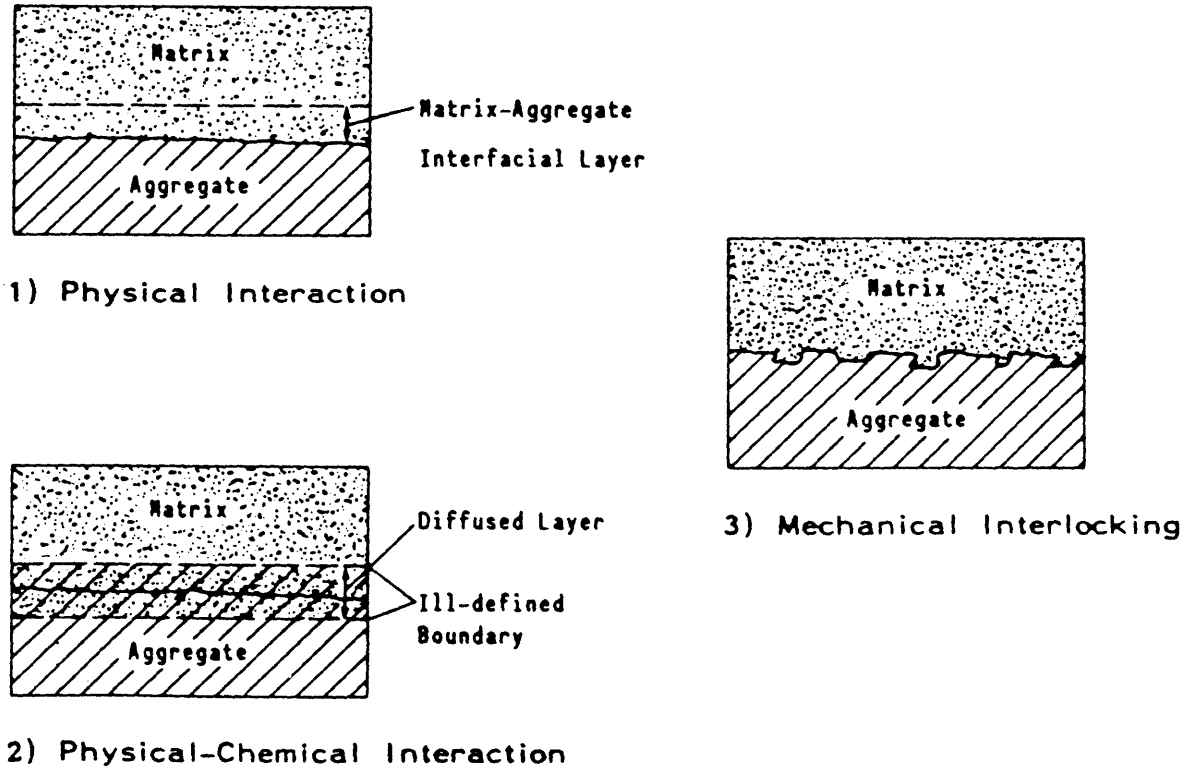

Figure 5.6 Interaction between Aggregate and Mortar Paste.

[*Zhang and Gjørv, 1990*]

Chapter 6

Experimental Results

The average failure loads for the three point bending specimens, tensile strengths, compressive strengths and critical stress intensity factors for the laboratory tests are reported in Table 6.1. Also included are the characteristic lengths for each mixture. This one measure is representative of the average of three to four beams' K_{Ic} divided by the average tensile strength of two cylinders. The compressive strength reported is representative of one or the average of two cylinders.

Visual inspection of the tested specimens shows that the two crack paths were evident. In all the specimens containing limestone, the failure was observed to be brittle and the crack path planar, as can be seen in Figure 6.1. This trend is in agreement with Oumera and Lee. Oumera found that the only case of limestone resulting in interfacial failure was a few with small angles of incidence [*1991*]. Lee found that limestone deflected the crack only for the highest strength limestone mixture with the angle of incidence equal to 90° [*1993*].

Interfacial crack propagation was found with the specimens containing granite. The rough crack face compared to limestone can be seen in Figure 6.2. Oumera [*1991*] and Lee [*1993*] also found that a crack impinging a granite aggregate was deflected through the interface in every case regardless of the angle of incidence. For different mortar strengths Oumera [*1991*] found the critical angles to increase with strength. However, in this research the failure path for NSC and HSC incorporating granite were

found to be interfacial in every case.

6.1 Ductility of Concretes

For each of the graphs referred to in section 6.1, the data for each mixture is represented by only one point. The point is calculated from equation 3.17 and is representative of the average of three or four beams and two split cylinder tensile tests. The data was compressed to one point for ease of presentation and interpretation of the following graphs.

6.1.1 Normal Strength Mortar with Limestone (Normal/Limestone)

When concrete is made with a coarse aggregate that is weaker than the bond strength such as limestone, the crack penetrates the aggregate and the fracture path is planar. Since the crack is not deflected by the limestone in normal strength mixtures the properties of the transition zone have little contribution to the behavior of the system. Therefore, the differences in behavior of limestone mixes may be directly attributed to the properties of the coarse aggregate.

The ductility of the normal/limestone mixtures, as shown in Figure 6.3, decreases with an increasing volume fraction, v. This may be attributed to the greater surface area of limestone on the resulting crack face. Ductility is also shown to decrease with a larger MSA. This can be observed in Figure 6.3 or in Table 6.1 by comparing mixtures that are consistent except for MSA. Trends similar to this have been concluded to be caused by a weaker transition zone, poorer packing and a higher probability of critical microflaws in larger aggregates [*Mehta and Aitcin, 1990*]. The effect of the transition zone in limestone mixtures is suspected to have a negligible effect since the crack rarely propagates interfacially. Therefore the other properties may be responsible for the improvement. Improved packing can significantly improve the properties of the interface because less

trapped water exists between the aggregates. Ordinarily excess water will reduce the strength of the interface because upon evaporation pores are left which act as weak-links. Additionally, large aggregates tend to be weaker because during the size reduction process, whether natural or man-made, a majority of internal flaws are eliminated in the creation of smaller aggregates. Therefore, aggregates which remain large are still likely to contain flaws [*Mehta and Aitcin, 1990*].

6.1.2 High Strength Mortar with Limestone (High/Limestone)

As with normal/limestone mixtures, the fracture path of high/limestone concrete is planar, that is there is no crack arrest by the aggregate. However, in contrast to normal/limestone there is an increase in ductility with an increase in volume fraction. Evidence is shown in Figure 6.4. The increased area of limestone on the crack face leads to greater ductility because the aggregate itself is more ductile than the mortar. From this argument one could suggest increasing the volume fraction above 45% however workability limitations constrain the volume fraction that can realistically be used.

In Figure 6.4 the ductility is also shown to decrease with an increasing MSA. It is well known that fracture energy, as well as other fracture characteristics such as K_{Ic}, increases with increasing MSA [*Hilsdorf and Brameshuber, 1991*]. Therefore, by using equation 3.17, the decrease in ductility can be seen to be attributable to a larger increase in tensile strength. This change in ductility could also be a property of the same characteristics outlined in the previous section: namely, larger aggregates being weaker, improved packing and improvements to the transition zone with smaller MSA.

6.1.3 Normal Strength Mortar with Granite (High/Granite)

Normal/granite mixtures exhibited an interfacial cracking path which was characterized by numerous crack bends and bifurcations. This cracking scenario was

predicted for granite based on its mechanical properties by Oumera [*1991*] through the analysis of two phase models. Normally, one would expect the ductility to increase with an increase in the number of deflections. However, by examining Figure 6.5 one can observe that the compared to the normal/limestone mixtures the normal/granite mixtures were less sensitive to changes in volume fraction. The insensitivity could be attributed to a competition between things which are suspected to increase ductility and those which decrease it. For example, with granite the crack will be deflected and this usually consumes more energy, however the bond may be so brittle that it will detract from the composite's performance. Further, higher percentages are known to create a more tortuous crack path, but with an increase in aggregate percentage there is more likelihood that the transition zones will overlap and yield a relatively weak crack path.

Figure 6.5 demonstrates that the concretes comprised of smaller MSA are most ductile, followed by the medium and large MSA. Theoretically, a larger MSA that deflects the crack as granite does would result in a longer crack path. However, knowing that a larger MSA also leads to weaker transition zones and poorer packing, it appears that a competition between the negative and positive affects explains the apparent insensitivity of ductility as related to MSA. Additionally, the shape of the granite used may also be responsible. The granite aggregates were relatively flat which increases the trapped water in the transition zone and decreases the strength of the region due to poor packing. With larger aggregates these influences could be more pronounced.

6.1.4 High Strength Mortar with Granite (High/Granite)

With high/granite mixtures the crack path is again interfacial. Contrary to normal/granite the insensitivity to volume fraction is not apparent. Figure 6.6 shows that as the volume fraction increases there is a pronounced increase in ductility. Knowing that energy is required for each bend and bifurcation, the increase is most likely attributable to

an increase in tortuosity with higher volume fractions. The potential for a weak crack path due to overlapping transition zones is diminished for high strength mixtures due to the improved properties of the interface through the addition of silica fume.

As seen in Figure 6.6, similar to all the other mixtures the ductility decreases with an increase in MSA. This increase could be attributed to the several reasons already mentioned. For completeness, they are again: higher probability of critical microflaws in larger aggregates, decreased heterogeneity of the transition zone with larger aggregates, larger transition zone and poorer packing. By the same argument with volume fraction, a smaller MSA will require more aggregates to attain a given volume fraction which will yield a longer crack path with more deflections, and thus energy consumption. This is evident because with the same aggregate percentage, there is generally an increase in ductility with a decrease in size despite the increase in the number of transition zones.

6.2 Recommendations for Material Selection

Recommendations can now be made about material selection. From this work it is apparent that MSA is a crucial parameter of mix design. Recommendations regarding volume fraction can be made, however ductility may not be the motivation for them. For HSC workability rather than ductility seems to be the controlling factor of volume fraction. Consequently, 35% seems to be the best compromise between workability and economy. For NSC smaller volume fractions lead to greater ductilities, however again economy may lead to the selection of 35%.

The ductilities versus aggregate percentage for all normal strength mixtures is reported in Figure 6.7. With NSC there is a definite decrease in ductility with an increase in aggregate percentage regardless of whether the aggregate deflects or is penetrated by the crack. Also regardless of the aggregate type, an increase in ductility with a decrease in

MSA was observed. Therefore mix design of NSC should call for a low volume fraction, if economy is not a concern, and a small MSA.

As seen in Figure 6.8, with high strength concretes the same argument can be made regarding MSA. That is, ductility was observed to increase with a decrease in MSA. However, in contrast to the normal strength mixtures, with HSC ductility is enhanced with an increase in aggregate percentage. In the case of limestone mixtures this can be explained by the corresponding increase of limestone on the resulting crack face with higher percentages. Since limestone is more ductile than the mortar, this leads to an improved composite behavior. Therefore, this work suggests that if high strength is desired while using an weak aggregate a small MSA and a high volume fraction should be specified by the mix designer. In the past, it has proven to be somewhat difficult to make HSC with weak aggregates so the applicability of this information is uncertain [*Aitcin and Laplante, 1992*]. For granite mixtures the impinging crack is deflected, therefore an increase in percentage leads to a longer crack path that consumes more energy upon fracture. However despite the improved properties, the volume fraction should be limited to 35% due to a decrease in workability with higher fractions.

In some cases of Figure 6.8 the limestone mixtures are observed to be more ductile than the corresponding granite mixtures. However due to the difference in silica fume used for the two mixtures a definite conclusion regarding this behavior can not be made. It was hoped to ascertain the composite performances based on isolating one variable however the silica fume donated to this work was changed for the two mixtures.

Table 6.1. Average Failure Loads and Observed Failure Paths.

Series	v (vol. Fraction)	MSA	Avg. P_{ult}	Failure	K_{Ic} (Pa $m^{1/2}$)	f'_t (MPa)	f'_c (MPa)	l_{ch} (m)
Normal/Limestone	0.25	½"	2.724	transgranular	621.9	1.92	36.0	0.1051
Normal/Limestone	0.35	½"	2.360	transgranular	538.7	1.94	25.1	0.0772
Normal/Limestone	0.45	½"	2.531	transgranular	577.9	2.16	27.1	0.0719
Normal/Limestone	0.25	¾"	2.953	transgranular	674.1	2.33	34.3	0.0834
Normal/Limestone	0.35	¾"	2.895	transgranular	661.0	2.69	32.7	0.0603
Normal/Limestone	0.45	¾"	2.680	transgranular	611.9	2.62	30.5	0.0544
Normal/Limestone	0.25	1"	2.728	transgranular	622.9	2.29	34.2	0.0737
Normal/Limestone	0.35	1"	2.991	transgranular	682.9	2.61	31.0	0.0685
Normal/Limestone	0.45	1"	2.969	transgranular	677.7	2.58	34.5	0.069
Normal/Granite	0.25	½"	3.077	interfacial	702.5	2.61	33.1	0.0727
Normal/Granite	0.35	½"	2.744	interfacial	626.3	2.19	33.6	0.0814
Normal/Granite	0.45	½"	2.933	interfacial	669.6	2.61	36.8	0.0658
Normal/Granite	0.25	¾"	3.287	interfacial	750.5	2.22	38.4	0.1144
Normal/Granite	0.35	¾"	3.470	interfacial	792.1	3.05	33.8	0.0676
Normal/Granite	0.45	¾"	xxxx	interfacial	xxxx	Tested	early	xxxx
Normal/Granite	0.25	1"	2.847	interfacial	650.0	2.59	34.1	0.0628
Normal/Granite	0.35	1"	3.002	interfacial	685.3	2.77	37.5	0.0612
Normal/Granite	0.45	1"	2.898	interfacial	661.7	2.45	28.2	0.0727
High/Limestone	0.25	½"	4.007	transgranular	914.8	3.29	40.8	0.0771
High/Limestone	0.35	½"	3.542	transgranular	808.6	2.39	49.4	0.1149
High/Limestone	0.45	½"	3.170	transgranular	723.7	2.08	43.0	0.1214
High/Limestone	0.25	¾"	4.567	transgranular	1042.5	3.20	52.8	0.1060
High/Limestone	0.35	¾"	3.632	transgranular	829.0	2.86	42.6	0.0841
High/Limestone	0.45	¾"	4.135	transgranular	944.0	2.83	47.8	0.1109
High/Limestone	0.25	1"	3.220	transgranular	735.2	3.15	43.7	0.0543
High/Limestone	0.35	1"	3.243	transgranular	740.4	2.97	36.4	0.0621
High/Limestone	0.45	1"	3.456	transgranular	789.1	3.12	50.4	0.0640
High/Granite	0.25	½"	3.725	interfacial	850.5	3.45	58.6	0.0607
High/Granite	0.35	½"	4.305	interfacial	982.8	3.28	45.4	0.0898
High/Granite	0.45	½"	4.174	interfacial	952.8	2.87	38.8	0.1101
High/Granite	0.25	¾"	3.592	interfacial	819.9	3.69	35.7	0.0494
High/Granite	0.35	¾"	3.981	interfacial	908.7	3.74	40.3	0.0591
High/Granite	0.45	¾"	3.712	interfacial	847.3	3.51	48.4	0.0583
High/Granite	0.25	1"	2.961	interfacial	675.9	3.07	35.7	0.0484
High/Granite	0.35	1"	3.988	interfacial	910.5	2.93	43.8	0.0964
High/Granite	0.45	1"	3.336	interfacial	761.6	2.75	48.4	0.0767

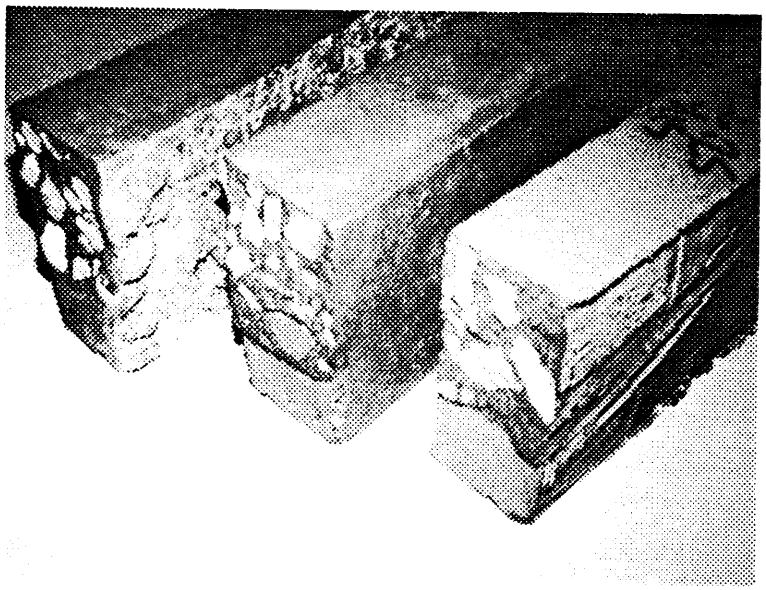

Figure 6.1 Planar Crack path with little or no Interfacial Crack Propagation.

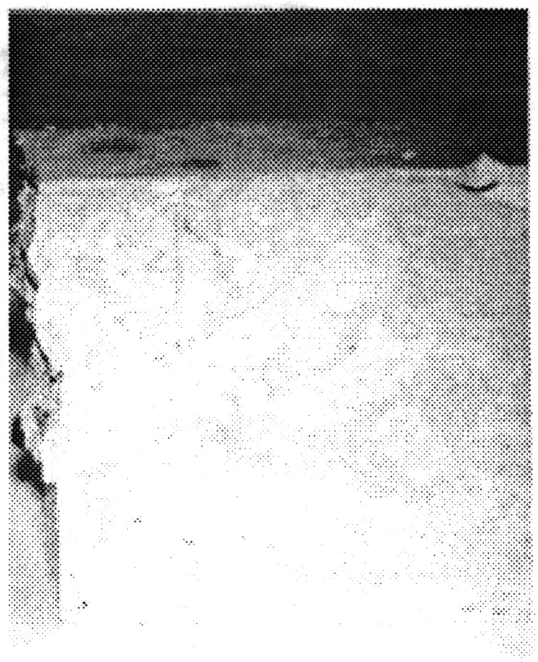

Figure 6.2. Interfacial Failure typical of Granite mixtures.

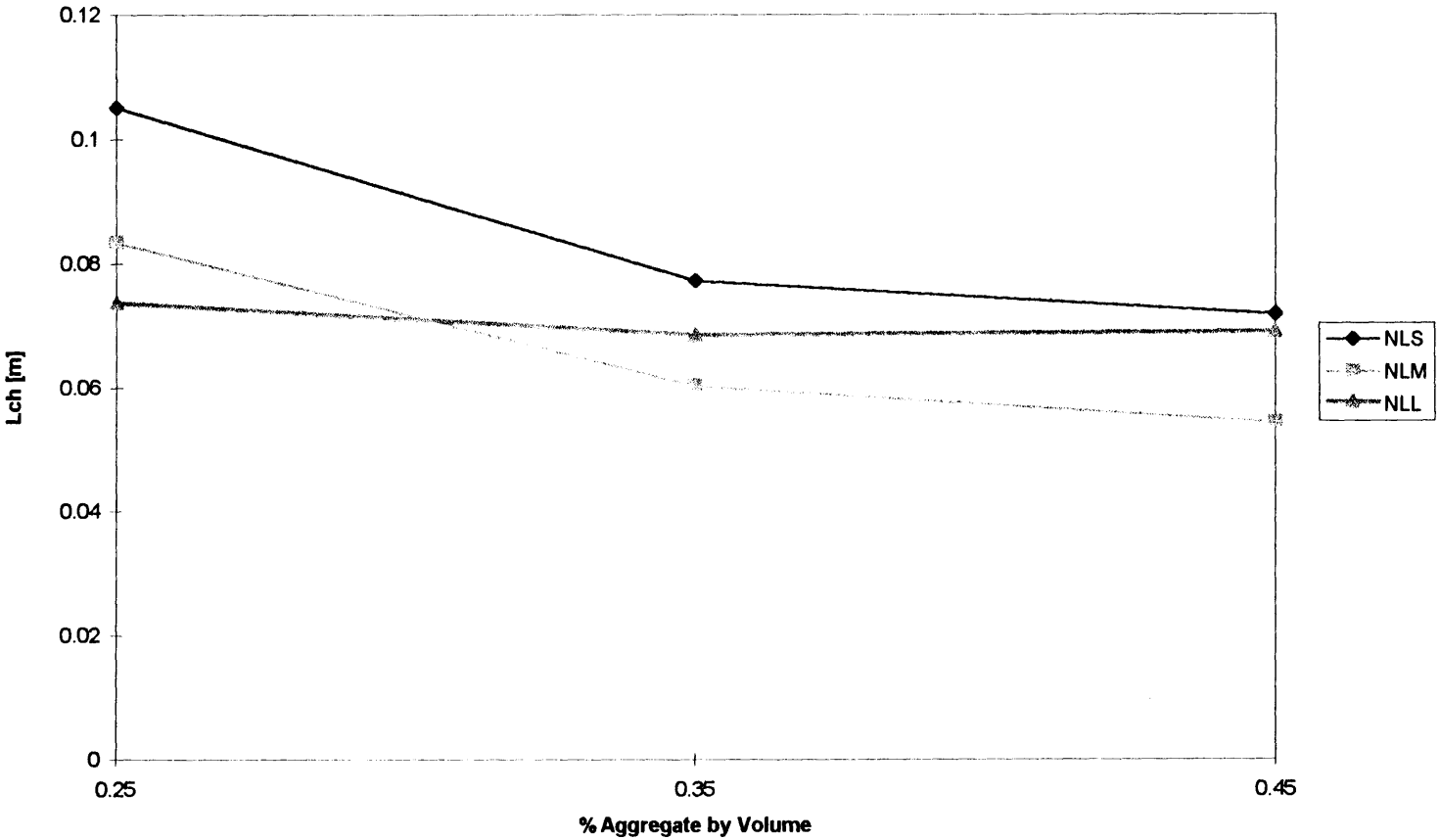

Figure 6.3 Ductility of Normal/Limestone Mixture

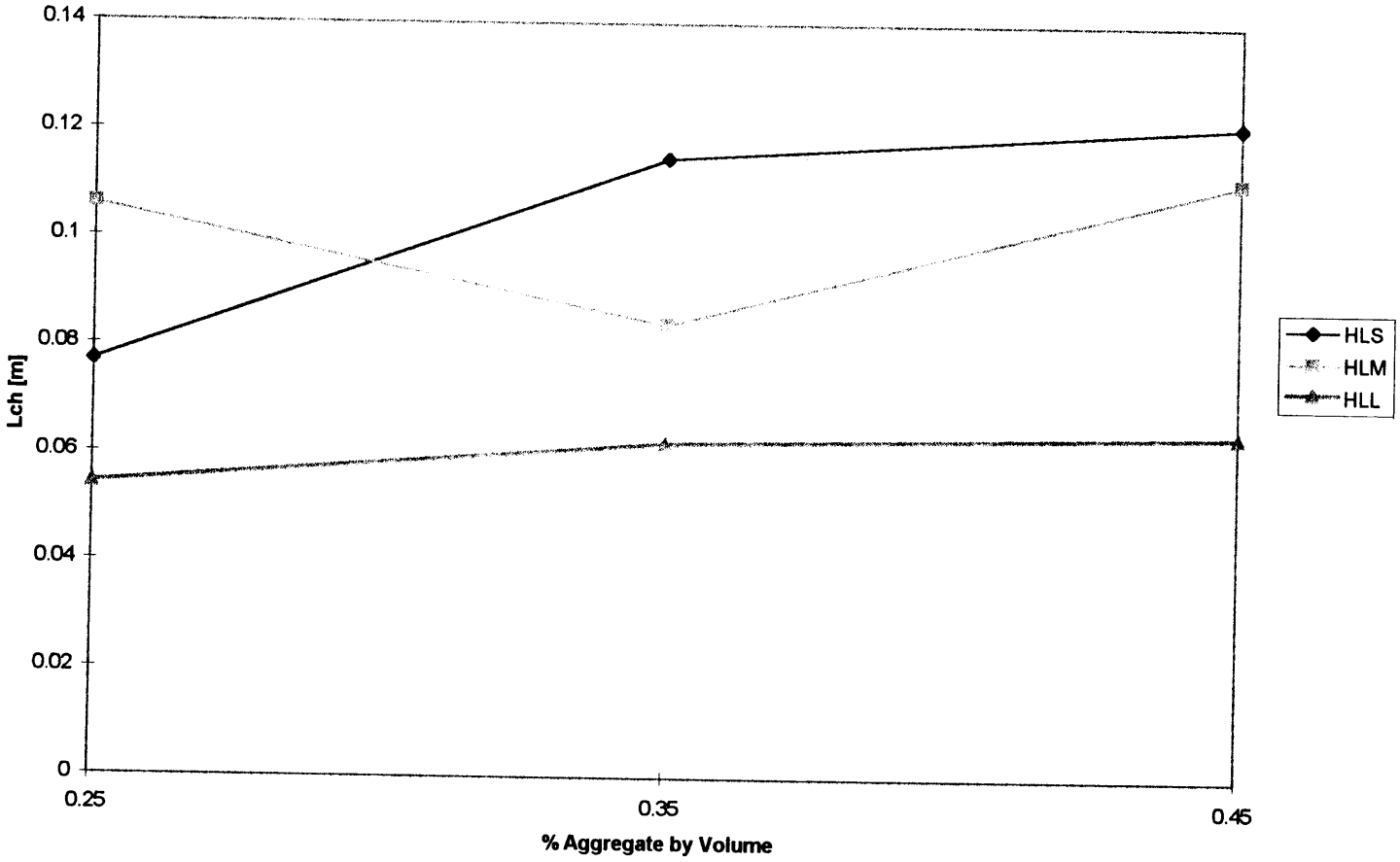

Figure 6.4 Ductility of High/Limestone Mixtures

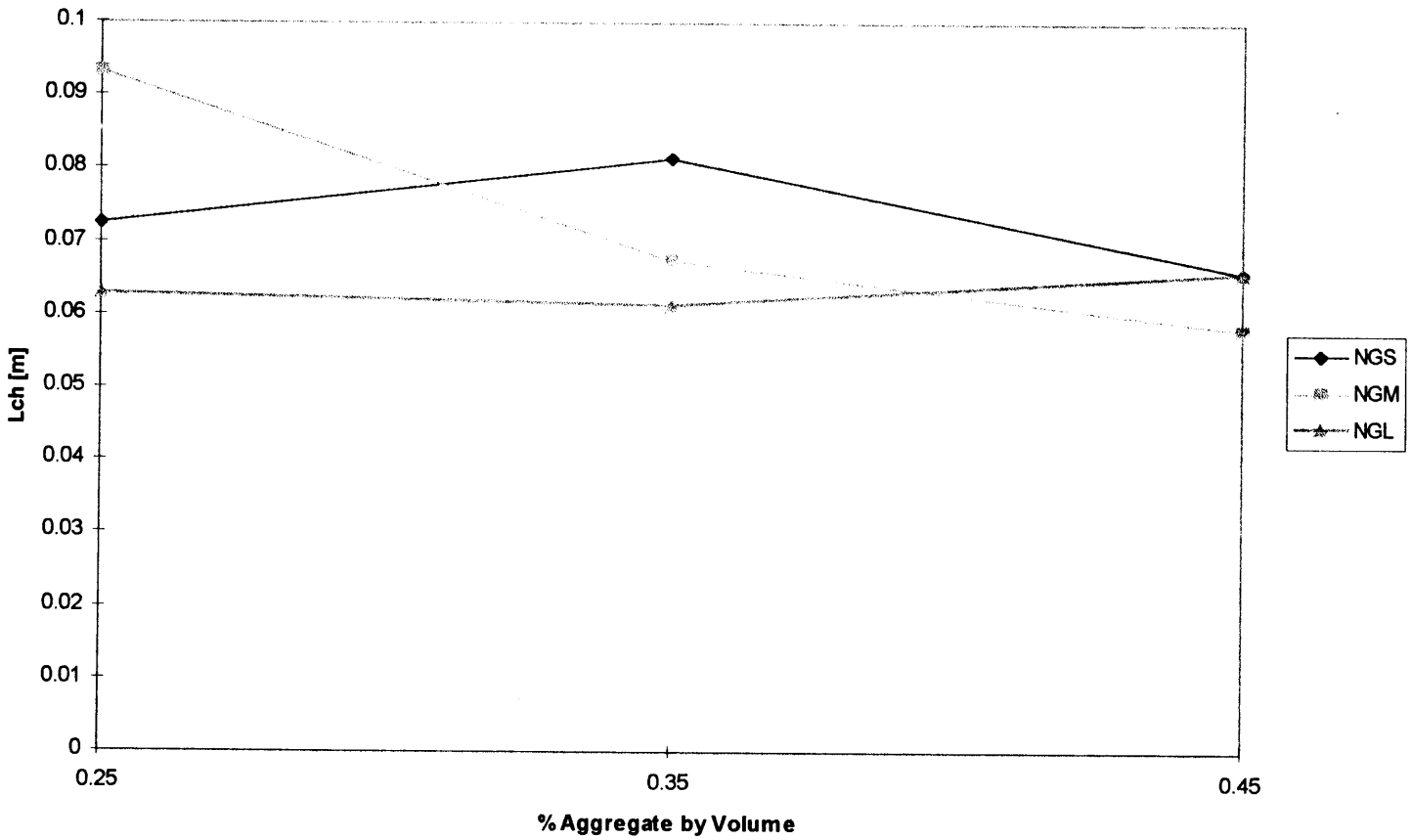

Figure 6.5 Ductility of Normal/Granite Mixtures

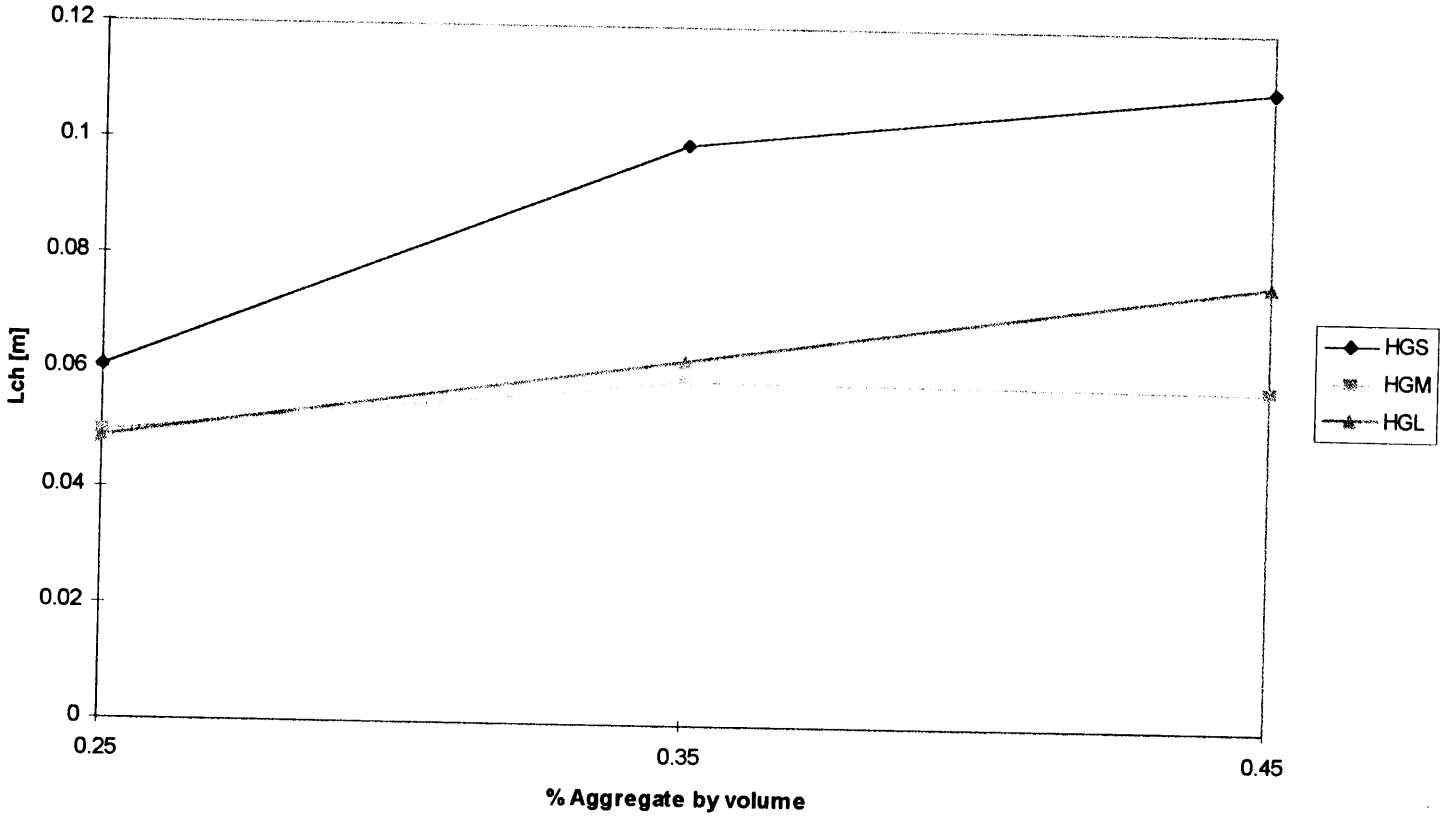

Figure 6.6 Ductility of High/Granite Mixtures

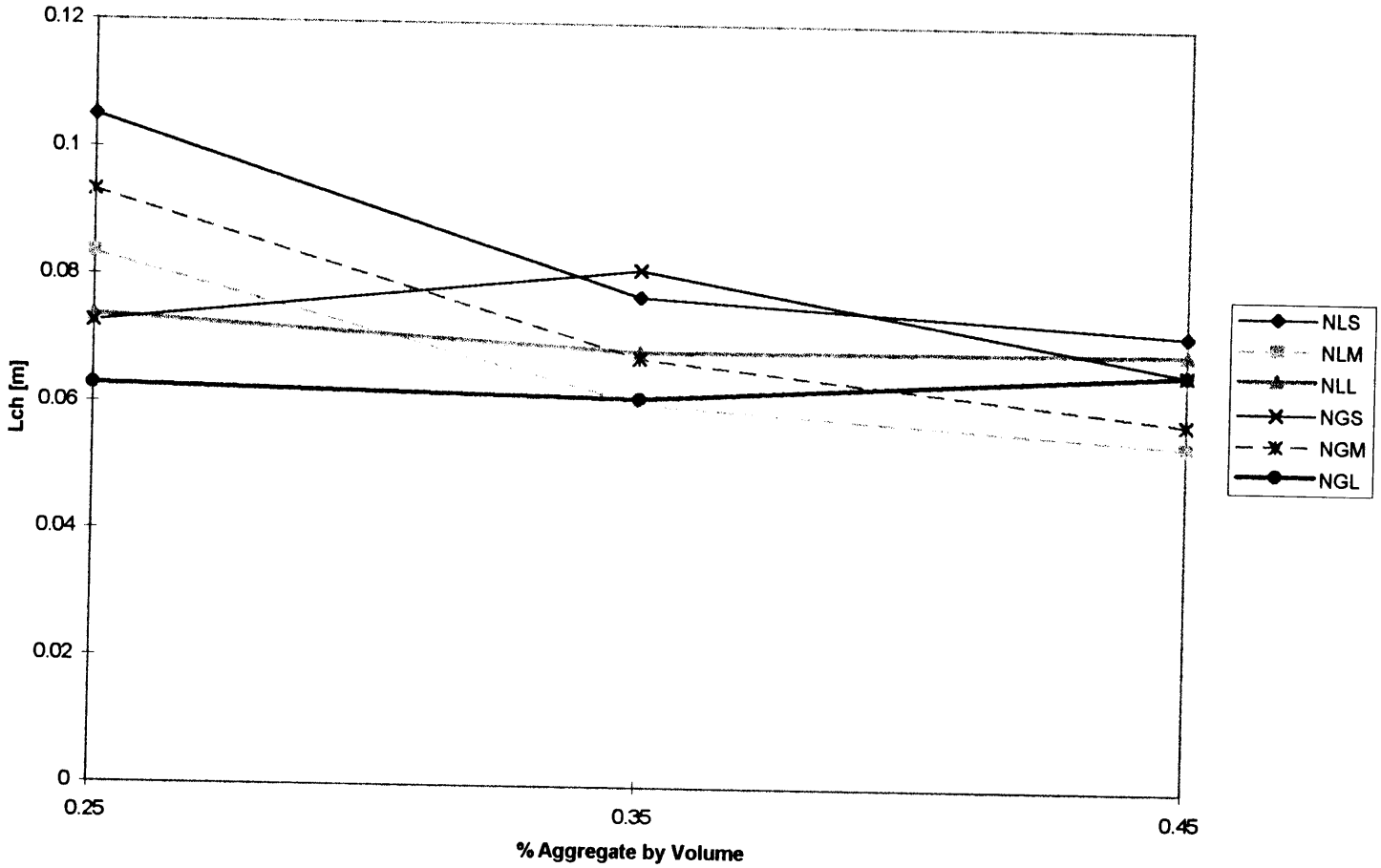

Figure 6.7 Ductility of All Normal Strength Mixtures

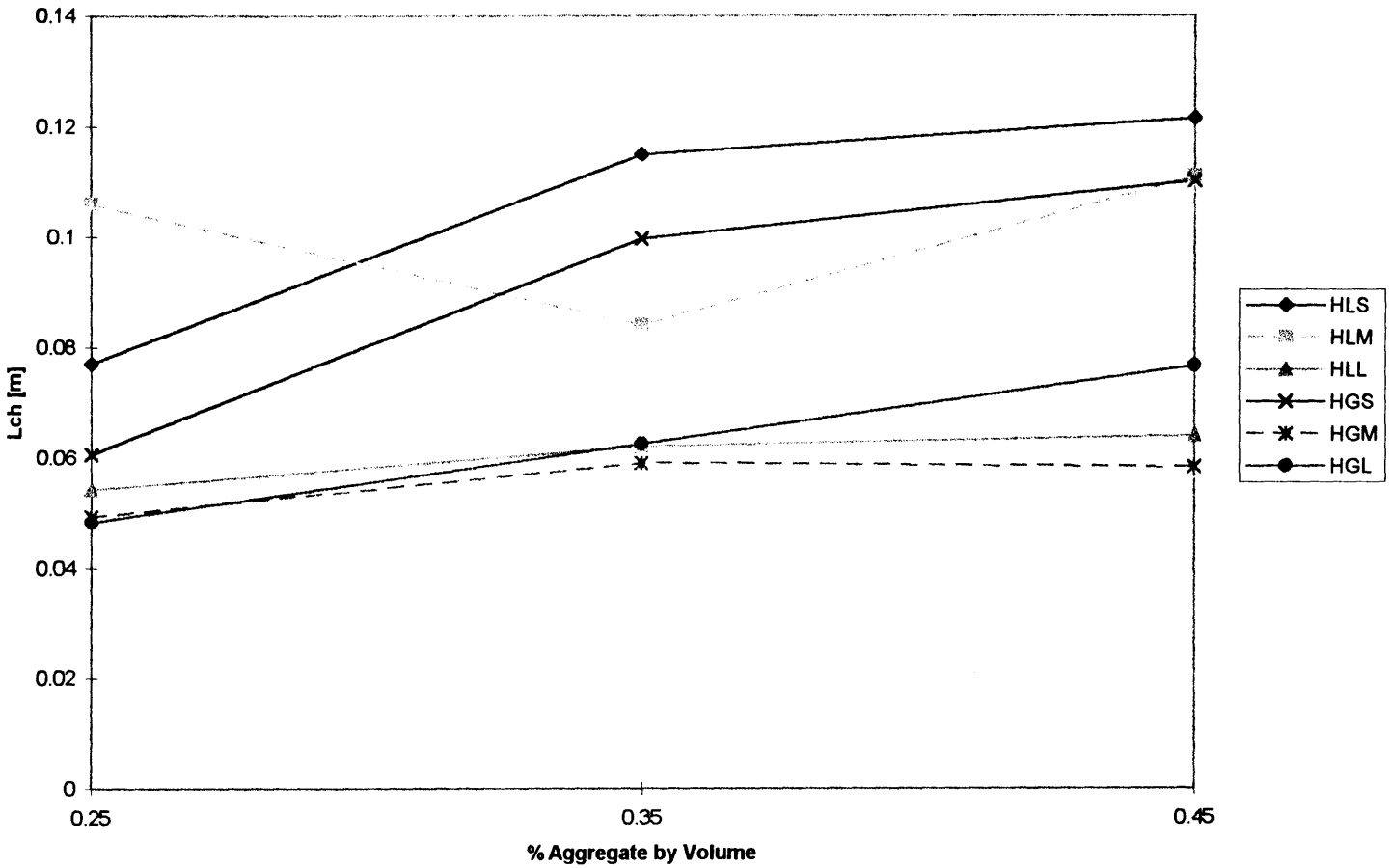

Figure 6.8 Ductility of All High Strength Mixtures

Chapter 7

Analytical Results

A motivation for this work was to asses analytical models' ability to adequately predict the behavior of real concrete composites. This chapter will detail a comparison between the analytical and laboratory results. Also included is a discussion pertaining to the applicability of several empirical equations suggested by other researchers. The empirical equations attempt to predict the characteristic length from the compressive strength of concrete and to predict the fracture energy based on, in one case material properties, and in the other aggregate properties and compressive strength. The strength-ductility equations are shown to not comply well with the data obtained in this research. The fracture energy equations are not expected to predict the behavior of the composite adequately because they fail to account for the properties of the constituents. Therefore, in this research a novel code-like equation is developed that accounts for more of the materials' properties.

7.1 Predictions Based on Analytical Procedures

Results of the analytical procedures developed prior to this work are compared with the data compiled. Table 7.1 shows the average peak loads obtained from the experimental work and physical models. The ratios of high strength to normal strength concretes' peak loads from the simulations are shown to agree with ratios from the experimental program. Figure 7.1 shows a comparison of the load/load-line displacements obtained from cohesive force simulations using normal and high strength mortars with a circular granite inclusion [*Büyüköztürk and Hearing, 1996*]. Similar to the laboratory, the

peak load and deflection of the system with high strength mortar is shown to be greater than with normal strength mortar. Figure 7.2 shows a comparison of load/line-displacements obtained with analytical simulations using normal and high strength mortars with limestone aggregate [*Kitsutaka et al., 1993*]. Here, as was the case in the experiments, the peak load of the system is higher with high strength mortar but the deflection is not shown to increase as in the model with granite inclusions. The analytical models are therefore concluded to agree well with the experimental results.

7.2 Ductility and Strength Relationships

7.2.1 Laboratory Data

Development of empirical equations usually are based on the assumption that as strength increases ductility inherently decreases. As seen in Figure 7.3, the ductility of specimens containing limestone were found to decrease with compressive strength. This trend is in agreement with other researchers [*Zhou et al., 1995*]. However, as shown in Figure 7.3, specimens containing granite were found to have an increasing ductility with an increase in compressive strength. This trend could be due to granite deflecting cracks. Fracture energy is required for each deflection so the ductility should increase with more deflections. It has also been established that compressive strength is improved with a decreasing MSA. For any given volume fraction, the use of a small MSA will require more aggregates which will in turn represent more deflections while achieving an increase in strength. This may be the cause of compressive strength increasing while ductility also does.

7.2.2 Empirical Equations

Several researchers have proposed empirical code-like equations to predict the characteristic length by knowing only the compressive strength of the concrete. Two such equations are those of Hilsdorf and Brameshuber [*1991*] and Zhou et al. [*1995*]. Hilsdorf

and Brameshuber suggest

$$l_{ch} = 600 f_{cm}^{-0.3} \text{ mm} \tag{7.1}$$

The work of Zhou et al., by curve fitting, yields

$$l_{ch} = -3.84 \times 10^{-3} f_c + 0.58 \text{ m} \tag{7.2}$$

The results of this work suggest that such an equation based solely on strength of the composite is not easily accomplished. The comparison of these equations to the data obtained in this work, as seen in Figure 7.4, shows that with varying constituents no one equation can adequately predict the characteristic length. Neither equation accounts for the possible cracking scenarios observed with different fracture strengths of aggregates. For example, it was observed in this research that mixtures of the same compressive strength were found to have drastically different characteristic lengths depending on the aggregate type, size and volume fraction. In defense of the work of Zhou et al., their compressive strengths were much higher than those obtained from this work and the accuracy of the empirical equation may not necessarily apply to lower strength as accurately.

7.3 Fracture Energy

7.3.1 Empirical Fracture Energy Equations

An equation suggested to characterize a concrete composite's behavior based on the constituents was proposed by Larrard and Malier [*1992*]. The equation is:

$$G_{1c} = (1 - v)G_{1m} + vG_{1a} \tag{7.3}$$

where v is the volume fraction of aggregate and the subscripts refer to mode I fracture and

the composite, mortar and aggregate [*Larrard and Malier, 1992*]. Fracture energies were not calculated for the mixtures examined in this testing series, however equation 7.3 can be studied. First, the equation does not take into account the effect of MSA, which has been shown in this work to be appreciable. Additionally, Larrard and Malier do not account for the possibility of interfacial fracture. With granite aggregates, the fracture path would most likely be interfacial and the fracture energy of the interface rather than the aggregate itself becomes important. Due to the absence of factors which have been shown to influence fracture energy this equation may not accurately predict the behavior of concretes.

Conversely, Hilsdorf and Brameshuber [*1991*] have suggested that fracture energy, in the absence of experimental data, can be predicted by

$$G_F = a_d f_{cm}^{0.7} \tag{7.4}$$

where a_d is a coefficient depending on MSA. For an MSA of 8, 16, and 32 mm, a_d is suggested as 4, 6 and 10 respectively. f_{cm} is equal to the mean compressive strength of concrete in MPa. The coefficients suggested do not correspond to the MSA used in this research and the fracture energy was not directly measured so the applicability of this equation can not be evaluated rigorously. Nonetheless, it is suspected that this equation is also lacking because it does not account for any variation in volume fraction, or fracture energy of the aggregate or mortar.

7.3.2 Novel Fracture Energy Equation

It seems apparent that some combination of the two previous equations could be developed to adequately predict the behavior of the system. Therefore development of an equation began by modifying equation 7.3 with a variable to account for the effect of

MSA similar to equation 7.4. This modifier is necessary because a pronounced effect has been shown to be due to MSA. The term, defined k_a, is placed outside the brackets because the aggregate size has also been shown to affect the properties of the mortar in the vicinity of the aggregate [*Metha and Aitcin, 1990*]. The novel equation proposed is

$$G_c = k_a\left[\nu G_a + (1-\nu)G_m\right] \tag{7.5}$$

where G_c, G_a, and G_m are the fracture energies of the concrete, aggregate and mortar, respectively and ν is the volume fraction of the coarse aggregate.

To apply this equation to the data obtained for this research it is necessary to perform some manipulation and make some basic assumptions. To convert from the stress intensity factors of Table 6.1 to fracture energies it is necessary to employ the empirical modulus of elasticity equations 2.2, 2.4 and 2.5 and then use an altered form of 3.16 to obtain the fracture energy. The average modulus of elasticity from the three cited equations was used. The fracture energy values are obtained from the work of Kitsutaka et al. [*1993*] and are reported in Table 7.2. Equation 7.5 was than converted to solve for k_a:

$$k_a = \frac{\dfrac{K_{Ic}^2}{E}}{\nu G_a + (1-\nu)G_m} \tag{7.6}$$

Because this equation does not account for interfacial fracture in any way, only the limestone test data was used as input. The values of k_a obtained, based on MSA, are reported in Table 7.3. The numbers reported in are representative of the average for all the three point beams of each mixture. The value of k_a is smallest for the small MSA, and largest for the medium MSA. Initially it was suspected that k_a would increase with

decreasing size, however other researches, as reported in chapter 5, have found that fracture energy was insensitive to MSA. Hilsdorf and Brameshuber [*1991*], for equation 7.4, found that k_a was directly related to fracture energy.

In order for any equation of the form of 7.5 to be applicable to concretes which fail interfacially, the addition of another modifier is necessary. Using the same k_a values obtained for limestone the second modifier, denoted k_v, can be found from

$$k_v = \frac{\frac{K_{Ic}^2}{Ek_a}}{\nu G_{a,I} + (1-\nu)G_m} \tag{7.7}$$

where $G_{a,I}$ is the fracture energy of the interface between the mortar and aggregate. The value used for the interface fracture energy of a mortar granite system was taken from Lee's thesis work [*1993*]. For normal/granite and high/granite the interface fracture energies are 1.33 and 2.22 J/m^2 respectively. The values of k_v obtained for granite concretes are shown in Table 7.4. The trend of these values is as was expected. For higher aggregate percentages, the crack path is longer and thus more energy is consumed upon failure.

It is now possible to propose a general equation that can be used to predict the fracture energy based on the properties of the constituents:

$$G_c = k_a k_v \left[\nu G_{a,I} + (1-\nu)G_m\right] \tag{7.8}$$

k_a is specified in Table 7.3. If penetration of the aggregates is expected, k_v is taken as 1. Also, in cases of penetration $G_{a,I}$, the Mode I fracture energy of the aggregate in J/m^2 is used in place of $G_{a,I}$. If interfacial failure occurs with granite aggregates, k_v is obtained

from Table 7.4 and the value of $G_{a,i}$ is taken as the interface fracture energy of the mortar aggregate system.

7.4 Accuracy of Novel Equation

The experimental results were compared to those predicted from equation 7.8. For each of the mixtures the experimental fracture energy is divided by that predicted by equation 7.8, yielding the ratio referred to in the following portion of this section. For normal/limestone mixtures the comparisons between the experimental and analytical values can be seen in Table 7.5. The average ratio is 1.05. The fracture energy values for high/limestone are reported in Table 7.6 and the average ratio is 0.98. The standard deviation for the normal/granite and high granite are 0.124 and 0.190, respectively. Based on the two ratios it seems that this equation is suitable for cases of aggregate penetration.

For the granite mixtures the accuracy of the ratio is diminished, however the standard deviations are on the same order. The comparisons for normal/granite and high/granite are shown in Tables 7.7 and 7.8, respectively. The ratios obtained for these mixtures are 1.28 for normal/granite and 0.85 for high/granite. The standard deviations are 0.150 for normal/granite and 0.167 high/granite. Due to the larger ratio discrepancy with aggregate deflection, further research should be undertaken in order to modify the factor k_v and asses whether the same k_a can be applied for cases of penetration and deflection. Nonetheless, the theory of the novel equation proposed here is a valuable first step towards a code-like equation to predict the fracture energy based on material combinations. In the future, a similar experimental analysis should be performed and the results can then be compared with the novel equation developed here. Further refinements to the factors k_v and k_a can then be made and perhaps the accuracy can be improved.

7.5 Parametric Study of Novel Equation

From equation 7.8 it is possible to predict the fracture energy of a composite based on the constituent properties and the interfacial strength in cases of deflection. For varied coarse aggregate volume fraction and fracture properties from Lee [*1993*] and Kitsutaka et al. [*1993*], fracture properties for each mixture are predicted and shown in Figure 7.5. For interface fracture with percentages not studied in this research the value of k_v is linearly interpolated. The predicted behavior of the normal/limestone mixtures is expected. As more limestone is added, which has a higher fracture energy than normal strength mortar, the composite will have a higher fracture energy. Conversely, the high strength mortar fracture energy is higher than the limestone so increasing the volume fraction has a detrimental effect.

For the granite mixtures an interesting trend in Figure 7.5 is evident. In both cases the fracture energy increases to a maximum for 35 % and then decreases for higher percentages. For example, with a constant value of k_a normal/granite mixtures are expected to have fracture energies of 13.7 J/m^2 , 14.2 J/m^2 and 13.3 J/m^2 for 25%, 35% and 45% respectively. Similar data can be calculated for high/granite mixtures. For equation 7.8, this peak arises due to the factor k_v. In practice this trend can also be observed. It is well known that at some volume fraction there is a transition after which there is a negative gain so this

For a given volume fraction of 35 %, composite fracture energies are depicted in Figure 7.6 for varied mortar fracture energy. In each case the fracture energy of the composite is shown to be highly dependent on that of the mortar. Meanwhile, for composites exhibiting interfacial failure, the interface strength is not exceptionally influential. In Figure 7.7, it can be observed that the fracture energy of the composite changes little with improved interface fracture strength. Finally, in Figure 7.8, the fracture

energy of concretes that fail by penetration are shown to be highly dependent on the fracture properties of the aggregate.

7.6 Summary

The experimental data obtained as part of this research has been shown to correspond well with the analytical programs developed at MIT as predecessors to this work. Empirical equations to predict the fracture properties of concrete developed by other researchers have been shown to not comply well with the data obtained in this work. The equations investigated all failed to account for each of the parameters that have been shown in this research to influence the fracture properties of concrete. Therefore a novel fracture energy equation was developed to account not only for the fracture properties of the constituents but also for the cracking scenario and the MSA. To the author's knowledge no other equation taking both of these parameters into account has been developed. Due to the lack of sufficient data to base empirical constants on, the equation should be carefully used. Nonetheless, it is felt that the theory is sound and with future work in the same are could make the equation useful in predicting the fracture properties of concretes.

Table 7.1 Comparison of analytical models developed at MIT to the values obtained in the laboratory for this work.

(a) Comparison to aggregate penetration analytical model of Kitsutaka et al. [*1993*]

Material Combination	Physical Model Fracture Load [kN]	Real Concrete Beam Fracture Load [kN]
High strength limestone	1.200	3.631
Normal strength limestone	0.893	2.771
Ratio	1.340 Aggregate Penetration	1.310 Aggregate Penetration

(b) Comparison to interfacial propagation analytical model of Büyüköztürk and Hearing [*1996*].

Material Combination	Physical Model Fracture Load [kN]	Real Concrete Beam Fracture Load [kN]
High strength granite	1.357	3..800
Normal strength granite	1.099	3.066
Ratio	1.23 Interfacial Failure	1.24 Interfacial Failure

Table 7.2 Mechanical Properties of Aggregates.

[*Kitsutaka et al., 1993*]

Materials	Compressive Strength (MPa)	Tensile Strength (MPa)	Young's Modulus (Gpa)	Poisson's ratio ν	Critical Energy Release Rate (J/m^2)	Fracture Energy (J/m^2)
Limestone	57.5	3.1	34.5	0.18	11.8	29.2
Granite	140.1	6.2	55.3	0.16	17.5	59.7

Table 7.3. Empirical Factors of k_a from Equation 7.6 for Limestone.

	Small	Medium	Large
NL 0.25	.449	.539	.461
NL .35	.385	.514	.562
NL 0.45	.416	.442	.512
HL 0.25	.532		.333
HL 0.35	.395	.445	.382
HL 0.45			.388
AVERAGE k_a	.435	.485	.440

k_a calculated from Equation 7.6 with fracture properties from Table 7.2 and interface fracture properties from Lee [*1993*].

$$\frac{\frac{K_{Ic}^2}{E}}{\nu G_a + (1-\nu) G_m} = k_a$$

Table 7.4 Values of Interfacial Fracture Modifier, k_v, for Volume Fractions

	25 %	35 %	45 %
k_v	1.43	1.74	1.85

k_v calculated from Equation 7.7 with fracture properties from Table 7.2 and interface fracture properties from Lee [*1993*]. Normal Granite interface strength is 1.33 J/m^2 and High Granite is 2.22 J/m^2.

$$k_v = \frac{\frac{K_{Ic}^2}{Ek_a}}{\nu G_{a,i} + (1-\nu)G_m}$$

Table 7.5. Comparison of Experimental Data and Proposed Equation for Normal/Limestone.

	NLS 0.25	NLS 0.35	NLS 0.45	NLM 0.25	NLM 0.35	NLM 0.45	NLL 0.25	NLL 0.35	NLL 0.45
G_C from Eqn.	13.77	14.19	14.62	15.35	15.83	16.3	13.93	14.36	14.79
G_C from Data	14.19	12.58	13.96	17.04	16.74	14.84	14.57	18.32	17.20
Data/Eqn.	1.03	0.89	0.95	1.11	1.06	0.91	1.05	1.28	1.16

Average: 1.05

Standard Deviation: 0.124

Table 7.6. Comparison of Experimental Data and Proposed Equation for High/Limestone.

	HLS 0.25	HLS 0.35	HLS 0.45	HLM 0.25	HLM 0.35	HLM 0.45	HLL 0.25	HLL 0.35	HLL 0.45
G_C from Eqn.	23.72	22.82	21.92	26.44	25.44	24.44	23.99	23.08	22.17
G_C from Data	29.00	20.76	17.71	33.34	23.30	28.68	18.11	19.99	19.51
Data/Eqn.	1.22	0.91	0.81	1.26	0.92	1.17	0.75	0.87	0.88

Average: 0.98

Standard Deviation: 0.190

Table 7.7. Comparison of Experimental Data and Proposed Equation for Normal/Granite.

	NGS 0.25	NGS 0.35	NGS 0.45	NGM 0.25	NGM 0.35	NGM 0.45	NGL 0.25	NGL 0.35	NGL 0.45
G_C from Eqn.	13.73	14.21	13.33	15.31	15.84		13.89		13.49
G_C from Data	18.86	14.86	16.30	20.02	23.70		15.90		18.01
Data/Eqn.	1.37	1.05	1.22	1.31	1.50		1.14		1.34

Average: 1.28

Standard Deviation: 0.150

Table 7.8. Comparison of Experimental Data and Proposed Equation for High/Granite.

	HGS 0.25	HGS 0.35	HGS 0.45	HGM 0.25	HGM 0.35	HGM 0.45	HGL 0.25	HGL 0.35	HGL 0.45
G_C from Eqn.	28.00	28.93		28.00	28.93	27.08	28.00	28.93	27.08
G_C from Data	21.13	31.82		24.78	28.79	22.94	16.84	27.73	18.57
Data/Eqn.	0.75	1.10		0.89	1.00	0.85	0.60	0.96	0.69

Average: 0.85

Standard Deviation: 0.167

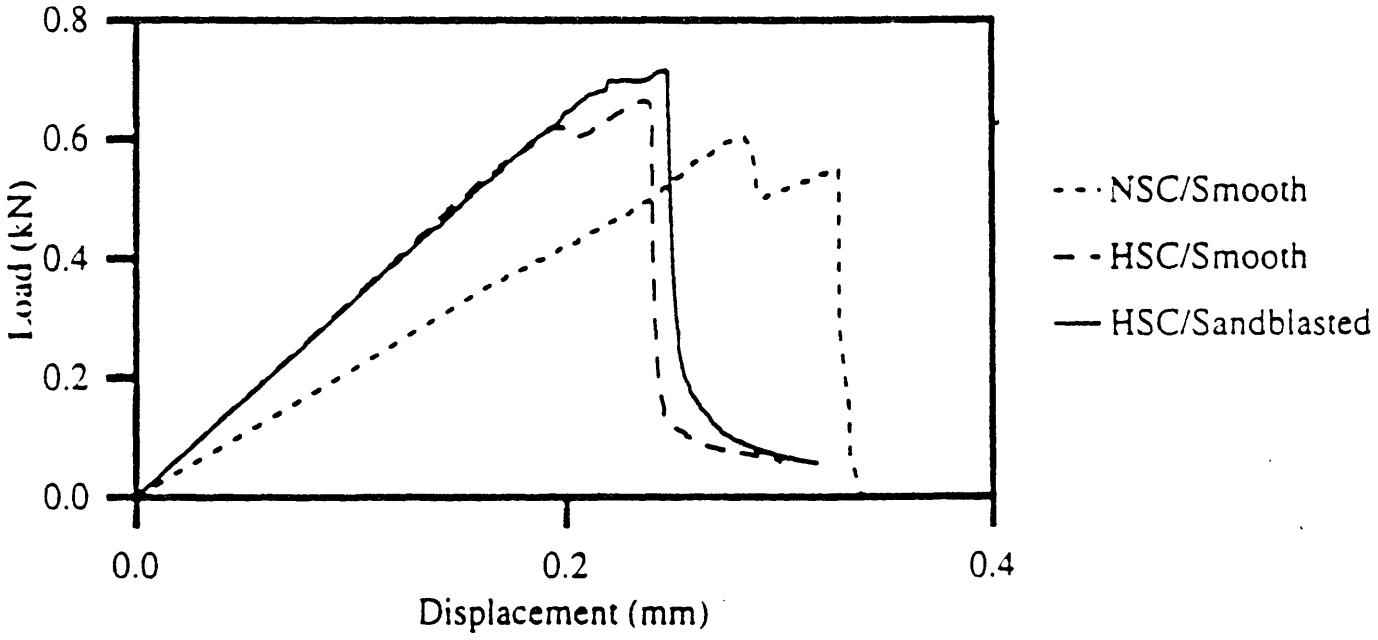

Figure 7.1 Comparison of the load/load-line displacements obtained from cohesive force simulations using normal and high strength mortars with a circular granite inclusion [*Büyüköztürk and Hearing, 1996*]

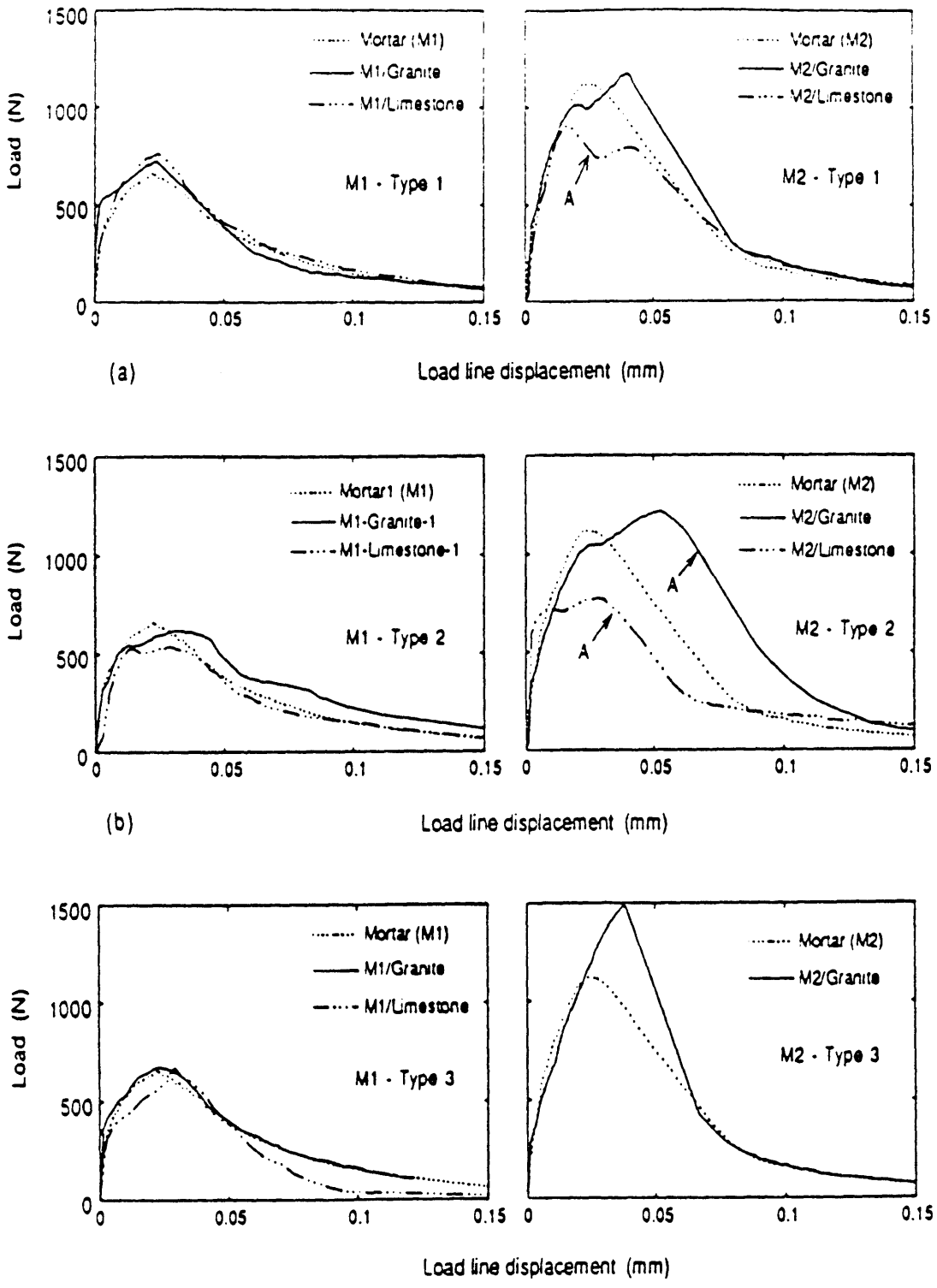

Figure 7.2 Comparison of load/line-displacements obtained with analytical simulations using normal and high strength mortars with limestone aggregate [*Kitsutaka et al., 1993*]

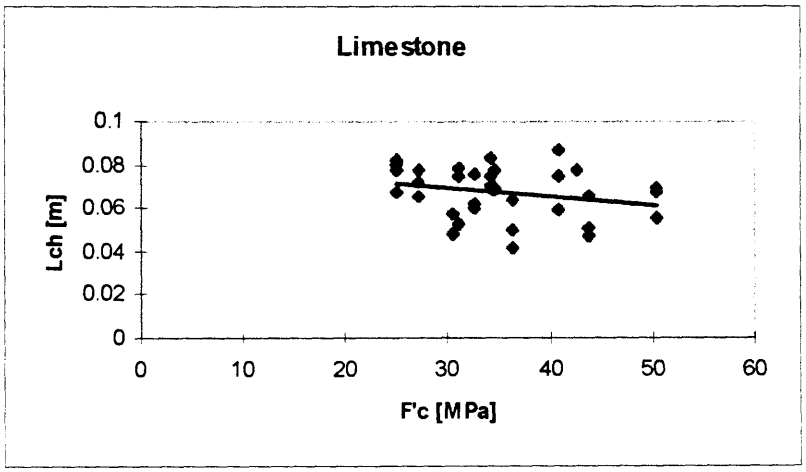

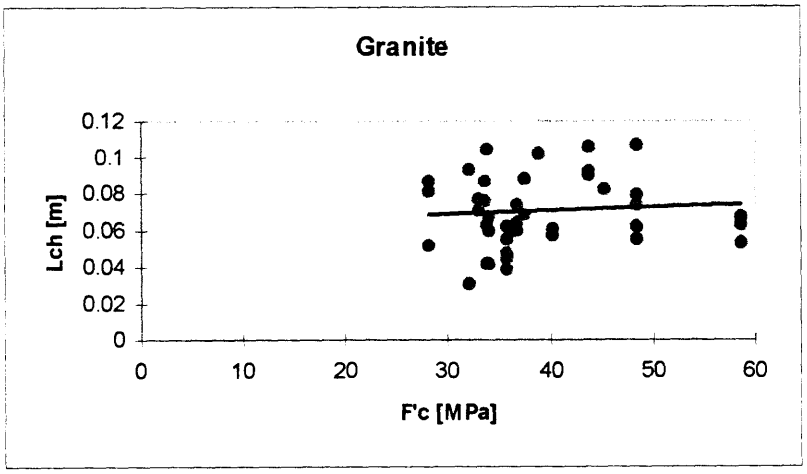

Figure 7.3 Ductility Strength Relations for Limestone and Granite Mixtures

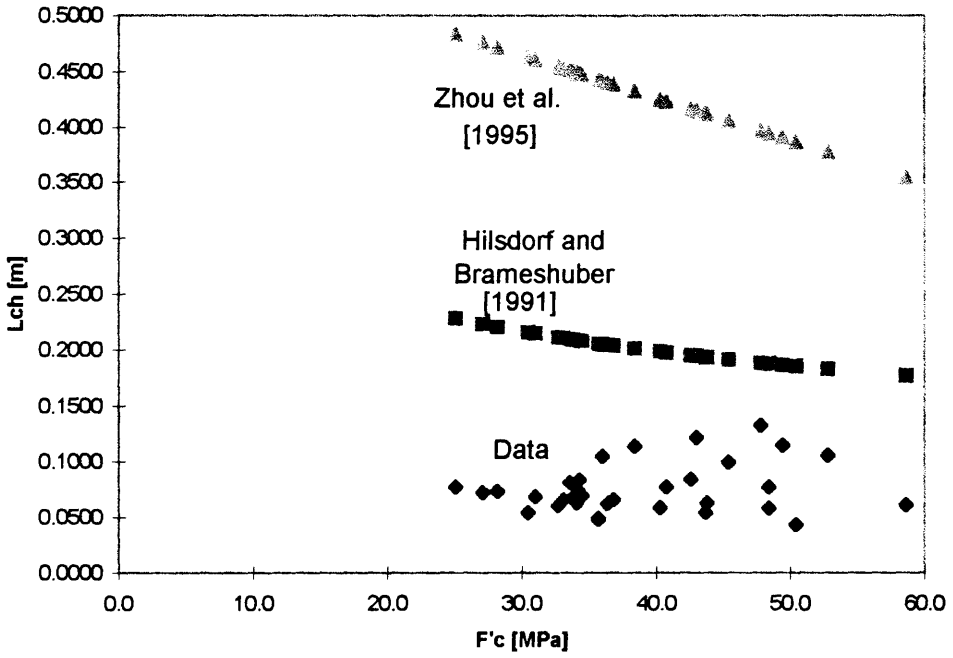

Figure 7.4 Comparison of Empirical Strength-Characteristic Length Relationships to Data Obtained from this Research

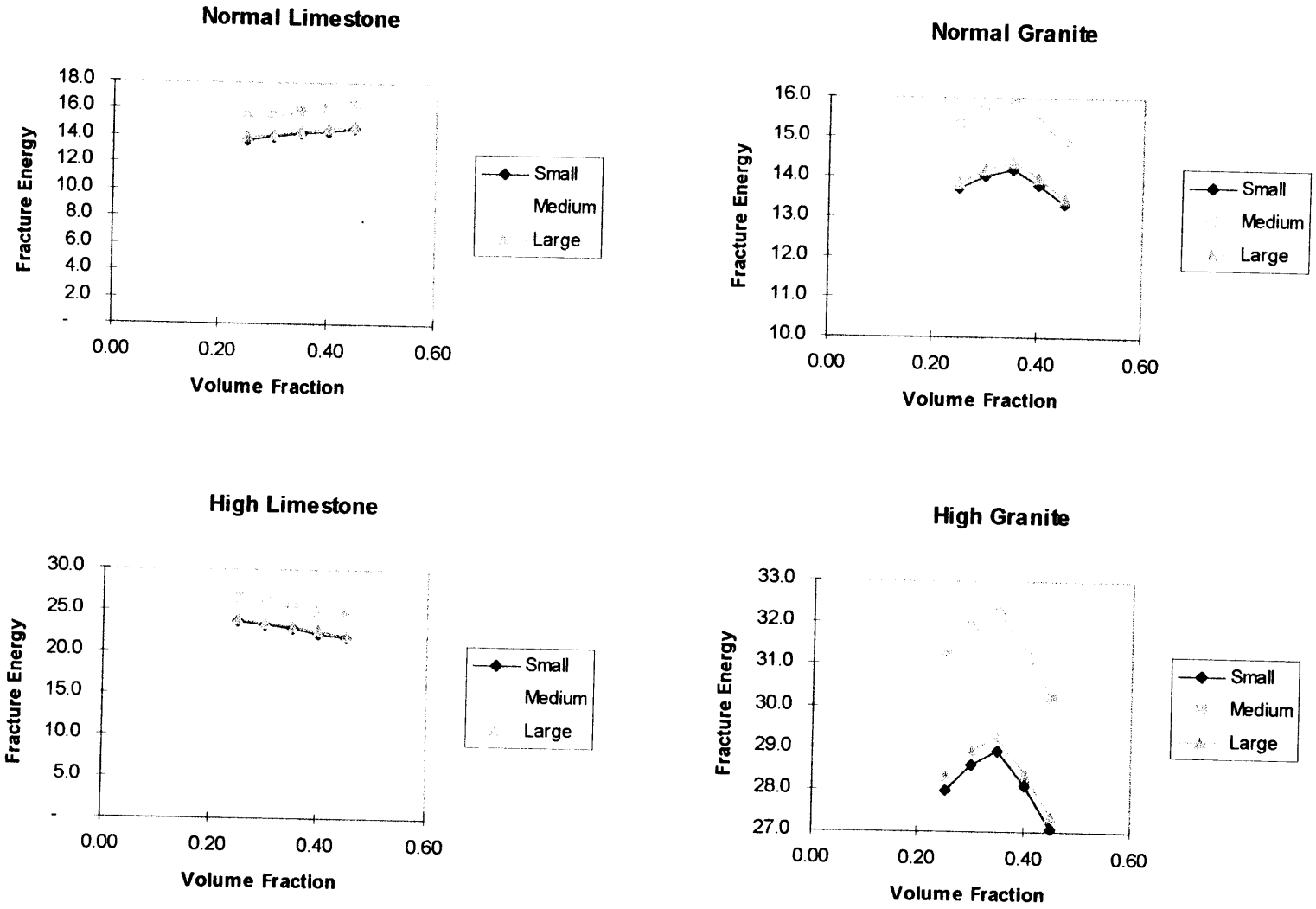

Figure 7.5 Parametric Study for Variable Volume Fractions

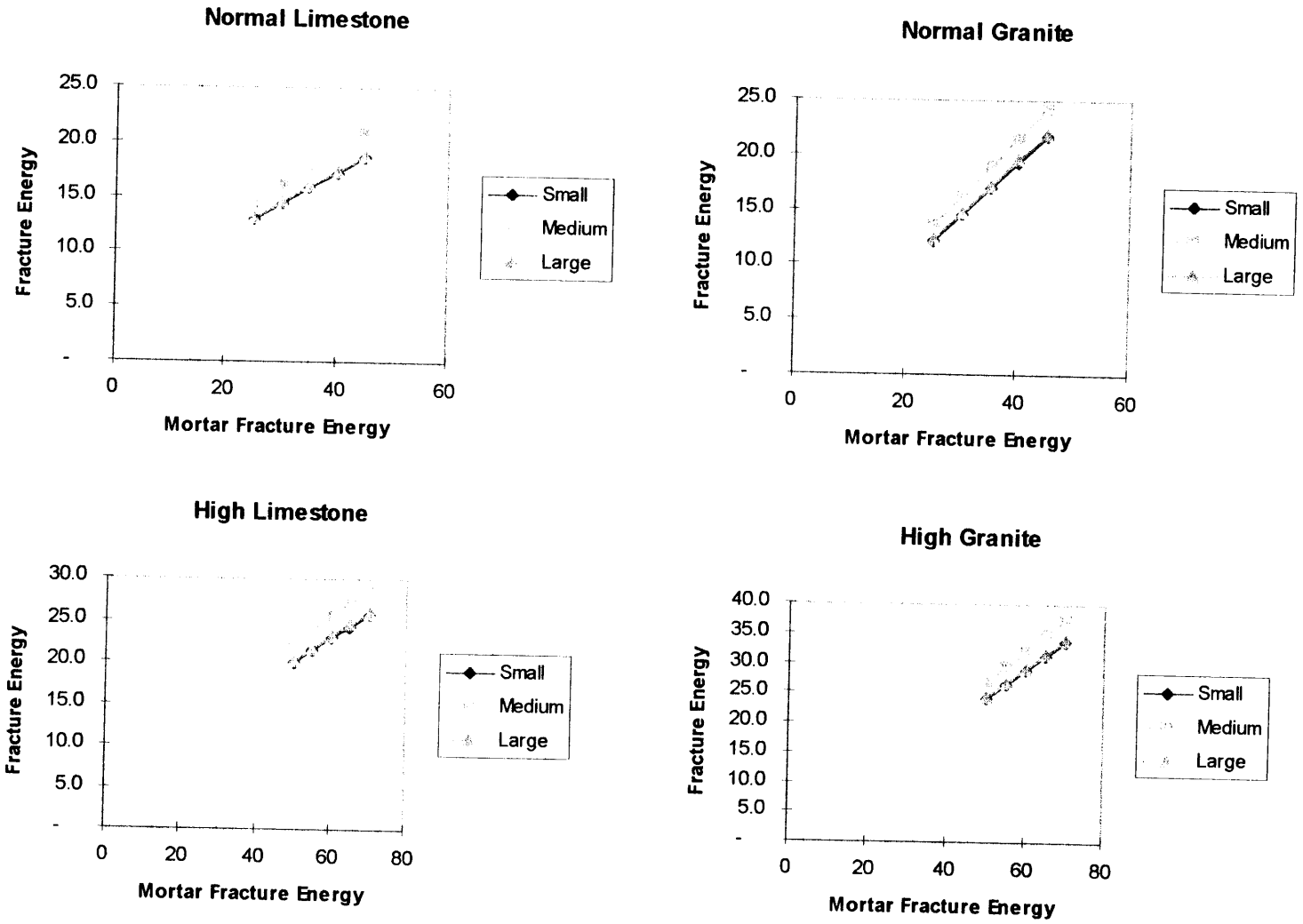

Figure 7.6 Parametric Study for Varied Mortar Fracture Energy

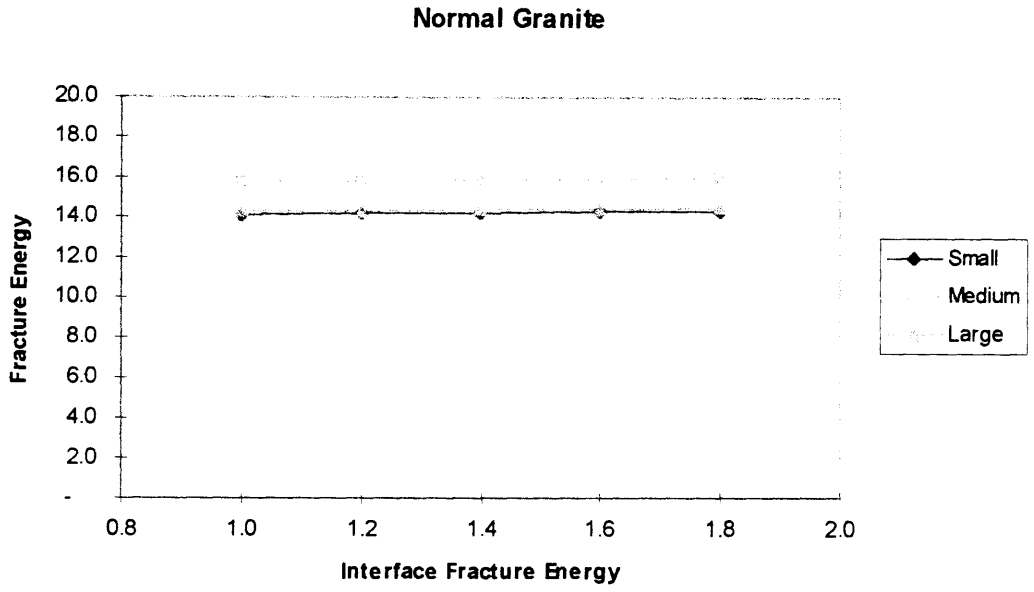

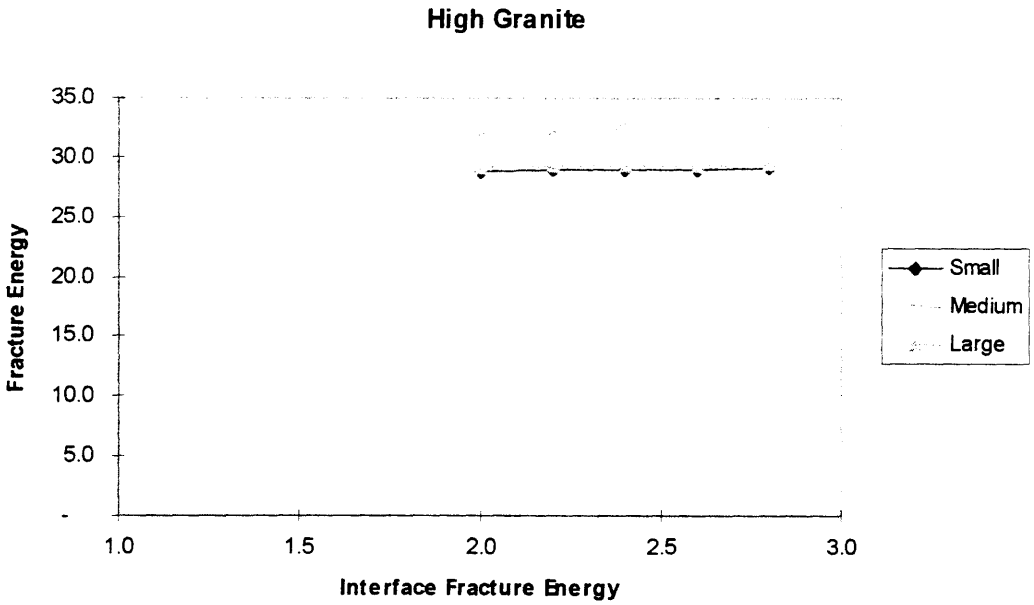

Figure 7.7 Parametric Study of Variable Interface Fracture Energy

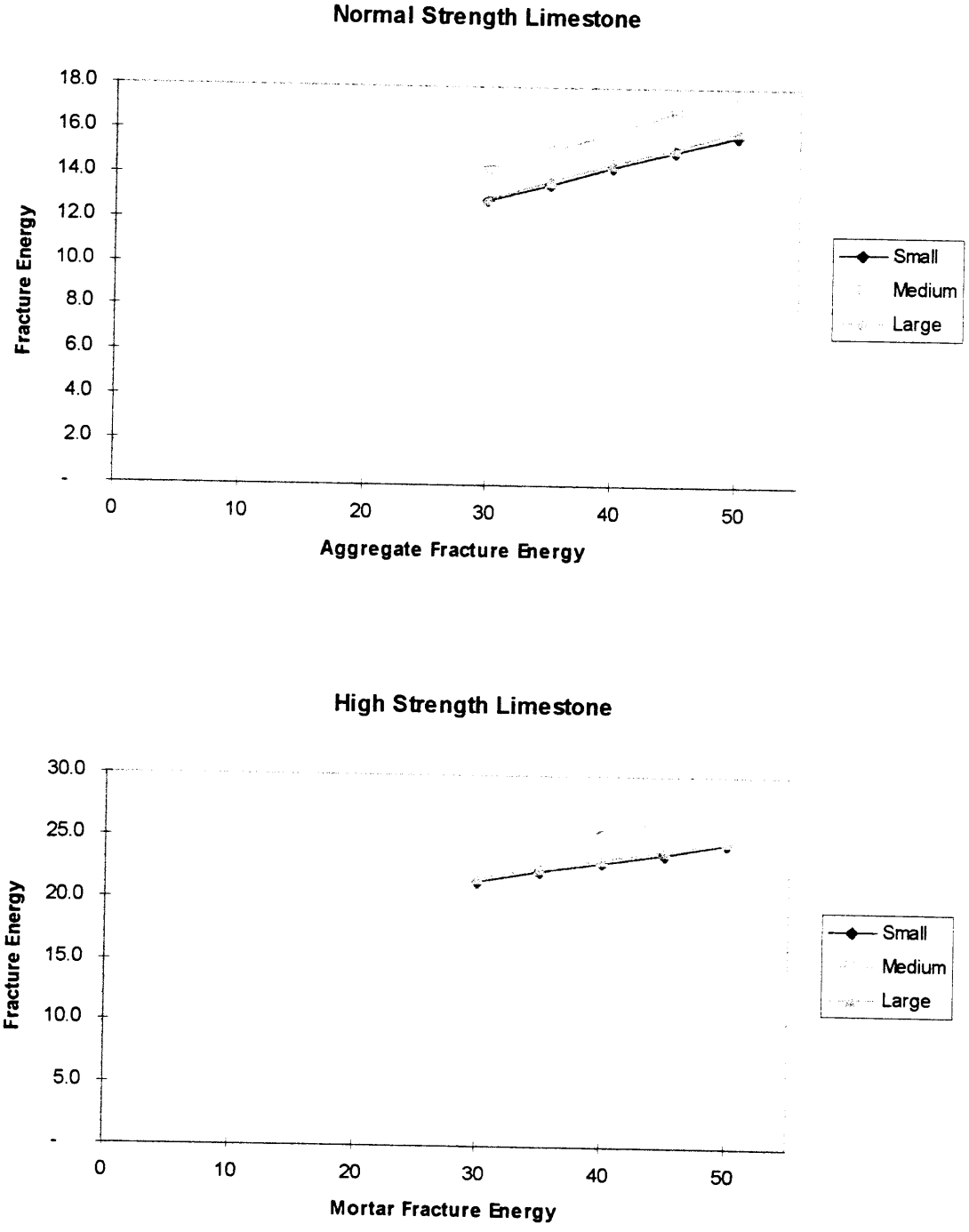

Figure 7.8 Parametric Study of Variable Aggregate Fracture Energy

Chapter 8

Summary, Conclusions and Future Work

8.1 Summary

This research was undertaken in order to assess the parameters which affect the ductile failure of high strength cementitious composites. The effect of some properties on fracture and ductility are not well known at this time, therefore study in this area can contribute to a greater understanding. The parameters which were investigated here include varying MSA, aggregate type and volume fraction in combination with both normal and high strength mortar. For each of the 36 mixtures obtained with the previously mentioned variables, several three point bending beams meeting RILEM specifications and cylinders were cast in order to obtain the fracture values necessary to calculate the results. The characteristic length, a measure proposed by Hillerborg [*1989*], is used to quantify ductility. The data is also used in the development of a novel code-like equation to predict fracture energy based on the material constants.

This work is a continuation of other works completed at MIT. The previous research, discussed in detail in Chapter 4, was different from this in that they investigated concrete as a two phase model consisting of mortar and aggregate as opposed to the true concrete studied here. This work is a continuation in that the knowledge acquired from the two phase models and analytical schemes are compared to the fracture properties of true concrete.

8.2 Conclusions

8.2.1 Conclusions with Respect to Ductility

For the normal strength mixtures with both limestone and granite, the ductility was found to decrease with an increase in volume fraction. The decrease in the granite mixtures was less pronounced due to the longer fracture path resulting from interfacial failure. However, despite the longer crack path the ductility's decrease may be due to the ductility of the interface being less than that of the mortar.

Both high strength mixtures were found to increase in ductility with an increase in volume fraction. The limestone mixtures have improved ductilities because the ductility of the limestone is greater than the mortar's. The granite mixtures have an increasing ductility with volume fraction due to the increase in deflections found with aggregates that produce interfacial failure.

High strength and normal strength mixtures comprised of either limestone or granite were found to have improved ductilities with a smaller MSA. This may be due to improved packing, improved transition zone, and a smaller transition zone with small MSA.

For normal strength mixtures there was not much of a difference in ductility between the limestone and granite mixtures. This may be because the ductility of the limestone is comparable to the ductility of the interface between mortar and granite. For HSC, no valid comparison can be made between the limestone and granite mixtures because different forms of silica fumes were used for these concretes.

8.2.2 Conclusions with Respect to Novel Equation

The novel equation to predict fracture energy based on material properties was

shown to be most accurate for the limestone mixtures. The accuracy with granite mixtures was diminished, however sufficient correlation between the laboratory data and the equation may come with future research. The discrepancy with granite concretes may be due to the fact that the maximum size of aggregate modifier, k_a, found for the limestone mixtures is applied to the granite in order to calculate the volume fraction modifier, k_v. It would be desirable to have the coefficient independent of the aggregate type however whether that is possible is unknown. Nonetheless the theory is sound and the equation is a valuable preliminary step in the development of a code-like fracture energy.

8.3 Future Work

Future work, as a continuation of this and other MIT interface fracture work, could progress in the following ways:

- An experimental series similar to this with higher strength concretes than obtained in this research could be undertaken,

- The portion of this work which addressed the ductility could be expanded to include other aggregate characteristics such as surface roughness and aggregate shape,

- The novel fracture energy equation should be researched further for higher strength concretes and for other material combinations in order to improve the factors k_a and k_v.

Bibliography

Aitcin, P. -C. and Laplante, P. (1992), "The Development of High Strength Concrete in North America," *High Performance Concrete: From Material to Structure*, Y. Malier, ed., E & FN Spon, PLACE, pp.412-420.

Bjerkeli, L, Tomaszewicz, and Jensen, J. J. (1990), "Deformation Properties and Ductility of High Strength Concrete," *High Strength Concrete*, ACI SP-121, W. T. Hester, ed. pp.215-238.

Broek, D. (1978), *Elementary Engineering Fracture Mechanics*, Sijthoff & Noordhoff, Alphen aan den Rijn-The Netherlands.

Büyüköztürk, O. and Hearing, B. (1996), "Improving the Ductility of High Performance Concrete through Mortar-Aggregate Interfaces. In Iyer, S. L., ed., *To appear in Proceedings for the ASCE 4th Materials Conference*, New York, NY. American Society of Civil Engineers.

Büyüköztürk, O. and Lee, K. -M. (1993), "Assessment of Interfacial Fracture Toughness in Concrete Composites," *Cement and Concrete Research*, Vol. 15, No. 3, pp. 143-152.

Carrasquillo, R. L., Nilson, A. H. and Slate, F. O. (1981), "Properties of High Strength Concrete Subject to Short-Term Loads," *ACI Journal*, Vol. 78, No. 3, pp. 179-186.

Causse, G., and Montens, S., (1992), "The Roize Bridge," *High Performance Concrete from Material to Structure*, Y. Malier, ed., pp. 525-536.

Collins, T. M., (1989), "Proportioning High-Strength Concrete to Control Creep and Shrinkage," *ACI Materials Journal*, Vol. 86, No. 6 pp. 576-580.

DeChamps, J. -F and Monachon, P. (1992), "High Performance Concrete in the Arch of the Bridge over the Rance," *High performance Concrete from Material to Structure*, Y. Malier, ed., pp. 510-524.

Dundurs, J. (1969), "Edge-bonded dissimilar orthogonal elastic wedges," *Journal of Applied Mechanics*, Vol. 36, pp. 650-652.

Ghosh, S. and Nasser, K. W., (1995), "Creep, shrinkage, frost and sulphate resistance of high-strength concrete," *Canadian Journal of Civil Engineering*, Vol. 22, No. 3, pp. 621-636.

Giaacio, G., Rocco, C., Violini, D., Zappitelli, J., and Zerbino, R. (1992), "High-Strength Concretes Incorporating Different Coarse Aggregates," *ACI Materials Journal*, Vol. 89, No. 3, pp.242-246.

Goldman, A. and Bentur, A. (1989), "Bond Effects in High-Strength Silica Fume Concretes," *ACI Materials Journal*, Vol. 86, pp. 440-447.

Hammer, T. A., and Sellevold, E. J. (1990), "Frost Resistance of High-Strength Concrete," *High Strength Concrete*, ACI SP-121, W. T. Hester, ed. pp. 457-488.

Haug, A. K. and Jakobsen, B. (1990), "In situ and Design Strength for Concrete in Offshore Platforms," *High Strength Concrete*, ACI SP-121, W. T. Hester, ed. pp. 369-398.

He, M. Y. and Hutchinson, J. W. (1989), "Crack Deflection at an Interface between Dissimilar Elastic Materials," *International Journal of Solids and Structures*, Vol. 25, No. 9, pp. 1052-1067.

Helland, S. (1990), "High-Strength Concrete used in Highway Pavements," *High Strength Concrete*, ACI SP-121, W. T. Hester, ed. pp. 757-766.

Hillerborg, A. (1989), "Existing methods to determine and evaluate fracture toughness of aggregative materials-RILEM recommendation on concrete," *Fracture Toughness and Fracture Energy Test methods for concrete and rock*, H. Mihashi, H. Takahashi, and F. H. Wittman, editors, pp. 145-152.

Hilsdorf, H. K. and Brameshuber, W. (1991), "Code-type formulation of fracture mechanics concepts for concrete," *International Journal of Fracture*, Vol. 51, pp. 61-72.

Hussain, M. A., Pu, S. L. and Underwood, J., (1974), "Strain Energy Release Rate for a Crack under Combined Mode I and II", Fracture Analysis, ASTM STP 560, American Society of Testing Materials, pp. 2-28.

Hutchinson, J. W. and Suo, Z. (1992), "Mixed mode cracking in layered materials," *Metal-Ceramic Interfaces*, pp. 295-306.

Jeng, Y. S. and Shah, S. P. (1985), "A fracture toughness criterion for concrete," *Engineering Fracture Mechanics*, Vol. 21, No. 5, pp. 1055-1069.

Kitsutaka, Y., Büyüköztürk, O., and Lee, K. M. (1993), "Fracture behavior of high strength concrete composite models. *Submitted to ACI Journal of Materials.*

Larrard, F. (1990), "Creep and Shrinkage of High Strength Field Concretes," *High Strength Concrete*, ACI SP-121, , W. T. Hester, ed., pp.577-598.

Larrard, F., Ithurralde, G., Acker, P. and Chauvel, D. (1990), "High-Performance Concrete for a Nuclear Containment," *High Strength Concrete*, ACI SP-121, , W. T. Hester, ed., pp.549-576.

Larrard, F., and Malier, Y. (1992), "Engineering properties of very high performance concrete," *High Performance Concrete from Material to Structure*, Y. Malier, ed., 85-114.

Lee, K.-M. (1993), *Interface Fracture in High Strength Concrete*, Ph.D. Thesis, Department of Civil and Environmental Engineering, Massachusetts Institute of Technology, Cambridge, MA.

Lee, K. -M. and Büyüköztürk, O. (1995), "Fracture Toughness of Mortar-Aggregate Interface in High-Strength Concrete," *ACI Materials Journal*, Vol. 92, No. 6, pp. 634-642.

Liu, T. C., Nilson, A. H., and Slate, F. O. (1972), "Stress-strain Response and Fracture of Concrete in Uniaxial and Biaxial Compression," *ACI Journal*, Vol. 69, No. 5, pp. 291-295.

Malier, Y (1992), Introduction, *High performance Concrete from Material to Structure*, Y. Malier, ed., pp. xiii-xxiv.

Malier, Y., Brazillier, D. and Roi, S. (1992), "The Joigny Bridge: An Experimental High Performance Concrete Bridge," *High performance Concrete from Material to Structure*, Y. Malier, ed., pp. 424-431.

Mehta, P. K. (1986), *Concrete: structure, properties, and materials*, Prentice Hall, Englewood Cliffs, NJ.

Mehta, P. K. and Aitcin, P.-C. (1990), " Microstructural Basis of Selection of Materials and Mix Proportions for High-Strength Concrete," *High Strength Concrete*, ACI SP-121, , W. T. Hester, ed., pp.265-286.

Mihashi, H. Nomura, N. and Izumi, M. (1989), "Influence of internal structure on tension softening and fracture energy of concrete," *Fracture Toughness and Fracture Energy Test methods for concrete and rock*, H. Mihashi, H. Takahashi, and F. H. Wittman, editors, pp. 87-100.

Mitsui, K., Zongjin, L., Lange, D. A., and Shah, S. P. (1992), " Influence of mineral admixtures in the transition zone of concrete," *Interfrace in Cementitious Composites*, J. C. Maso , editor, pp. 65-70.

Oumera, A. A. (1991), *Crack Propagation in the Aggregate-Mortar Interface Regions of Concrete*, M. S. Thesis, Department of Civil and Environmental Engineering, Massachusetts Institute of Technology, Cambridge, MA.

Paulson, K., Nilson, A. H. and Hover, K. C. (1991), "Long-Term Deflection of High-Strength Concrete Beams," *ACI Materials Journal*, Vol. 88, no. 2, pp. 197-206

Penttala, V. and Rautanen, (1990), "Microporosity, Creep, and Shrinkage of High Strength Concretes," *High Strength Concrete*, ACI SP-121, W. T. Hester, ed. pp.409-432.

Popovics, S. (1979), *Concrete-Making Materials*, Hemisphere Publishing Corporation, Washington.

Rice, R. (1988), "Elastic Fracture Concepts for Interfacial Cracks," *Journal of Applied Mechanics*, Vol. 55, pp. 98-103.

RILEM Draft Recommendations (1989), "TC 89-FMT Fracture Mechanics of Concrete-Test Methods."

Shih, T. S., Lee, G. C. and Chang, K. C. (1989),"On Static Modulus of Elasticity of Normal-Weight Concrete," *Journal of Structural Engineering, ASCE,* Vol. 115, No. 10, pp. 2579-2587.

Snyder, K. A., Winslow, D. N., Bentz, D. P., and Garboczi, E. J., (1992), "Interfacial zone percolation in cement-aggregate composites," *Interface in Cementitious Composites*, J. C. Maso, ed., pp. 259-268.

Tasdemir, C., Tasdemir, M. A., Lydon, F. D., and Barr, B. I. G., (1996), "Effects of Silica Fume and Aggregate Size on the Brittleness of Concrete," *Cement and Concrete Research*, Vol. 26, No. 1, pp. 63-68.

Trende, Uwe. (1995), *Interface Fracture of High Strength Concrete: Size Effect and Roughness*, M. S. Thesis, Department of Civil and Environmental Engineering, Massachusetts Institute of Technology, Cambridge, MA.

Troxell, G. E., Davis, H. E. and Kelley, J. W. (1968), *Composition and Properties of Concrete*, McGraw-Hill Book Company, New York.

Wang and Salmon, (1985), *Reinforced Concrete Design*, Harper & Row, Publishers, Cambridge.

Wittman, F. H. (1989), "Structure and fracture mechanics of composite materials," *Fracture Toughness and Fracture Energy Test methods for concrete and rock*, H. Mihashi, H. Takahashi, and F. H. Wittman, editors, pp. 3-12.

Zhang, M. H., and Gjørv, O.E. (1990), "Microstructure of the Interface Zone between Lightweight Aggregate and Cement Paste," *Cement and Concrete Research*, Vol. 20, pp. 610-618.

Zhou, F. P., Barr, B. I. G., and Lydon, F. D. (1995), "Fracture properties of high strength concrete with varying silica fume content and aggregates," *Cement and Concrete Research,* Vol. 25, No. 3., pp. 543-552.

Appendix

Mix Proportions

Same mix proportions for limestone and granite concretes.

	N 0.25	N 0.35	N 0.45 (3 Beams)
Aggregate:	21.720 kg	30.408 kg	39.069 kg
Cement:	19.720 kg	17.091 kg	14.460 kg
Sand:	39.460 kg	34.199 kg	28.940 kg
Water:	9.860 kg	8.545 kg	7.230 kg

	H 0.25	H 0.35	H 0.45 (3 beams)
Aggregate:	16.290 kg	30.408 kg	29.320 kg
Cement:	19.730 kg	17.099 kg	10.852 kg
Sand:	39.460 kg	34.199 kg	21.703 kg
Water:	4.341 kg	3.762 kg	2.387 kg
Silica Fume:	4.120 kg	3.571 kg	2.266 kg
HRWR:	0.442 kg	0.383 kg	0.243 kg

Data

CONCRETE	BEAM (KN)	BEAM (KN)	BEAM (KN)	BEAM (KN)	TEN. LOAD	TEN. LOAD	COMP. LOAD	COMP. LOAD	f'_t (MPa)	f'_c (MPa)
NLS .25	2.687	2.842	2.682	2.686	7,850		36,850		1.92	36.0
NLS .35	2.411	2.214	2.440	2.373	8,440	7,430	25,700		1.94	25.1
NLS .45	2.634	2.532	2.428		8,800	8,840	27,750		2.16	27.1
NLM .25	3.379	2.719	3.024	2.689	9,260	9,840	35,500	34,750	2.33	34.3
NLM .35	2.936	3.250	2.500		10,860	11,160	33,450		2.69	32.7
NLM .45	2.762	2.529	2.750		10,540	10,930	31,170		2.62	30.5
NLL .25	2.671	2.761	2.753		9,340	9,440	34,000	36,000	2.29	34.2
NLL .35	3.140	3.203	2.631		10,680		29,525	34,000	2.61	31.0
NLL .45	2.981	2.956	3.156		10,560	10,260	34,000	36,500	2.58	34.5

CONCRETE	BEAM (KN)	BEAM (KN)	BEAM (KN)	BEAM (KN)	TEN. LOAD	TEN. LOAD	COMP. LOAD	COMP. LOAD	f'_t (MPa)	f'_c (MPa)
HLS .25	4.254	3.499	3.950	4.325	13,480		41,700		3.29	40.8
HLS .35	3.255	3.709	3.542	3.662	9,760		50,500		2.39	49.4
HLS .45	2.769	3.17	2.694		8,500		44,000		2.08	43.0
HLM .25	4.748	4.372	4.291	4.855	13,100		54,000		3.20	52.8
HLM .35	3.671	3.627	3.499	3.729	11,700		43,560		2.86	42.6
HLM .45	3.944	4.326			11,600		48,850		2.83	47.8
HLL .25	3.110	3.544	3.007	11,350	14,460		44,700		3.15	43.7
HLL .35	2.652	3.290	3.788	12,160	12,150		37,250		2.97	36.4
HLL .45	3.554	3.216	3.599	15,520	10,000		51,600		3.12	50.4

CONCRETE	BEAM (KN)	BEAM (KN)	BEAM (KN)	BEAM (KN)	TEN. LOAD	TEN. LOAD	COMP. LOAD	COMP. LOAD	f'_t (MPa)	f'_c (MPa)
NGS .25	3.027	3.179	3.026		10,660	11,740	35,000	32,750	2.61	33.1
NGS .35	2.651	2.836			9,020	8,940	35,650	33,000	2.19	33.6
NGS .45	2.801	3.097	2.901		10,360	11,000	37,650		2.61	36.8
NGM .25	2.967	3.292	3.603		10,560	7,600	39,250		2.20	38.4
NGM .35	3.354	2.740	4.315		13,240	11,700	34,550		3.04	33.8
NGM .45										
NGL .25	2.313	2.758	2.936		12,625	8,600	34,850		2.59	34.1
NGL .35	3.180	3.603	2.824		11,340	8,900			2.77	
NGL .45	3.069	3.180	2.446		9,920	10,160	28,800		2.45	28.2

CONCRETE	BEAM (KN)	BEAM (KN)	BEAM (KN)	BEAM (KN)	TEN. LOAD	TEN. LOAD	COMP. LOAD	COMP LOAD	f'_t (MPa)	f'_c (MPa)
HGS .25	3.458	3.930	3.788		14,600	13,640	59,950		3.45	58.6
HGS .35	4.468	5.000	4.142		13,600	13,240	46,400		3.28	45.4
HGS .45	4.404	4.086	4.031		11,500	12,000	39,650		2.87	38.8
HGM .25	3.180	4.003			10,440	15,100	36,475		3.69	35.7
HGM .35	4.038	3.923			15,300	12,260	41,210		3.74	40.3
HGM .45	3.815	3.608			14,300	14,420	49,500		3.51	48.4
HGL .25	2.93	3.145	2.824		12,980	12,160	36,475		3.07	35.7
HGL .35	3.914	3.870	4.181		12,000	12,000	44,850		2.93	43.8
HGL .45	3.269	3.403	3.936		12,160	10,350	49,500		2.75	48.4